'

**European Joint Programme
on Radioactive Waste Management**

Deliverable 15.7: Elucidation of critical irradiation parameter

Work Package 15 ConCorD

Document information

Project Acronym	**EURAD**
Project Title	**European Joint Programme on Radioactive Waste Management**
Project Type	**European Joint Programme (EJP)**
EC grant agreement No.	**847593**
Project starting / end date	**1st June 2019 – 30 May 2024**
Work Package No.	**15**
Work Package Title	**Container corrosion under disposal conditions**
Work Package Acronym	**ConCorD**
Deliverable No.	**15.7**
Deliverable Title	**Elucidation of critical irradiation parameter**
Lead Beneficiary	**Jacobs**
Contractual Delivery Date	**30/09/2023**
Actual Delivery Date	**06/02/2024**
Type	**Report**
Dissemination level	**Public**
Authors	**Clayton Bevas (Jacobs), James Hesketh (Jacobs), Andy Rance (Jacobs), Leigh-Anne Stevenson (Jacobs), Shorubhi Uthayakumaran (Jacobs) Ben Pateman (Jacobs), Cristiano Padovani (Jacobs), Šárka Šachlová (UJV), Vlastislav Kašpar (UJV), David Dobrev (UJV), Daniel Götz (UJV), Kateřina Kolomá (UJV), Petr Večerník (UJV)**

To be cited as:

Clayton Bevas (Jacobs), James Hesketh (Jacobs), Andy Rance (Jacobs), Leigh-Anne Stevenson (Jacobs), Shorubhi Uthayakumaran (Jacobs) Ben Pateman (Jacobs), Cristiano Padovani (Jacobs), Šárka Šachlová (UJV), Vlastislav Kašpar (UJV), David Dobrev (UJV), Daniel Götz (UJV), Kateřina Kolomá (UJV), Petr Večerník (UJV). (2024): Elucidation of the effect of radiation on the corrosion of canister materials. Final version as of 06/02/2024 of deliverable D15.7 of the HORIZON 2020 project EURAD. EC Grant agreement no: 847593.

Disclaimer

All information in this document is provided "as is" and no guarantee or warranty is given that the information is fit for any particular purpose. The user, therefore, uses the information at its sole risk and liability. For the avoidance of all doubts, the European Commission or the individual Colleges of EURAD (and their participating members) has no liability in respect of this document, which is merely representing the authors' view.

Acknowledgement

EURAD (Deliverable n° 15.7) – Elucidation of critical irradiation parameter
Dissemination level: Public
Date of issue of this report: 06/02/2024

Page 1

Status of deliverable		
	By	Date
Delivered (Lead Beneficiary)	James Hesketh	05/02/2024
Verified (WP Leader)	Nikitas Diomidis	06/02/2024
Reviewed (Reviewers)	Satoru Suzuki, Valerie Maillot, Mehran Behazin, Christina Lilja, Fraser King	29/01/2024
Approved (PMO)		
Submitted to EC (Coordinator)		

EURAD (Deliverable n° 15.7) – Elucidation of critical irradiation parameter
Dissemination level: Public
Date of issue of this report: 06/02/2024

Page 2

Executive Summary

This document is deliverable 15.7 of the EURAD WP15 ConCorD and aims to elucidate the critical parameters associated with radiation exposure when considering the corrosion performance of candidate canister materials for deep geological disposal of radioactive waste.

The document describes three separate sets of experiments to evaluate the corrosion resistance of candidate canister materials while exposed to gamma irradiation under simulated disposal conditions. The experiments were performed by Jacobs and UJV as part of ConCorD's Task 3 – Influence of Radiation.

The Jacobs tests were performed on copper and carbon steel and investigated a wide range of dose rates (0.1 to 1000 Gy h^{-1}) and total radiation doses (1 to 100 kGy) on corrosion, whilst specimens were exposed to a simulated porewater solution under initially anoxic conditions. The results demonstrated that for copper, the presence of radiation results in an increase in corrosion rate measured under all dose rates investigated (0.1 to 10 Gy hr^{-1}), with an increasing effect at higher dose rates. The increase in corrosion rate due to the presence of radiation varied from 0.03 to 1.15 μm yr^{-1}, for dose rates from 0.1 to 10 Gy h^{-1}, respectively. However, due to the very low corrosion rate of copper in the absence of radiation of 0.02 μm yr^{-1}, the additional corrosion loss due to radiation reflected a very large relative increase compared to unirradiated conditions. For carbon steel, the influence of radiation on corrosion rate was less substantial than for copper. A significant increase in corrosion rate was only detected above 10 Gy hr^{-1}. At 10 Gy h^{-1} the presence of radiation led to an increase in corrosion rate by 0.90 and 1.41 μm yr^{-1}, following exposure durations of 10000 and 5000 hours respectively. However, since the corrosion rate of carbon steel in the absence of radiation was between 1.57 and 3.51 μm yr^{-1}, the increase in corrosion loss due to radiation was modest relative to corrosion rate in unirradiated conditions.

The UJV tests were performed on carbon steel specimens embedded within either MX-80 bentonite or Bentonite Cerny Vrch (BCV) that were saturated and tested under anoxic conditions at 90 °C and 150 °C. Specimens were irradiated at a representative dose rate of 0.4 Gy h^{-1} and were tested for durations between 6 and 18 months. Corresponding unirradiated control tests were set up to determine the influence of radiation on corrosion. It was found that at 150 °C, the presence of radiation resulted in a significant inhibition of the corrosion rate for all durations tested and in both types of bentonite. A more modest inhibition was also observed for tests performed in BCV at 90 °C, but in MX-80 bentonite the influence of radiation on corrosion rate was negligible.

Keywords

Carbon steel, Container, Corrosion, Copper, Geological Disposal, Radiation, Radioactive Waste, Radiolysis, Waste Management

EURAD (Deliverable n° 15.7) – Elucidation of critical irradiation parameter
Dissemination level: Public
Date of issue of this report: 06/02/2024

Page 3

Table of contents

EURAD (Deliverable n° 15.7) – Elucidation of critical irradiation parameter
Dissemination level: Public
Date of issue of this report: 06/02/2024

Page 4

EURAD (Deliverable n° 15.7) – Elucidation of critical irradiation parameter
Dissemination level: Public
Date of issue of this report: 06/02/2024

Page 5

EURAD (Deliverable n° 15.7) – Elucidation of critical irradiation parameter
Dissemination level: Public
Date of issue of this report: 06/02/2024

Page 6

List of figures

EURAD (Deliverable n° 15.7) – Elucidation of critical irradiation parameter
Dissemination level: Public
Date of issue of this report: 06/02/2024

Page 7

EURAD (Deliverable n° 15.7) – Elucidation of critical irradiation parameter
Dissemination level: Public
Date of issue of this report: 06/02/2024

Page 8

EURAD (Deliverable n° 15.7) – Elucidation of critical irradiation parameter
Dissemination level: Public
Date of issue of this report: 06/02/2024

Page 9

EURAD (Deliverable n° 15.7) – Elucidation of critical irradiation parameter
Dissemination level: Public
Date of issue of this report: 06/02/2024

Page 10

EURAD (Deliverable n° 15.7) – Elucidation of critical irradiation parameter
Dissemination level: Public
Date of issue of this report: 06/02/2024

Page 11

List of Tables

EURAD (Deliverable n° 15.7) – Elucidation of critical irradiation parameter
Dissemination level: Public
Date of issue of this report: 06/02/2024

Page 12

EURAD (Deliverable n° 15.7) – Elucidation of critical irradiation parameter
Dissemination level: Public
Date of issue of this report: 06/02/2024

Page 13

Glossary

Acronym / Abbreviation	Definition
AAS	Atomic absorption spectroscopy
BCV	Bentonite Cerny Vrch
CS	Carbon steel
CSC	Cold-sprayed copper
CSZ	Capillary Zone Electrophoresis
Ctot	Total Carbon Content
CZE	Capillary Zone Electrophoresis
DP	Depth profile
EDM	Electrical discharge machining
EDX/EDS	Energy dispersive X-ray spectroscopy
GDF	Geological disposal facility
IR	Irradiated
LOM	Light Optical Microscopy
NIR	Unirradiated
RAC	Radiation assisted corrosion
RH	Relative humidity
RIC	Radiation induced corrosion
RT	Room Temperature
SEM	Scanning electron microscopy
Stot	Total Sulphur Content
WC	Wrought copper
XRD	X-ray diffraction
XRF	X-ray fluorescence
X-SEM	Cross-section scanning electron microscopy
XPS	X-ray photoelectron spectroscopy

EURAD (Deliverable n° 15.7) – Elucidation of critical irradiation parameter
Dissemination level: Public
Date of issue of this report: 06/02/2024

Page 14

1. Introduction

1.1 Background

1.1.1 Geological disposal of radioactive waste

Currently the preferred option for the disposal of high-level radioactive waste and spent fuel is deep geological disposal. Geological disposal involves emplacement of the waste package several hundred meters underground within a geological disposal facility (GDF), with the aim of isolating radioactive nuclides from the biosphere for a period ranging from thousands to potentially millions of years. Disposal in a geological facility mitigates many of the risks associated with surface storage such as climate change, human intervention, and seismic activity.

The key design philosophy behind a GDF is the multibarrier concept, whereby isolation of radionuclides is provided by a series of engineered and natural barriers. The natural rock formation itself serves as the outermost barrier limiting the movement of radioactive nuclides if they escape from the engineered barrier. Within the rock formation is the buffer layer, which is an engineered barrier between the rock and the canister. The buffer typically comprises bentonite clay or cementitious grout and serves several key functions. The buffer provides mechanical stability to the canister, and a favourable chemical environment that results in a low corrosion rate as well as providing further containment of radionuclides in the event of a breach of the canister. The innermost barrier is the canister itself, which fulfils an integral role in the multibarrier system by providing absolute containment of radionuclides over its design life.

To fulfil its role, the canister must be designed to resist external stress placed upon it during emplacement (e.g., hydrostatic and lithostatic stress) and corrode at a rate low enough to prevent breaching within its design life. To achieve the desired corrosion performance, canisters are either made of corrosion resistant materials, which corrode at an inherently low rate ensuring a minimal loss of thickness at the outermost surface, or they are made of materials that corrode at a very predictable rate allowing a corrosion allowance to be specified, which will prevail over a specified period. Copper and carbon steel are the two most popular canister materials for the disposal of radioactive waste within a GDF, however there is also interest into the use of more modern engineering materials such as stainless steels, superalloys, ceramics etc. A drawback of more modern materials is the lack of data underpinning their degradation characteristics in the long-term (e.g., thousands of years), which can be gained for copper and carbon steel thanks to the presence of natural and archaeological analogues.

A key question that arises when predicting the lifetime of copper and carbon steel containers in a GDF is the impact of radiation on the corrosion behaviour. At present there is no consensus on how much of an additional allowance has to be made to take account of an increase in corrosion rate following saturation of the buffer due to the presence of radiation emitted by the waste package as it decays. One perspective is that the radiation dose rate is the key factor to consider as this will have an impact on the redox conditions at the canister surface owing to radiolysis of the solution close to the metal surface [1]. If this perspective is accurate, then the impact of radiation, if any, would be relatively short-lived as the dose rate experienced by the surface of the canister will attenuate by many orders of magnitude over its design life. However, an alternative perspective is that the total radiation dose is more relevant than the dose rate. Conceptually, this can be thought of in terms of mass balance, whereby the total additional corrosion that is attributable to radiation is a function of the amount of radiolysis products that are generated. If this perspective is correct, then the impact of radiation is likely to be relevant over a significant fraction of the design life of the canister due to the very long timescales that the total dose is able to accumulate [1]. The distinction is also necessary from a testing perspective. Given the long design lives of canisters designed for use in a GDF, testing the corrosion resistance of materials must be performed over a considerably shorter timescale. Where radiation is to be considered, previous testing has been undertaken with dose rates exceeding those anticipated at the canister surface in order to deliver a representative total dose within a practical timeframe [2]. However, without an improved mechanistic understanding of the system, it is not clear to what extent this approach will alter the results

EURAD (Deliverable n° 15.7) – Elucidation of critical irradiation parameter
Dissemination level: Public
Date of issue of this report: 06/02/2024

Page 15

compared to that where a representative dose rate is applied, and therefore how to interpret and compare data produced using accelerated test methods.

1.1.2 Influence of radiation on corrosion in repository environments

Throughout this report, the process by which corrosion occurs in the presence of gamma radiation and is influenced by gamma radiation induced radiolysis of the local electrolyte will be referred to by the general term radiation induced corrosion (RIC). Given that corrosion of waste canisters under anticipated disposal conditions will proceed in the absence of radiation, the term radiation assisted corrosion (RAC) may be a more accurate description of the process. However, RAC more typically is used in relation to mechanisms that also involve neutron radiation effects that can influence a material's corrosion or stress corrosion cracking resistance due to alteration of the microstructure [3, 4]. Hence, RIC is referred to here to maintain consistency with the body of literature reporting on the influence of gamma radiation on the corrosion of candidate canister materials for the disposal of radioactive waste due to radiolysis of the local electrolyte [1, 5-10]. Such processes could include the direct influence of radiolytically generated redox species on the corrosion rate, but also indirect processes such as an alteration in the structure and or chemistry of the corrosion product, which could influence the rate of attenuation of corrosion.

In the case of copper corrosion, it has been proposed that the influence of radiation on corrosion will be dominated by the dose rate as opposed to the total dose, due to its influence on the concentration of radiolytic species and the corrosion potential E_{corr} [1]. In simple, dilute groundwater, the predominant oxidants arising from radiolysis are anticipated to be $OH^\bullet$, O_2^-, H_2O_2 and O_2 and the main reducing species would be $H^\bullet$ $e^-_{(aq)}$ and H_2, whereas, in the presence of chloride ions, ClO^-, ClO_2^-, ClO_3^-, ClO_4^-,Cl_2^- and Cl_2 could also be formed [11]. Previously it has been claimed that for copper corrosion under disposal conditions, O_2 and H_2O_2 are the main oxidants that should be considered owing to their higher concentration than the oxychloride species [12]. Elsewhere, it has been stated that H_2O_2 does not oxidise copper directly but forms molecular oxygen due to catalytic decomposition at the oxide surface [13]. However, it should be considered that modelling of the speciation of groundwater under radiolysis is complex, leading to a high number of chemical reactions that increases considerably when the number of species within the ground water is also increased [14]. Hence, for a real system or a more complex groundwater chemistry (e.g., including sulphur species) it is not yet certain what redox species will dominate the behaviour of the system. In general, in deaerated conditions for dose rates in the range expected at a canister surface (0 to 25 Gy h^{-1} [15, 16]) and total doses up to 100 kGy, the corrosion rate is lower than in the presence of radiation [1]. This inhibitory effect was observed for copper exposed to 0.1 M NaCl [17], groundwater [17] and standard Canadian shield saline solution [18]. Instances in which an enhancement of the corrosion rate was observed were in the presence of $NaNO_3$ and Na_2SO_4 + Fe_2SiO_4 [17], which presumably leads to the formation of additional redox species beyond those considered above. Elsewhere, the RIC of copper in deaerated deionised water was assessed over much higher dose rates of 80 to 770 Gy h^{-1}, which far exceed those anticipated at a container surface in a GDF [7]. It was found that radiation led to a substantial increase in the amount of soluble copper in solution for total doses exceeding 74 kGy, with further increases observed at higher total doses. A dose rate effect was also observed, whereby a greater amount of copper in solution was observed when the total dose was achieved by using a lower dose rate for a longer duration [7]. Comparable observations have been made when modelling the RIC of copper in both pure water and water containing 10^{-4} M HCO_3^- over a range of dose rates from 0.18 to 180 Gy h^{-1}. The model predicted a greater corrosion loss for a given total dose when the dose is achieved via a lower dose rate, which is due to the sublinear dependence of corrosion rate on dose rate. It should be noted that the aforementioned model did not include an attenuation in corrosion rate due to formation of protective films or any other kinetic limitation, which would diminish the impact of increasing duration/total dose on corrosion loss.

For carbon steel, H_2O_2 is considered to be one of the dominant oxidants that influences the corrosion rate during radiolysis of water in deaerated conditions [5, 19]. The concentration of H_2O_2 was found to have a strong influence on E_{corr} in the region where the potential is governed by the anodic half reaction of the carbon steel and the cathodic half reaction for formation of OH^- from H_2O_2 [5, 19]. The influence of radiation dose rate on corrosion has been studied for carbon steel and other ferrous materials such as iron and low alloy steel in a

EURAD (Deliverable n° 15.7) – Elucidation of critical irradiation parameter
Dissemination level: Public
Date of issue of this report: 06/02/2024

Page 16

range of different solutions including concentrated brines and various groundwater chemistries. For dose rates between 0 to 10^6 R h^{-1} (~0 to 10^4 Gy h^{-1} in water), a range of behaviours have been observed in different solutions. In seawater a higher dose rate led to a higher corrosion rate at each dose rate investigated [20], whereas, in some concentrated brines that exhibited high corrosion rates in the absence of radiation (10's μm yr^{-1}), little or no influence of radiation was observed up to dose rates of 10^3 R h^{-1} (~10 Gy h^{-1}) [21-23]. Where dose rate effects were observed, the effect on corrosion rate under increasing dose rate was sublinear [11, 20]. It has been shown that in the presence of a high dose rate of ~6.2 kGy h^{-1} the corrosion potential of carbon steel in a 0.01 M borate buffer increased from ~ -650 mV$_{SCE}$ to ~0 mV$_{SCE}$ within a few hours, and led to a change in the surface oxide from predominantly Fe_3O_4 to one containing both Fe_3O_4 and γ -Fe_2O_3 [5]. In ambient, deaerated water at a dose rate of 50 Gy h^{-1}, radiation was found to cause a slight inhibition of corrosion up to a total dose of 18 to 20 kGy, but it was proposed that over longer durations radiolytic species in solution could deteriorate the protective magnetite layer leading to an increase in corrosion rate [24]. At a higher dose rate of 0.55 kGy h^{-1} and at a higher temperature of 100 °C, radiation caused the corrosion rate of carbon steel in deaerated water to increase by approximately 6 times over exposure periods of 300-900 hours [25]. In the presence of Gaomiaozi bentonite containing 17% Beishan groundwater, radiation at a dose rate of ~3 kGy h^{-1}, was found to increase the corrosion rate of carbon steel by roughly a third when tested up to a total dose of 3 MGy. The presence of radiation also led to changes in the chemistry of the corrosion product, namely the additional formation of siderite and maghemite, whereas previously only magnetite, hematite and goethite were formed [2]. Elsewhere an increase in corrosion rate was observed in Allard ground water and bentonite equilibrated groundwater at dose rates of 11 Gy h^{-1} and 300 Gy h^{-1}. However, at the lower dose rate the corrosion rate tended towards that observed in the absence of radiation at longer durations (2000 hour) and was ascribed to the formation of a protective oxide. At the higher dose rate of 300 Gy h^{-1} the corrosion rate was 0.8 μm yr^{-1} after an exposure duration of 5000 hours, compared to 0.05 μm yr^{-1} in unirradiated conditions [26].

Overall, the influence of radiolysis on corrosion is complex and influenced by a multitude of factors including the material, the solution chemistry, the environmental conditions, the radiation dose rate and the total dose. Furthermore, assessing the relative impact of radiation in different environments is complicated by the tendency for authors to report the influence of radiation as the increase in corrosion rate relative to unirradiated conditions. This can lead to some confusion due to the wide variety in corrosion rates observed in unirradiated conditions arising from the different test conditions. For both copper and steel, dose rates in the range of those anticipated at a container surface in a GDF have in some instances been reported to reduce the corrosion rates due to the influence of radiation on the chemistry of the corrosion product [16]. Typically, substantial increases in corrosion rate are only observed at higher dose rates beyond those expected at canister surfaces in a GDF, and were observed for total doses that were close to, or lower than those anticipated over a canister lifetime. Where a dose dependent increase in corrosion was observed, the effect was usually sublinear, requiring a substantial increase in dose rate to cause a modest increase in corrosion rate.

1.2 Aim and motivation

The motivation for this work is the need to determine whether a specific corrosion allowance is required to address a possible increase in waste container corrosion loss owing to the presence of radiolysis products at the canister surface. If such an allowance is required, there is also a need to determine how it should be quantified for canisters exposed to different radiation doses and dose rates.

The aim of this work is to investigate and elucidate the influence of gamma radiation on the corrosion rate of carbon steel and copper in a range of conditions. This includes conditions that simulate those anticipated within a GDF, as well as conditions that extend beyond those expected e.g. higher dose rates. It is intended that the data provided will help to underpin future safety assessments of the corrosion processes occurring at a container surface within a GDF.

EURAD (Deliverable n° 15.7) – Elucidation of critical irradiation parameter
Dissemination level: Public
Date of issue of this report: 06/02/2024

Page 17

1.3 Structure of the report

This report comprises results from thee independent sets of experiments performed by two separate organisations (Jacobs and UJV) within the Task 3 group in ConCorD. Given that the methodology and design of these experiments are quite different from one another, they are initially discussed in isolation of the other parallel studies as follows:

- Jacobs experiments – Sections 2, 3 and 4
- UJV experiments – Sections 5, 6 and 7

The findings from the independent experiments are then discussed as an ensemble in Section 8 along with the results of other radiation corrosion experiments performed within Task 3 that are reported in Deliverable 15.8 [27].

1.4 Summary of the different experiments

A high-level summary of the different experiments performed by Jacobs and UJV is provided in Table 1-1.

Table 1-1. High-level summary of the experiments described in this report.

Organisation	Type of experiment	Environment	Material	Durations (h)	Dose rates (Gy h^{-1})	Total doses (kGy)
Jacobs	exposure testing	simulated porewater (0.1 M NaCl + 0.2 M NaHCO$_3$)	copper carbon steel	1 to 10000	0 to 1000	0 to 100
UJV	exposure testing	MX-80 bentonite BCV bentonite	carbon steel	4380 to 13140	0 and 0.4	0 to 5.256

2. Methodology for tests performed by Jacobs

2.1 Overview

The Jacobs testing program involves corrosion testing by exposure to a simulated bentonite porewater solution for different durations over a wide range of dose rates, some of which far exceed those anticipated at a container surface in a GDF. The reason for selecting such conditions is to attempt to discern the underlying mechanisms that govern the key corrosion processes under radiation, rather than to try to quantify specific corrosion rates for repository conditions. The key is to elicit the overall trends in the data which are easier to resolve when using a model solution and a very wide range of test conditions than when focussing in on a precise range of highly representative environments.

2.2 Test specimens

Carbon steel (CS), wrought copper (WC), and cold-sprayed copper (CSC) specimens of dimensions 50.0 mm x 2.0 mm x 1.2 mm were prepared by electrical discharge machining (EDM). To remove any surface material deposited by the EDM process, all specimens were ground using a Metaserv universal rotary. Specimens were adhered to glass microscope slides using a Cyanoacrylate based super glue (supplied by RS) and mounted

EURAD (Deliverable n° 15.7) – Elucidation of critical irradiation parameter
Dissemination level: Public
Date of issue of this report: 06/02/2024

Page 18

on a microscopy glass slide holder (Figure 2-1). Surfaces were ground until parallel concentric grinding marks were observed, rotated 180°, and ground again in the opposite direction. This process was repeated with P320[1] and P1200 (600 grit) silicon carbide grinding paper. After grinding all samples were ultrasonicated in acetone for 20 minutes followed by a static 24 hours immersion in acetone before drying under vacuum.
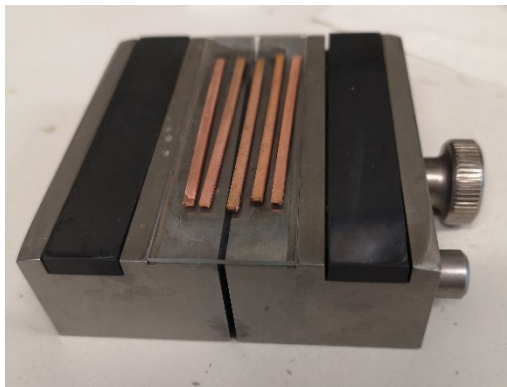
Figure 2-1. Wrought copper specimens adhered to a glass microscope slide and mounted in a microscope slide holder.

The dimensions of all specimens were measured with a micrometre to allow for nominal corrosion rate calculations by mass loss. The width and thickness were measured at thee equally spaced positions along the specimen and the length was measured three times at the same position. All specimens were weighed three times on an Ohaus Explorer balance whilst exposed to laboratory atmosphere for 60 minutes.

2.3 Solution preparation

A one litre solution of 0.1 M NaCl in deionised water was sparged with argon gas for 2 hours (flow rate 100 mL min^{-1}) then transferred into an argon glovebox. The NaCl solution was added to approximately 16.8 g of NaHCO$_3$ equating to a NaHCO$_3$ concentration of 0.2 M. The solution was then sealed and stirred for ten minutes with a magnetic stirrer.

An airtight seal was attained on the solution container with a plastic screw cap and a circular nitrile membrane to maintain a steady pH by preventing loss of evolved CO$_2$. Two holes were punched though the nitril membrane to insert a pH probe and a metal outlet tube fitted with a compression fitting. This allowed for pH measurements and the removal of the buffer solution whilst maintaining the airtight seal. The pH of the buffer solution was measured following ten minutes of stirring, after which aliquots of solution were drawn up though the outlet tube and transferred to the assembled ampoules (see Section 2.4). When drawing up solution, an open-ended needle was inserted though the nitrile seal to allow argon gas from the glovebox atmosphere to enter the sealed glass bottle. The initial pH of the buffer solution was 8.0 for all tests; pH 8 was selected to be close to that anticipated in bentonite, but also low enough to not cause passivation of the copper, chloride was added to further reduce the chance of copper passivation.

2.4 Assembly

The experimental configuration comprised a quartz glass ampoule which housed an inner glass carousel that could support up to six individual samples. The ampoules were assembled in an anoxic argon glovebox and was partly filled with test solution to give a fixed liquid to ullage volume ratio. The ampoules were sealed using a polyurethane radiation tolerant adhesive. Two different ampoule designs were employed in this experiment. All 10000 h samples and two ampoules exposed for 5000 h (carbon steel and wrought copper ampoules at 0.2 Gy h^{-1} dose rate) used Design One. All other experiments employed ampoule Design Two. The use of two different designs was a necessity owing to the limited availability of components to make enough experimental

---

[1] No American National Standards Institute (ANSI) equivalent exists for P320 but it is greater than 240 grit and less than 280 grit.

EURAD (Deliverable n° 15.7) – Elucidation of critical irradiation parameter
Dissemination level: Public
Date of issue of this report: 06/02/2024

Page 19

cells using Design One. As a consequence, Design Two was aimed to be as similar to Design One as possible using the alternative components that were available.

Ampoule Design One had a tall, open-ended neck offset to one side (see Figure 2-2). The neck of the outer ampoule was sealed with polyurethane adhesive and allowed to cure for a minimum of 60 seconds. Once the adhesive in the neck had cured, a quartz glass cap was filled with polyurethane adhesive and pressed over the neck of the outer ampoule (see Figure 2-3). This ensured the ampoule was properly sealed and provided a long diffusion path to limit oxygen ingress via diffusion though the adhesive. The carousel used in this design comprised six equally spaced glass tubes that were fixed together in a hexagonal arrangement. The carousel was raised off the base of the outer ampoule by approximately 3 mm, using glass beads, to allow mass transport between the bottom openings of the six tubes and the bulk solution within the rest of the ampoule.

Instead of a sealed long neck, ampoule Design Two had a tapered ground glass joint and a glass stopper that was sealed shut using the same polyurethane radiation tolerant adhesive (see Figure 2-4). The inner carousel in Design Two comprised six separate glass tubes arranged into a ring by positioning them around a 12 mm diameter central glass cylinder and were raised off the base of the ampoule by approximately 5 mm using a glass disc (see Figure 2-4b).

In each of the designs, one metal test sample was placed into each of the six glass cylinders. Ampoules were loaded with one of the following arrangements: 6 x CS, 6 x WC, or 4 x WC plus 2 x CSC. To ensure that the design of the cell prevented the ingress of oxygen, the concentration of oxygen within the longest exposure duration ampoules was measured using an oxygen sensor placed on the inside of the ampoule (see Figure 2-2a)[2].

A buffer solution of 0.2 M sodium hydrogen carbonate and 0.1 M sodium chloride in deaerated, deionised water was used in all assembled test cells (see Section 2.3 above). After the test specimens were placed in the glass tubes in each carousel, the buffer solution was added until all specimens were submerged. Ampoule Design One had a total volume of 56 mL of which approximately 46 mL was filled with buffer solution giving a solution : ullage volume ratio of 4.6 : 1. Ampoule Design Two had a total volume of 109 mL of which approximately 60 mL was filled with solution giving a solution : ullage volume ratio of 1.2 : 1.

Although the solution : ullage volume ratio differs between the two ampoule designs[3] it is not expected to significantly alter the equilibrium concentration of radiolytically generated species. However, the proportionately larger ullage of Ampoule Design Two is expected to increase the time taken to reach equilibrium. These points are discussed further in Section 2.7 and Section 3.3.

All samples were designated with unique sample codes based on the nomenclature VV W – X #Y Z, where:

VV = CS (carbon steel), WC (wrought copper) or CSC (cold-sprayed copper) and indicates the sample material

W = 1 – 6 and indicates the immersion duration where 1 = 1 hour and 6 = 10000 hours

X = 1 – 9 and indicates the exposure dose rate where 1 = 0 Gy h^{-1} and 9 = 1000 Gy h^{-1}.

#Y = #1 - #6 and indicate each replica ribbon in the ampoule

Z = A, B, C, or D which is only given to sub-sectioned samples for spectroscopic analysis (see Section 2.6.1) and indicates each sub-section.

---

[2] The oxygen sensors work via fluorescence decay and can be operated through glass.
[3] This was unavoidable based on the geometry of ampoule Two and the lack of available alternatives.

EURAD (Deliverable n° 15.7) – Elucidation of critical irradiation parameter
Dissemination level: Public
Date of issue of this report: 06/02/2024

Page 20
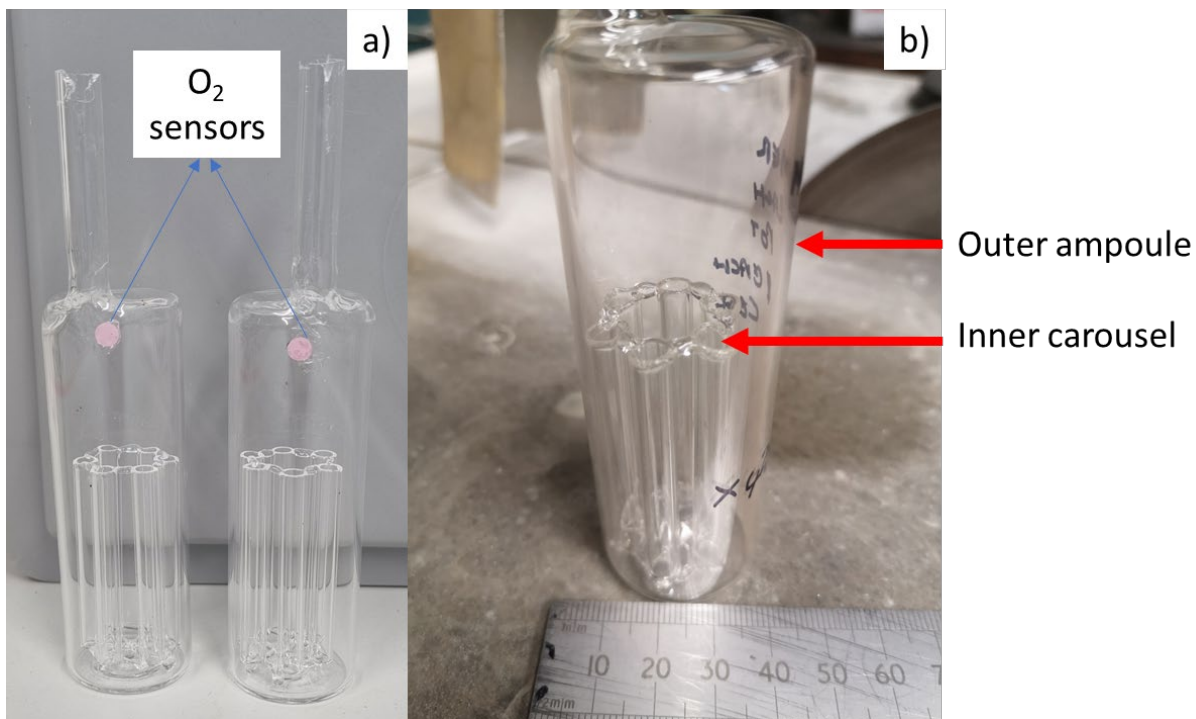
Figure 2-2. Ampoule Design One, a) empty ampoules with O$_2$ sensor spots shown b) empty ampoule with inner carousel highlighted.

Figure 2-3. Ampoules 25 and 26 (Design One) with carbon steel and wrought copper specimens/cold-sprayed copper specimens immersed in the buffer solution.

EURAD (Deliverable n° 15.7) – Elucidation of critical irradiation parameter
Dissemination level: Public
Date of issue of this report: 06/02/2024

Page 21
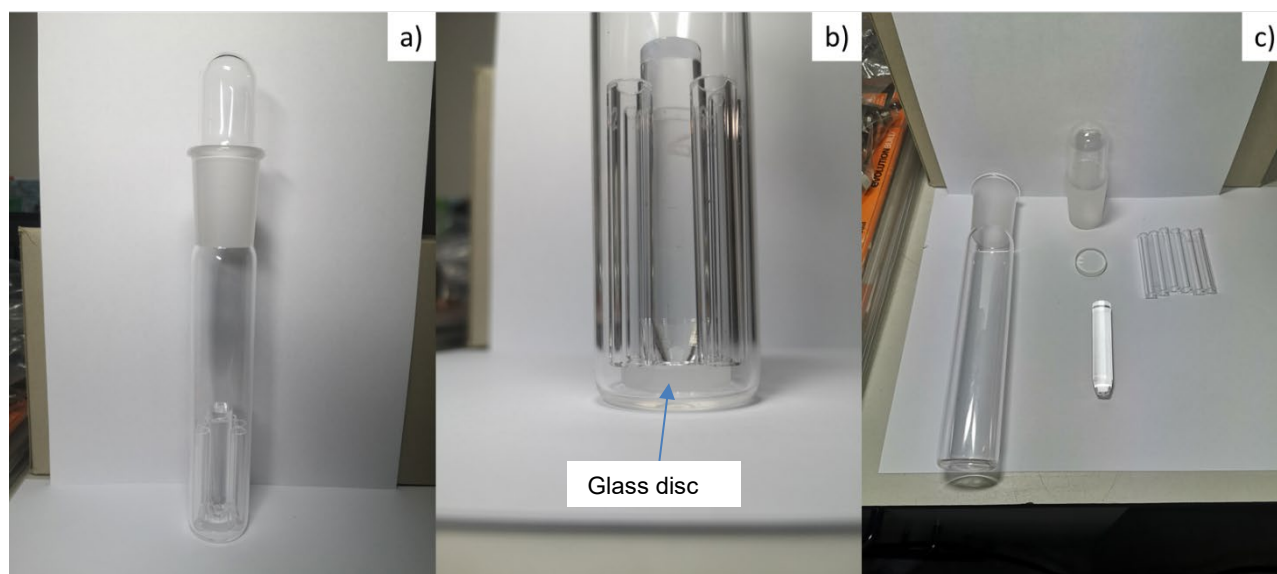
Figure 2-4. Ampoule Design Two, a) empty ampoule b) empty inner carousel c) unassembled individual components of the ampoule.

2.5 Irradiation

Ampoules were irradiated with gamma radiation from a ^{60}Co source at the Harwell Irradiation Facility, Harwell, Oxfordshire. Dosimetry measurements were taken to determine the locations with dose rates ranging from 0.1 to 1000 Gy h^{-1}. A variety of different dose rates and exposure durations were calculated to achieve total dosages of 1, 10 and 100 kGy. The matrix detailing all dose rates, exposure durations and total dosages is shown in Table 2-1.

Ampoules exposed for 1, 100 and 1000 h were rotated 180° halfway through their exposure duration to ensure all sample positions were exposed to equal total gamma radiation dosages. Ampoules exposed for 5000 and 10000 h were rotated once a month throughout their exposure duration. Ampoules exposed for 10 h were exposed overnight and therefore were not rotated halfway through their exposure period. Due to other facility users accessing the radiation facility, the ^{60}Co sources were periodically removed resulting in periods of unirradiated "downtime". Because of downtime, the total duration of exposure of each test cell is greater than the period of exposure to radiation. The radiation exposure period is the total time the irradiated ampoules were exposed to gamma radiation from the ^{60}Co source. The total exposure period is the duration between emplacement and final removal from the radiation facility.

The radiation exposure duration was set to equal the nominal exposure duration outlined in Table 2-2 below, therefore the immersion exposure period was larger as it included the periods of downtime in which the cells were not exposed to radiation. Instances of downtime were on average 76 minutes, and typically not more than a couple of hours with the exception of one instance during the exposure period of 5000 and 10000 h samples, where irradiation was stopped for 24 days for annual facility maintenance. In addition to the unirradiated "downtime", samples were also exposed to the buffer solution in the absence of radiation whilst in transit to and from the glovebox and radiation facility during assembly and dismantling. This equated to approximately 90 to 120 minutes of additional unirradiated solution exposure for all ampoules (including unirradiated control samples). Throughout this report the nominal radiation exposure durations will be referenced when referring to exposure durations of different samples.

EURAD (Deliverable n° 15.7) – Elucidation of critical irradiation parameter
Dissemination level: Public
Date of issue of this report: 06/02/2024

Page 22

Table 2-1. Matrix detailing the combination of dose rates and exposure durations for all ampoules. Numbers 0, 1, 10 and 100 in bold denote the total radiation dosage received in kGy by ampoules containing carbon steel (CS), wrought copper (WC) or cold-sprayed copper (CSC) specimens. Note. Where cold-sprayed copper (CSC) is listed, cold-sprayed copper specimens replaced two out of the six wrought copper specimens in the same ampoule.

Exposure Duration (h)	Dose Rate (Gy h^{-1})								
	0.0	0.1	0.2	1	2	10	20	100	1000
1	**0** (CS, WC)								**1** (CS)
14	**0** (CS, WC)							**1** (CS)	**10** (CS)
100	**0** (CS, WC-CSC)					**1** (CS, WC-CSC)		**10** (CS, WC-CSC)	**100** (CS)
1000	**0** (CS, WC-CSC)			**1** (CS, WC-CSC)		**10** (CS, WC-CSC)		**100** (CS, WC)	
5000	**0** (CS, WC)		**1** (CS, WC-CSC)		**10** (CS)		**100** (CS)		
10000	**0** (CS, WC)	**1** (CS, WC)		**10** (CS, WC)		**100** (CS, WC)			

Table 2-2. Nominal exposure durations with the corresponding actual radiation exposure and total immersion durations. Note the significantly larger difference for 5000 and 10000 h duration samples was due to annual maintenance of the radiation facility which resulted in an additional 24 days of downtime for these samples.

Nominal duration (h)	Irradiation exposure (hh:mm)	Total Immersion (hh:mm)	Difference (hh:mm)
1	01:00	01:02	00:02
14	14:10	14:10	00:00
100	114:07	114:27	00:20
1000	998:00	1024:00	26:00
5000	5001:00	5780:00	779:00
10000	10001:00	11058:00	1054:00

2.6 Disassembly and post-test analysis

2.6.1 Disassembly

After the samples had reached their target immersion durations/radiation dosages, test cells were transferred to a glovebox where they were photographed before being dismantled. A line was scored/etched into the rim of the ampoule along its circumference. The glass along the scored line was fractured by tapping with a hammer allowing separation of the lid/ground cone from the base of the ampoule. The pH of the buffer solution was recorded immediately after fracturing and the reading was taken approximately 60 seconds after the probe was immersed in the solution. For tests with copper specimens, the pH at the end of the test was between 8.0 and 8.2. For steel tests, a greater increase in pH was observed, reaching values of between 8.5 and 8.7 following exposures of 5000 and 10000 hours. Note that the ampoule design (namely Design One or Design Two) did not influence the measured pH at the end of the test. Following pH measurements, specimens were removed from the inner carousel using tweezers.

Once removed from the buffer solution, specimens were individually immersed in deaerated, deionised water for approximately 20 s followed by light swirling for an additional 20 s. After immersion in water, the specimens were transferred to individual beakers of methanol where they were lightly swirled for 40 s. After methanol immersion, the specimens were dried under vacuum for a minimum of ten minutes. Once dry the specimens were photographed whilst still in the glovebox and sealed in argon filled Mylar bags until analysed as described in the following subsections.

Once dry, the samples designated for spectroscopic analysis were wrapped in aluminium foil and sectioned into quarters with a junior hacksaw. Aluminium foil was used to minimise the redeposition of sawing swarf on the samples' surfaces. All samples were rinsed in methanol once sectioned to remove any traces of swarf remaining. Each sample section was given a unique code as detailed in Section 2.4.

2.6.2 Mass loss

To calculate the average corrosion rate of the specimens, mass loss measurements were carried out on each specimen in accordance with procedure ASTM G1 [28], as summarised below:

EURAD (Deliverable n° 15.7) – Elucidation of critical irradiation parameter
Dissemination level: Public
Date of issue of this report: 06/02/2024

Page 24

1. Prior to assembly of the ampoules, all the specimens were weighed and their initial mass was designated as M_0.
2. After dismantling, the specimens were descaled in the selected descaling reagents, which were chosen for the two test materials as follows:
   - Carbon steel: 0.5 w/v% dibutyl thiourea in 18.5 w/v% hydrochloric acid for 5 minutes under sonication.
   - Wrought copper: 18% w/v deaerated hydrochloric acid for two minutes.
3. The specimens were then cleaned as follows:
   - Rinsed three times in deionised water.
   - Sonicated for five minutes in deionised water.
   - Sonicated for five minutes in methanol.
   - Vacuum dried for five minutes.
4. The specimens were reweighed (giving mass, M_1).
5. To account for possible weight loss due to dissolution of metal during the determination of M_1, and assuming all corrosion products had been removed at this point, steps 2-4 were then repeated twice for carbon steel and four more times for wrought copper. These additional measurements were designated M_2 and M_3 for carbon steel, and M_2 to M_5 for wrought copper.

The mass loss due to corrosion of the metal coupons was calculated by determining the y-intercept of the plot of mass loss versus cleaning cycle number, as per the methodology described in ASTM G1 [28]. The mass loss measurements were carried out for carbon steel samples from all exposure conditions and all wrought copper samples exposed for 10000 h. The radiation exposure duration (see section 2.5 and Table 2-2) was used as the exposure duration for corrosion rate calculation purposes.

2.6.3 Visual inspections

Photos of all samples pre- and post-exposure were taken with a Canon SX740 HS digital camera. Unique features on a select number of specimens post-exposure were imaged with a Opti-Tekscope Digital Microscope with a maximum magnification of x200.

2.6.4 Surface SEM-EDX

The surfaces of five carbon steel and two wrought copper samples were examined using scanning electron microscopy (SEM) and energy dispersive X-ray (EDX) analysis. A JEOL 6480 LV SEM equipped with an Oxford Instruments X-MAX80 SD X-ray detector and INCA X-ray analysis system was used to image the samples and perform the analysis using EDX. EDX analyses the characteristic X-rays produced by the interaction between the primary electron beam and the sample. The technique identifies all elements present with atomic numbers of five (i.e., boron) and greater, with a detection limit of approximately 0.1 weight %. The measurements are semi-quantitative. An accelerating voltage of 15-20 kV was used for imaging, mapping and point analysis.

2.6.5 SEM-EDX in cross-section

The surfaces of 11 carbon steel and four wrought copper samples were analysed in cross-section using SEM with EDX (X-SEM). Each sample was mounted as received into epoxy resin. The set resin block was then cross-sectioned using a hand saw and one half of the cross section was re-potted and mounted in further epoxy resin. The face of the cross section was then ground and polished flat. Prior to SEM-EDX analysis the sample was carbon coated to enhance the conductivity of any non-conducting materials. At each step, limited exposure to air and water was ensured and the samples were kept under vacuum between steps. EDX analysis of cross sectioned samples were collected with the same instrument parameters as the surface SEM-EDX analysis described above.

2.6.6 Raman spectroscopy

Raman spectroscopy was used to investigate the surface chemistry of carbon steel and wrought copper samples. The fingerprint Raman spectrum for the corrosion product can be used to identify corrosion

EURAD (Deliverable n° 15.7) – Elucidation of critical irradiation parameter
Dissemination level: Public
Date of issue of this report: 06/02/2024

Page 25

products to a high lateral resolution. Samples were analysed using a Horiba JY LabRam Aramis confocal Raman microscope. The exciting laser wavelength used was 532 nm. A x50 extra-long working distance objective lens was used to collect the 180° backscattered light. The specimens were loaded into sample holders inside an argon-purged glovebox and held in place using Menzel Gläser cover slips attached to the sample holders using Araldite® adhesive. This ensured that the specimens were not exposed to air before or during the analyses.

2.6.7 XPS

X-ray photoelectron spectroscopy (XPS) was used to investigate the surface chemistry of corroded metal specimens. Chemical state information obtained though peak fitting procedures can help identify the oxidation state of metal species and specific functional groups present. The surfaces of thee carbon steel and one wrought copper sample were analysed using XPS and ion beam depth profiling, to determine the surface composition and the oxidation state of the predominant species.

Samples were analysed using a Thermo Scientific K-Alpha XPS instrument equipped with a microfocussed, monochromated Al Kα X-ray source. The source was operated at 12 keV and a 400 μm (radial) spot size was used. The analyser operates at a constant analyser energy of 200 eV for wide binding energy survey scans and 50 eV for narrow binding energy detailed scans.

The data acquisition and analysis were performed with Casa XPS analytical software. Peak fitting (Lorentzian / Gaussian (L/G) 30%) was applied following removal of a Sherly background. Normalised atomic percentages were determined from the peak areas of the elemental main peaks detected on the survey scan following background subtraction and application of 'Wagner' sensitivity factors. Depth profiling was achieved using 2 kV Ar$^+$ ions at the medium current setting. Profiles were obtained in 15 steps with 20 seconds ion bombardment per step for a total of 300 s. Each sample was analysed in thee locations and depth profiled in one. Both wide binding energy and detailed scans were undertaken after each depth profiling step.

2.7 Radiolysis modelling

In support of the laboratory tests performed by Jacobs, Amphos 21 performed modelling to calculate the steady state concentrations of select radiolytically generated species (i.e., O_2, H_2O_2 and H_2). It has been shown that the presence of chloride impacts the concentrations of other radiolytically generated species and is therefore a key component to consider [12]. Therefore, the radiolysis model combines the generation of water and chloride radiolysis products into a single system which is implemented in COMSOL [29-31]. The model considered the radiolysis of a solution of 0.1 M NaCl up to 1,000 hours at ambient temperature in the absence of interfacial reactions including corrosion, with partition between gaseous and aqueous phases as per the design of the Jacobs experimental cells. Key differences between the experimental environment and the modelled system are the exclusion of NaHCO$_3$ from the modelled solution, and the exclusion of coupled interfacial reactions. For this reason, the model is used only to give a broad indication of equilibrium concentrations and rates of generation of O_2 and H_2 in the bulk solution and estimates of bounding corrosion rates based on mass balance with these oxidants.

3.   Results of tests performed by Jacobs

3.1 Summary of analysis

An outline of the spectroscopic analysis carried out on carbon steel and wrought copper samples is detailed in Table 3-1 and Table 3-2, respectively. Note only visual inspections were carried out on cold-sprayed copper samples. Mass loss measurements were carried out on all carbon steel samples and all wrought copper samples exposed for 10000 h and results are presented in Section 3.2. Images taken of all samples pre- and post-exposure are shown in Section 3.4.

EURAD (Deliverable n° 15.7) – Elucidation of critical irradiation parameter
Dissemination level: Public
Date of issue of this report: 06/02/2024

Page 26

Table 3-1. Outline of the spectroscopic analysis carried out on carbon steel specimens presented in this report. The total dose received in each condition is highlighted in bold. Note, X-SEM = cross-section SEM analysis.

Exposure Duration (h)	Dose Rate (Gy h^{-1})								
	0.0	0.1	0.2	1	2	10	20	100	1000
1									**1 kGy** X-SEM
14								**1 kGy** X-SEM	**10 kGy** X-SEM
100	**0 kGy** X-SEM					**1 kGy** X-SEM SEM Raman XPS		**10 kGy** X-SEM SEM Raman XPS	**100 kGy** X-SEM SEM Raman XPS
1000									
5000	**0 kGy** X-SEM		**1 kGy** X-SEM SEM Raman		**10 kGy** X-SEM SEM Raman		**100 kGy** X-SEM		
10000									

Table 3-2. Outline of the spectroscopic analysis carried out on wrought copper specimens presented in this report. The total dose received in each condition is highlighted in bold. Note, X-SEM = cross-section SEM analysis.

Exposure Duration (h)	Dose Rate (Gy h⁻¹)								
	0.0	0.1	0.2	1	2	10	20	100	1000
1									
10									
100	**0 kGy** X-SEM					**1 kGy** X-SEM SEM Raman XPS			
1000									
5000	**0 kGy** X-SEM		**1 kGy** X-SEM SEM Raman						
10000									

3.2 Mass loss

3.2.1 Copper

The corrosion rates for copper were determined from tests that were operated for 10000 hours, from triplicate specimens (the results for the unirradiated control test were acquired from quadruplet specimens). Average corrosion rates are listed in Table 3-3. In unirradiated conditions the average corrosion rate was just 0.02 μm yr^{-1}, which is consistent with the expectation that copper is largely immune to corrosion in unirradiated, anoxic solution at slightly alkaline pH. In irradiated conditions, the average corrosion rate exhibited a strong dose rate/total dose dependence from 0.1 to 10 Gy h^{-1} (1-100 kGy) as shown in Figure 3-1. Since the corrosion rates were only determined from tests conducted for 10000 hours, there is no indication of the trend in corrosion rate as a function of time. From Figure 3-1, although the average corrosion rate exhibits a strong dose rate/total dose dependence increasing from ~0.05 to 1.2 μm yr^{-1} from 0.1 to 10 Gy h^{-1}, this effect is sub-linear and decreases at the higher dose rates/total doses.
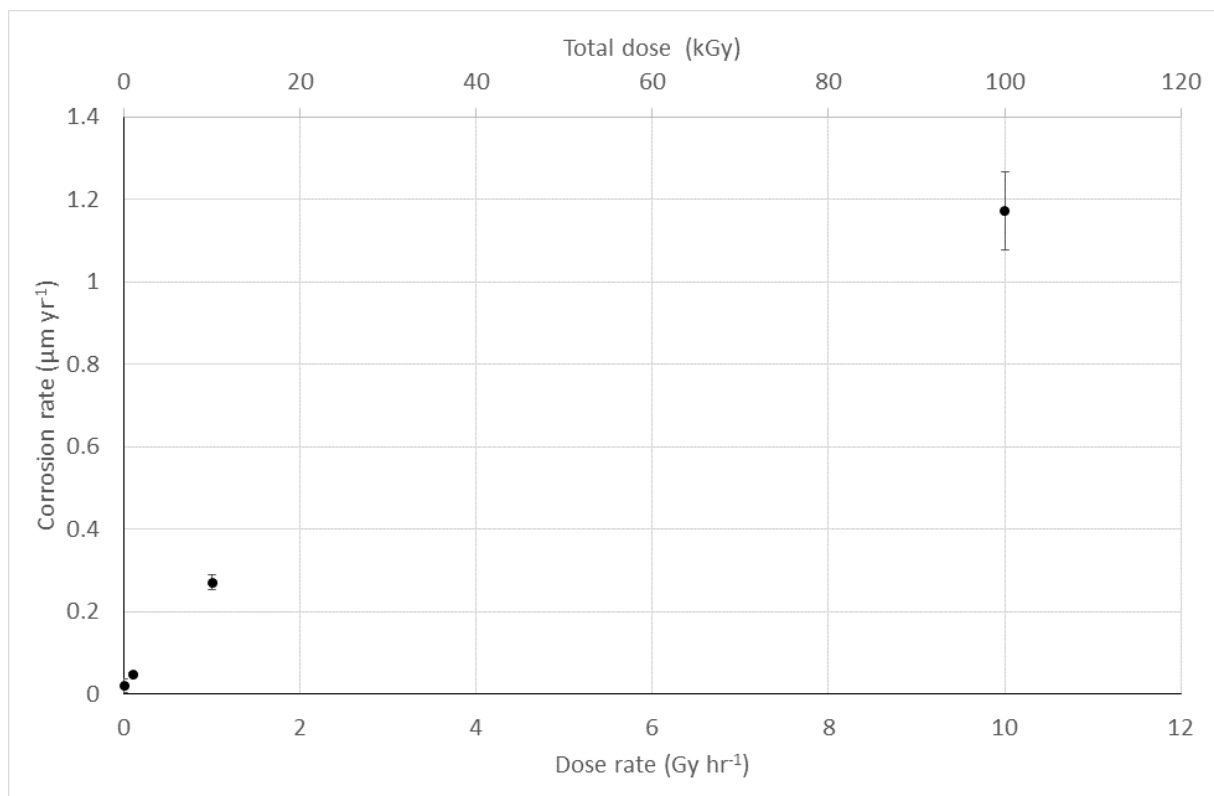
Figure 3-1. Copper average corrosion rate versus dose rate/total dose for tests operated for a duration of 10000 hours. Error bars indicate the standard deviation between different specimens within the same test.

EURAD (Deliverable n° 15.7) – Elucidation of critical irradiation parameter
Dissemination level: Public
Date of issue of this report: 06/02/2024

Page 29

Table 3-3. Average corrosion rate of wrought copper exposed for 10000 h. Standard deviation of repeat measurements in brackets.

Dose rate (Gy h^{-1})	Average corrosion rate (μm yr^{-1})
0	0.02 (0.02)
0.1	0.05 (<0.01)
1.0	0.27 (0.02)
10	1.17 (0.09)

3.2.2 Carbon steel

Carbon steel corrosion rates were determined from triplicate specimens except for the results from the unirradiated control test that was operated for 1 hour, and the test performed at a dose rate of 100 Gy h^{-1} that was operated for 14 hours, which had duplicate specimens. In unirradiated conditions, the magnitude of the thickness loss due to corrosion increased with time up to 5000 hours, after which no increase in thickness loss was observed (see dark red bars in Figure 3-2). From Figure 3-2, it can be seen that a smaller average thickness loss was observed on unirradiated specimens (dark red bar) after 10000 hours of exposure compared with 5000 hours. In practice, this is probably due to experimental error as there is no feasible way that the thickness loss could be lower after a longer duration. This perspective is supported by the large error on the measurements made at 10000 hours that indicate a maximum thickness loss comparable to that observed after 5000 hours. In most likelihood, these results indicate a high attenuation in instantaneous corrosion rate with time that reduces to below the uncertainty of measurement after 5000 hours of exposure.

Thickness loss due to corrosion was converted into average corrosion rate as shown on a log scale in Figure 3-4. In the absence of radiation, the corrosion rate decreases substantially with time, from an initial average corrosion rate of ~180 μm yr^{-1} in the first hour to less than 2 μm yr^{-1} after 10000 hours. The attenuation in corrosion rate approximately exhibits a power law decay but a good fit of the data could not be obtained for a simple decay equation of the form At^{-B} where t is time and A and B are constants. A rapid attenuation in corrosion rate was also observed in tests exposed to gamma radiation, except for results obtained at 1000 Gy h^{-1} between 14 and 100 hours of exposure, which indicated a possible increase in corrosion rate. For durations of exposure between 1000 and 10000 hours, the relative rate of attenuation in corrosion rate was similar between unirradiated samples and those irradiated at 1 and 10 Gy h^{-1}, with slightly lower rates of attenuation observed with increasing dose rates. Nevertheless, at 0, 1 and 10 Gy h^{-1} the increase in corrosion loss between 1000 and 10000 hours was less than 1 μm (Figure 3-2) indicating an average corrosion rate in this period of < 1 μm yr^{-1}.

For tests performed for durations of 5000 hours and longer, gamma radiation at dose rates greater than or equal to 10 Gy h^{-1} significantly increased the amount of corrosion that took place. Whilst it appears that the average corrosion loss exhibits a monotonic dose rate dependence in the 10000 hour tests, this apparent trend is most likely attributable to random variation in the data. This is more evident when comparing the data from the tests performed for 5000 and 10000 hours. Whilst the mean corrosion loss at 1 Gy h^{-1} is greater than at 0 and 0.1 Gy h^{-1} after 10000 hours of exposure, the corrosion loss at 0 Gy h^{-1} measured after 5000 hours exposure is greater than all the losses measured at 10000 hours with the exception of the test at 10 Gy h^{-1}. For tests performed for a duration of 1000 hour, the corrosion loss was significantly greater at a dose rate of 100 Gy h^{-1}; at 10 Gy h^{-1} the mean corrosion loss was greater than in the absence of radiation, but the difference was within the repeatability of the measurements. Following 100 hours of exposure, a significant increase in corrosion rate was observed at 100 and

EURAD (Deliverable n° 15.7) – Elucidation of critical irradiation parameter
Dissemination level: Public
Date of issue of this report: 06/02/2024

Page 30

1000 Gy h^{-1} compared to the unirradiated control test. Whereas, at shorter durations there is no clear trend in the data, which could be partly due to the very low corrosion losses observed at short durations. Hence, we have placed a greater importance in the trends of the mass loss data obtained from the longer duration tests. The average corrosion rate is plotted versus dose rate as shown in Figure 3-5 for the full range of test conditions, and the same data is shown over the range of dose rates anticipated at the external surface of canisters in a GDF, see Figure 3-6 and is summarised in Table 3-4.

One can also compare the increases in corrosion relative to unirradiated controls as a function of total dose, as shown in Figure 3-3. Doing so for total dosages of 100 kGy showed dose rates of 10 Gy h^{-1} and above lead to a significant increase in corrosion loss compared to corresponding 0 Gy h^{-1} control samples. This corrosion loss threshold increased to a dose rate of 100 Gy h^{-1} when exposed to a total dose of 10 kGy. The difference in corrosion loss between controls and irradiated samples of the same dose rate increases with increasing total dose/exposure duration. The figure implies that the impact of radiation is greater for higher total doses. However, it must be noted that this impact could be related to the increased test duration, particularly since the corrosion rate is observed to shown rapid attenuation over time.

Compared with the amount of corrosion that takes place in unirradiated conditions the increase in corrosion due to radiation was fairly modest, with the exception of the results measured at 100 Gy h^{-1} for 14 hours. Even at a comparatively high dose rate of 10 Gy h^{-1} the average corrosion rate after 10000 hours was only 2.2 µm yr^{-1}, compared with an unirradiated rate over the same time period of 1.5 µm.yr^{-1}. Furthermore, the results indicate that the corrosion rate is expected to decrease further over longer durations of exposure. In some tests a lower corrosion rate was observed in the presence of radiation than in the corresponding control test. However, where this was observed the difference between the corrosion losses from irradiated tests and the unirradiated control test were within the range of repeatability of the measurement. The largest reduction in corrosion rate compared to the unirradiated control was observed at 1 Gy h^{-1} after 1000 hour duration of exposure, but at the same dose rate and a longer duration of 10000 hours this apparent inhibiting effect was not observed, indicating it was possibly due to random variation.

EURAD (Deliverable n° 15.7) – Elucidation of critical irradiation parameter
Dissemination level: Public
Date of issue of this report: 06/02/2024

Page 31
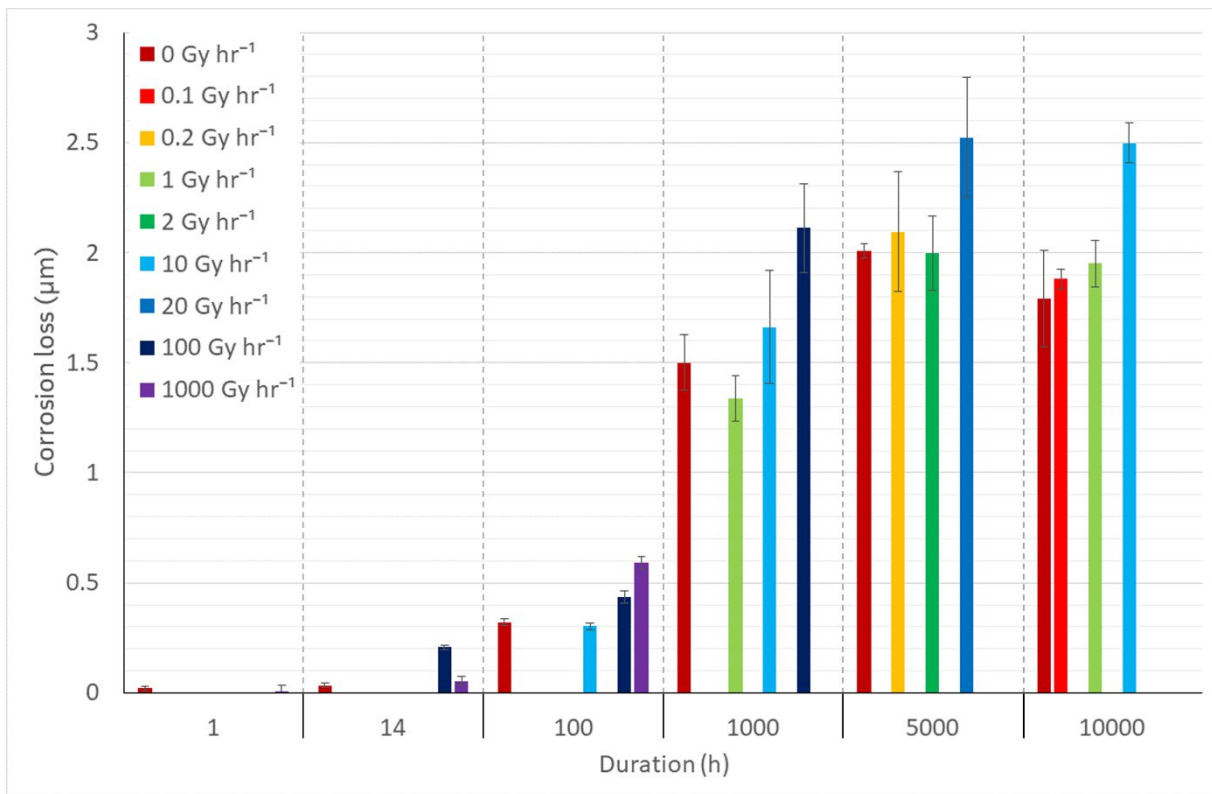
Figure 3-2. Thickness loss of carbon steel due to corrosion shown for each test duration (from 1 hour to 10000 hours) with dose rate increasing from left to right between 0 and 1000 Gy h^{-1}. Error bars indicate the standard deviation between different specimens within the same test.

EURAD (Deliverable n° 15.7) – Elucidation of critical irradiation parameter
Dissemination level: Public
Date of issue of this report: 06/02/2024

Page 32
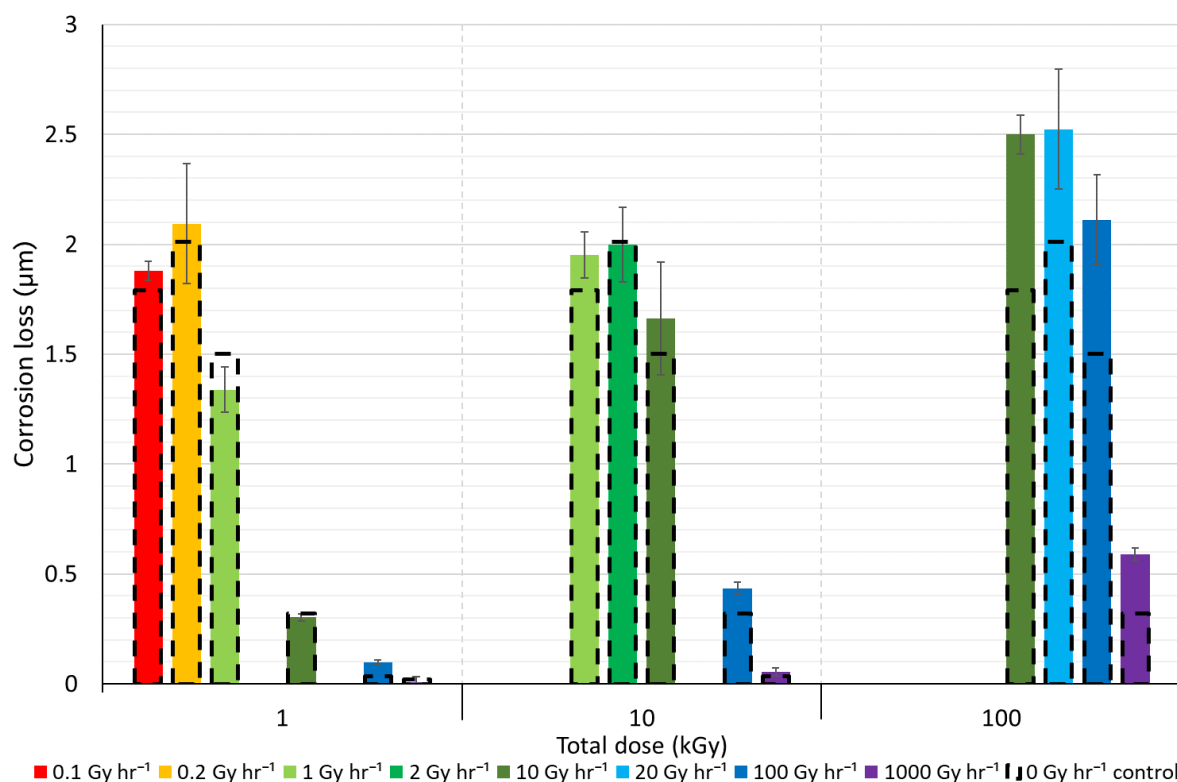
Figure 3-3. Thickness loss of carbon steel due to corrosion shown for each total dose (from 1 kGy to 100 kGy) with dose rate increasing from left to right between 0 and 1000 Gy hr^{-1}. Error bars indicate the standard deviation of irradiated samples between different specimens within the same test condition. Dotted columns indicate corrosion loss of corresponding control sample (0 Gy h^{-1}) at the same duration. Note, these results are from tests operated for durations between 1 and 10000 hours.

EURAD (Deliverable n° 15.7) – Elucidation of critical irradiation parameter
Dissemination level: Public
Date of issue of this report: 06/02/2024

Page 33
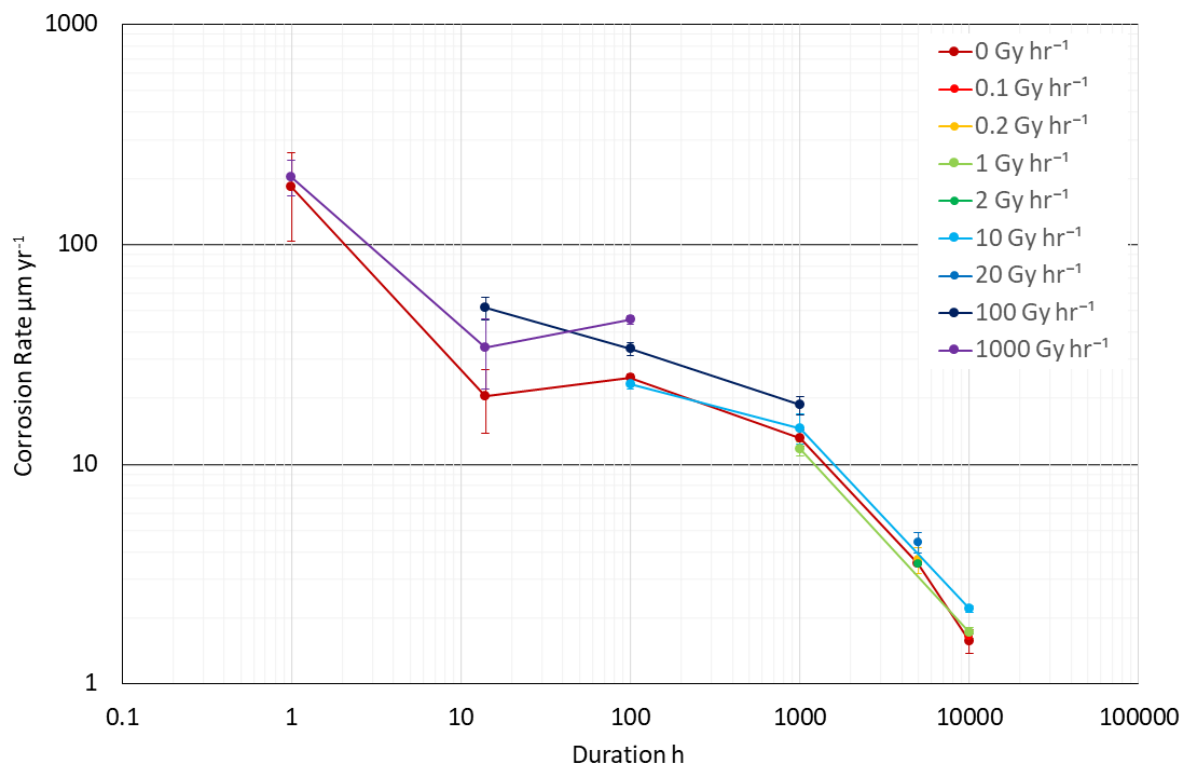
Figure 3-4. Change in carbon steel average corrosion rate versus time for dose rates between 0 to 1000 Gy h⁻¹ expressed on a log scale. Error bars indicate the standard deviation between different specimens within the same test.

EURAD (Deliverable n° 15.7) – Elucidation of critical irradiation parameter
Dissemination level: Public
Date of issue of this report: 06/02/2024

Page 34
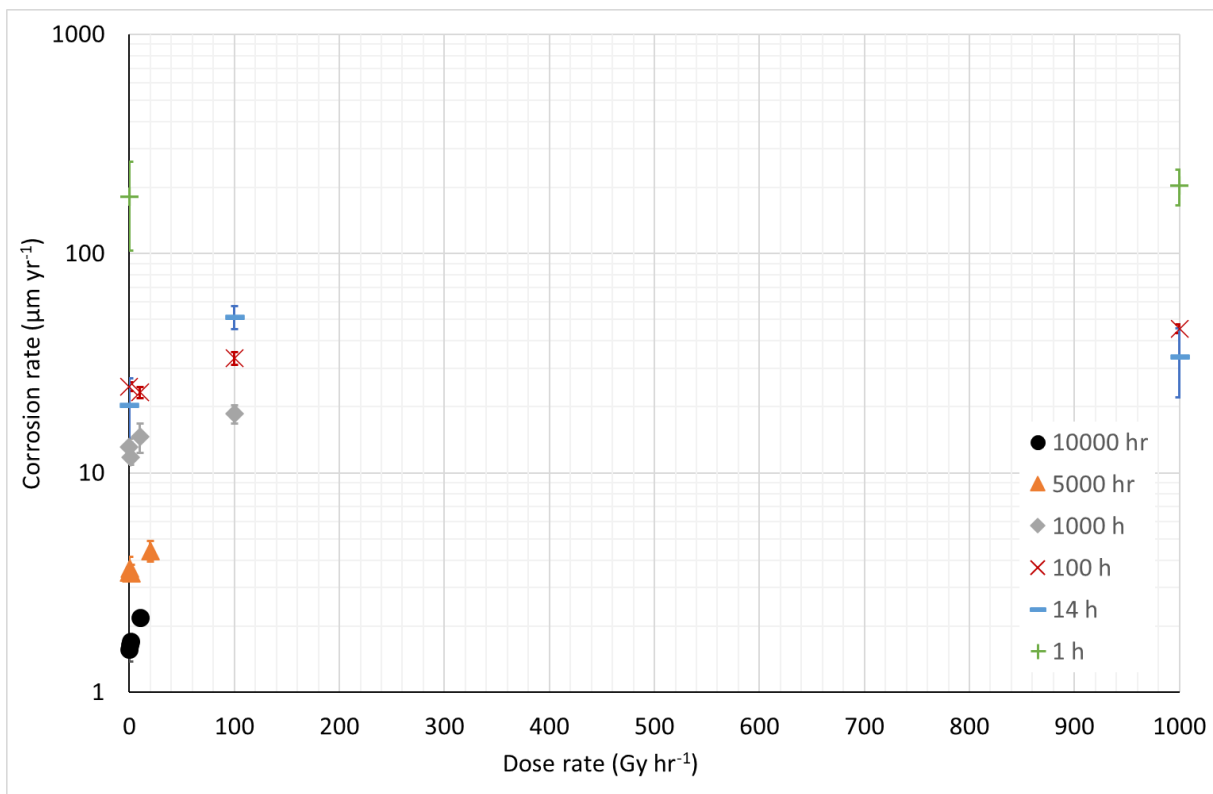
Figure 3-5. Carbon steel average corrosion rate expressed on a log scale versus dose rate for tests operated for durations of 1 to 10000 hours. Error bars indicate the standard deviation between different specimens within the same test.

EURAD (Deliverable n° 15.7) – Elucidation of critical irradiation parameter
Dissemination level: Public
Date of issue of this report: 06/02/2024

Page 35
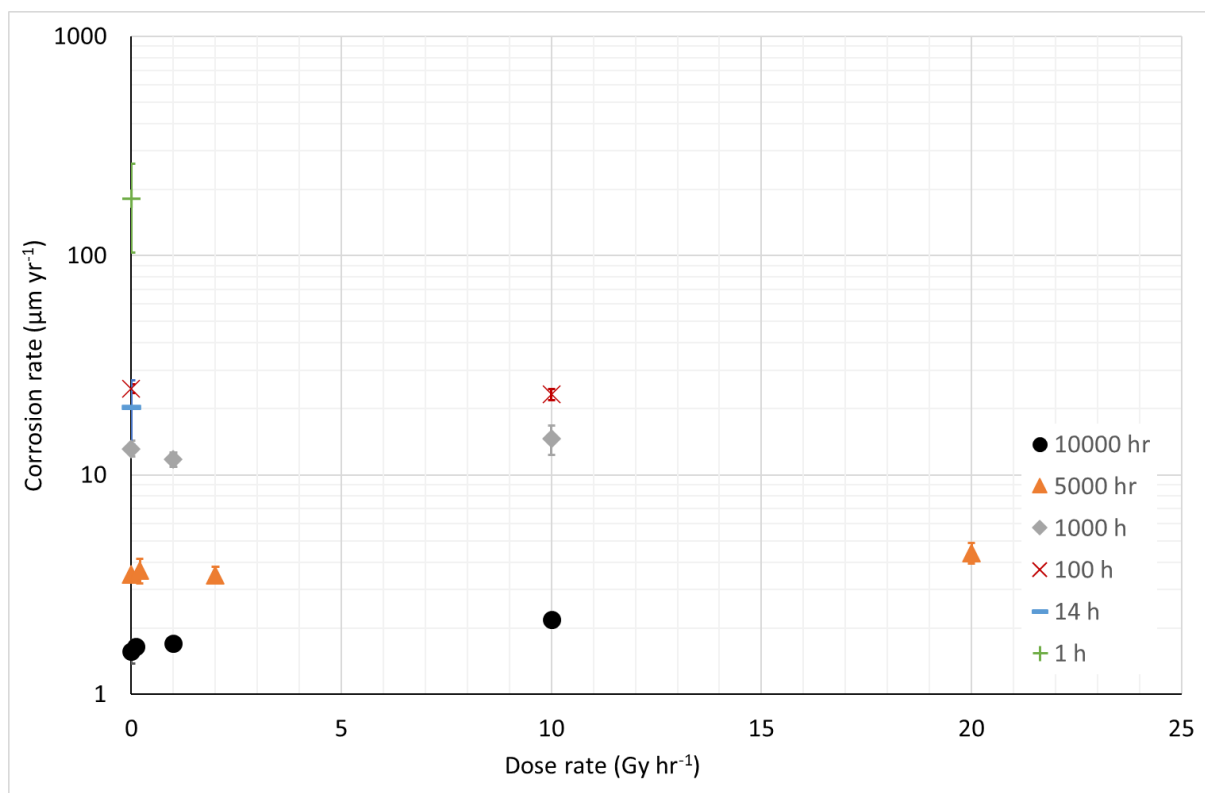
Figure 3-6. Carbon steel average corrosion rate expressed on a log scale versus dose rate for tests operated for durations of 1 to 10000 hours. Data is repeated from Figure 3-5 but with the x-axis limited to 25 Gy h^{-1} to better display the trend at lower dose rates. Error bars indicate the standard deviation between different specimens within the same test.

EURAD (Deliverable n° 15.7) – Elucidation of critical irradiation parameter
Dissemination level: Public
Date of issue of this report: 06/02/2024

European Joint Programme
on Radioactive Waste Management

Page 36

Table 3-4 Average corrosion rates in μm yr^{-1} of carbon steel samples. Note total dosages received are also included in bold. Standard deviation of repeat measurements in brackets.

Exposure Duration (h)	Dose Rate (Gy h^{-1})								
	0.0	0.1	0.2	1	2	10	20	100	1000
1	**0 kGy** 182.13 (78.84)								**1 kGy** 203.36 (37.21)
14	**0 kGy** 20.40 (6.65)							**1 kGy** 51.28 (6.19)	**10 kGy** 33.89 (11.84)
100	**0 kGy** 24.66 (1.11)					**1 kGy** 23.22 (1.28)		**10 kGy** 33.36 (2.21)	**100 kGy** 45.34 (2.04)
1000	**0 kGy** 13.17 (1.10)			**1 kGy** 11.74 (0.91)		**10 kGy** 14.58 (2.25)		**100 kGy** 18.53 (1.79)	
5000	**0 kGy** 3.52 (0.06)		**1 kGy** 3.67 (0.48)		**10 kGy** 3.50 (0.30)		**100 kGy** 4.42 (0.48)		
10000	**0 kGy** 1.57 (0.19)	**1 kGy** 1.65 (0.04)		**10 kGy** 1.71 (0.09)		**100 kGy** 2.19 (0.08)			

3.3 Radiolysis modelling by Amphos 21

Radiolysis of water and chloride was calculated as a function of dose rate between 0.1 and 1000 Gy h[-1] and for durations up to 1000 hours (shown in Figure 3-7, Figure 3-8, Figure 3-9 and summarised in Table 3-5 and Figure 3-10) for a solution of 0.1 M NaCl. The calculations considered the partition of both aqueous and gaseous species within the same solution volume and ullage volume as used in the experimental configuration for Ampoule Design Two, but results are only shown for the aqueous phase here. Ampoule Design Two had a larger relative ullage space than Ampoule Design One, which is expected to increase the time taken to reach steady state but is not expected to significantly influence the concentrations reached at steady state. Therefore, the figures reflect the estimated maximum time taken to reach steady state in the absence of consuming reactions e.g. corrosion. Furthermore, Ampoule Design Two was only implemented in tests run for 5000 and 10000 hours, hence the time taken to reach steady state (in the absence of corrosion) is predicted to be a small fraction of the total test duration. The figures show that at low concentrations, and short time scales, the concentration and the rate of formation of radiolytically generated O_2, H_2O_2 and H_2 are predicted to be roughly proportional to the dose rate. However, at longer timescales a steady state concentration is reached that increases logarithmically with increasing dose rate. These results imply that, over short timescales (where concentration is close to linear with dose rate), a similar yield of stable radiolytically generated oxidants (O_2 and H_2O_2) will be generated over the range of dose rates investigated, provided the total dose is the same. However, at longer timescales (times exceeding those required to reach steady state conditions), different yields of radiolytically generated oxidants will be produced at different dose rates, even if the total dose is the same. There are two ways to consider this. The first is if two solutions are given the same total dose at different dose rates (i.e., one is irradiated for longer); in this case the solution irradiated at the higher dose rate will contain a higher concentration of stable oxidants. The second is that if the two solutions are irradiated for an equal amount of time at different dose rates, the solution irradiated at the lower dose rate, and therefore a lower total dose, will contain a higher concentration of oxidants per Gy of radiation it received.

From Figure 3-8 and Figure 3-9 it can be seen that O_2 forms in greater abundance than H_2O_2. Furthermore, the steady state concentration of H_2O_2 exhibits a much stronger dose rate dependence than O_2 or H_2 over the range of 1 to 1000 Gr h[-1]. For H_2O_2 the dependence of steady state concentration is greater at lower dose rates, but for O_2 and H_2 the dependence is stronger at higher dose rates. It should be noted that the test solution also contained 0.2 M $NaHCO_3$, which was not included in the radiolysis model. The presence of $NaHCO_3$ in the test solution may influence the speciation under radiolysis, causing a discrepancy between the solution chemistry in the test environment and that predicted by modelling.

EURAD (Deliverable n° 15.7) – Elucidation of critical irradiation parameter
Dissemination level: Public
Date of issue of this report: 06/02/2024

Page 38
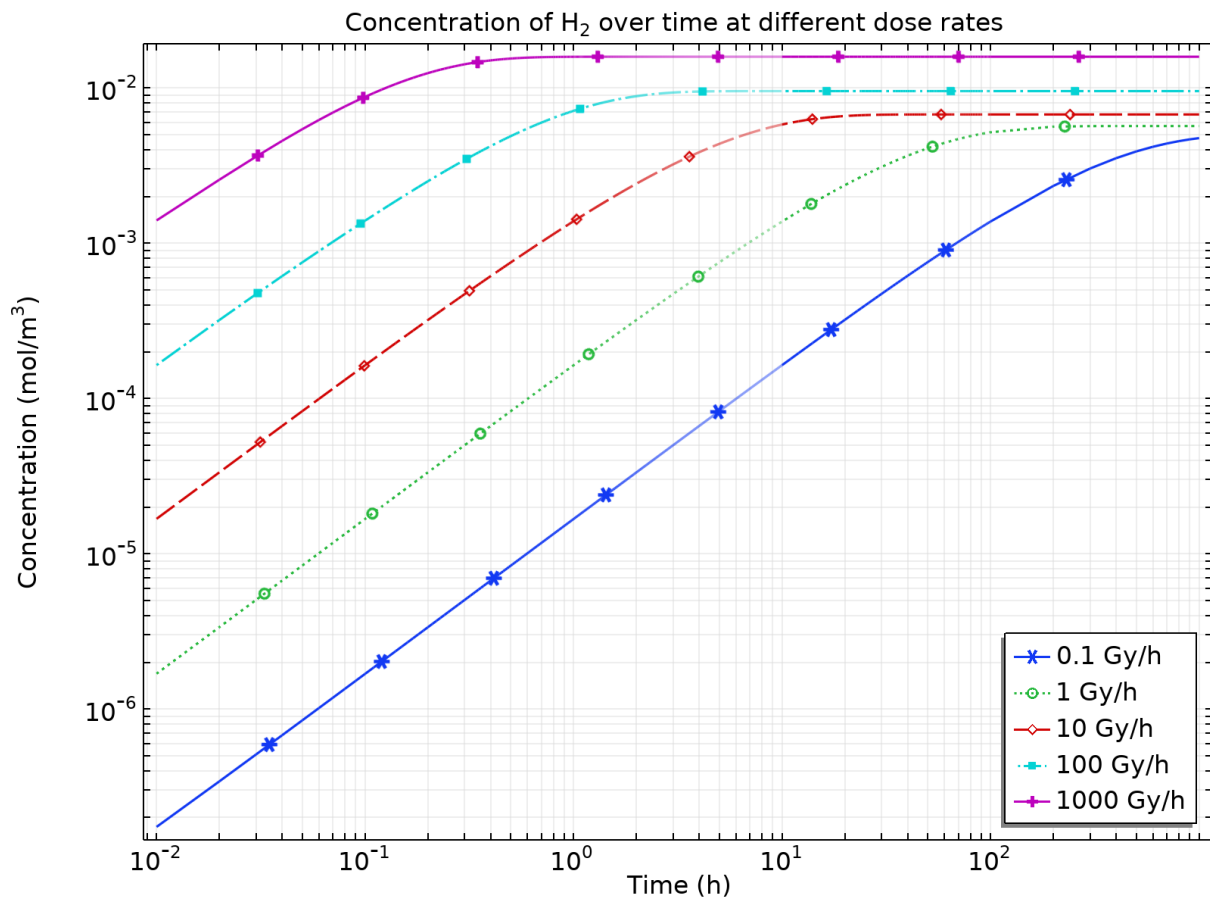
Figure 3-7. Concentration of H_2 over time up to 1000 hours at different dose rates, calculated for a solution of deaerated 0.1M NaCl by Amphos 21.

EURAD (Deliverable n° 15.7) – Elucidation of critical irradiation parameter
Dissemination level: Public
Date of issue of this report: 06/02/2024

Page 39
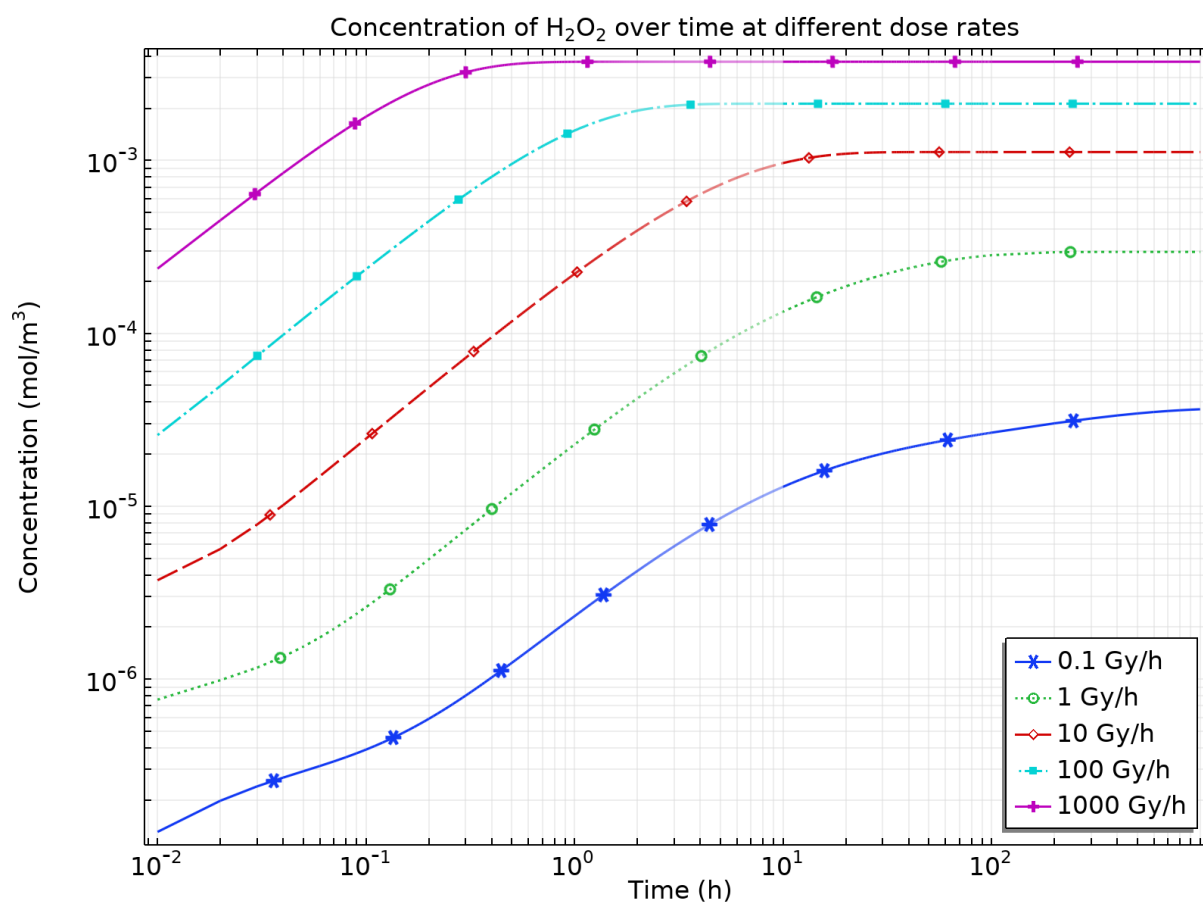
Figure 3-8. Concentration of H_2O_2 over time up to 1000 hours at different dose rates, calculated for a solution of deaerated 0.1M NaCl by Amphos 21.

EURAD (Deliverable n° 15.7) – Elucidation of critical irradiation parameter
Dissemination level: Public
Date of issue of this report: 06/02/2024

Page 40
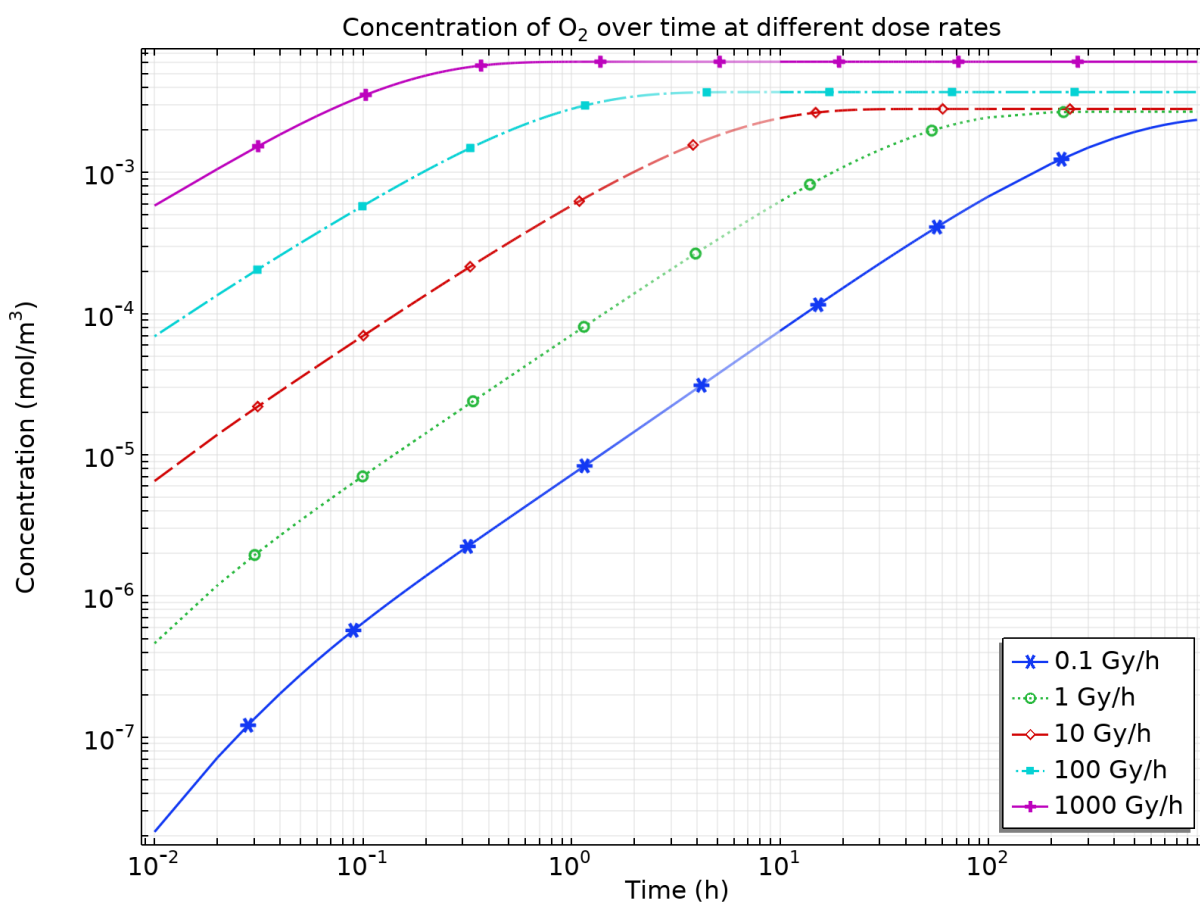
Figure 3-9. Concentration of O_2 over time up to 1000 hours at different dose rates, calculated for a solution of deaerated 0.1M NaCl by Amphos 21.

Table 3-5. Steady state concentrations[4] of H_2, O_2 and H_2O_2 calculated for a solution of deaerated 0.1M NaCl at different dose rates, calculated by Amphos 21.

Dose rate (Gy h^{-1})	Steady state concentration in (µM)		
	H_2	O_2	H_2O_2
0.1	4.75[4]	2.36[4]	0.0363[4]
1	5.68	2.69	0.295
10	6.74	2.81	1.12
100	9.54	3.71	2.12
1000	15.9	6.08	3.71

---

[4] At a dose rate of 0.1 Gy hr^{-1} the concentration only approached steady state after 1000 hours and a true steady state was not reached.

EURAD (Deliverable n° 15.7) – Elucidation of critical irradiation parameter
Dissemination level: Public
Date of issue of this report: 06/02/2024

Page 41
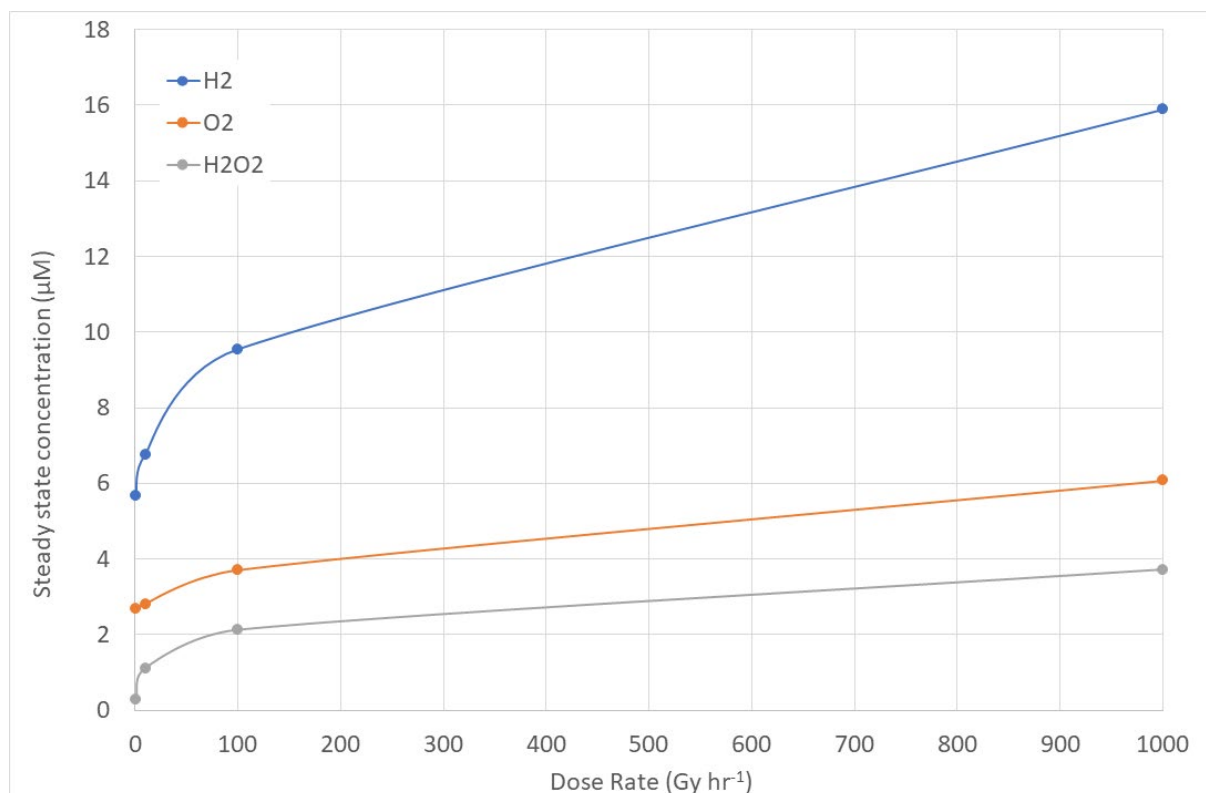
Figure 3-10. Steady state concentrations of H_2, O_2 and H_2O_2 calculated for a solution of deaerated 0.1 M NaCl plotted from Table 3-5.

3.4 Visual inspection

3.4.1 Copper

A general summary of the visual inspection of test specimens performed following testing is provided in Table 3-6 and images of all wrought and cold-sprayed copper specimens are shown in Figure 3-11 to Figure 3-16. In unirradiated conditions the coupons remained largely pristine for all test durations with only two exceptions. The first exception was specimen WC4-1#2, tested for 1000 hours, which had one dark spot on the edge of the coupon approximately 0.5 mm in diameter. The second exception was specimen WC6-1#5, which exhibited patches of black corrosion product on the surface after 10000 hours (see Figure 3-16). In both cases, the duplicate specimens that were also present in the test did not exhibit any visible corrosion products. Visual assessment of the extent of corrosion product on the surface of irradiated specimens indicated that it broadly correlated with the total dose received, i.e., it increased with both dose rate and duration of exposure to a similar extent. However, individual repeat specimens within a single test tended to show a wide variation in the extent of corrosion product present on the surface. Wrought and cold-sprayed copper generally exhibited a similar amount of corrosion, with the only exception being the results observed after 100 hours of testing at a dose rate of 10 Gy h^{-1}, which showed the presence of black patchy corrosion product on the two cold-sprayed copper coupons but not on the four wrought copper coupons (see Figure 3-13).

EURAD (Deliverable n° 15.7) – Elucidation of critical irradiation parameter
Dissemination level: Public
Date of issue of this report: 06/02/2024

Page 42

Table 3-6. Overview of the visual observation of copper specimens exposed to radiation dose rates between 0.1 and 100 Gy h⁻¹ for total doses of 1, 10 and 100 kGy.

Dose Rate (Gy h⁻¹)	Total dose (kGy)		
	1	10	100
0.1	Majority of specimen surface appears pristine, some small black/brown corrosion product on some specimens		
0.2	Majority of specimen surface appears pristine, some small black/brown corrosion product on some specimens		
1	Majority of specimen surface appears pristine, some small black/brown corrosion product on some specimens	Specimens covered in a significant fraction of black/brown corrosion product	
10	CSC coupons exhibiting small amount of black/brown corrosion, WC coupons appear pristine	Specimens covered in a significant fraction of black/brown corrosion product	Specimens covered in brown/black corrosion product with small green sections on ends of samples
100		Specimens covered in a significant fraction of black corrosion product	Specimens covered in green corrosion product with some areas covered in brown/black corrosion product

After 100 hours of testing, the only WC specimens that exhibited corrosion were those tested at 100 Gy h^{-1} (WC 3-8), with those tested at 10 Gy h^{-1} (WC 3-6) appearing pristine. As previously mentioned, the CSC coupons differed from the WC coupons by exhibiting black corrosion product at the lower dose rate of 10 Gy h^{-1} (CSC 3-6). However, following testing at 100 Gy h^{-1} the CSC and WC specimens showed a similar average amount of corrosion product (WC3-8 and CSC3-8), with some of the WC specimens appearing more corroded (#1 and #3) and others appearing less corroded (#2 and #4) than the CSC specimens. In all instances where corrosion products were observed, it was patchy and regions of seemingly pristine surface were still visible (see Figure 3-13).

Following exposure for 1000 hours, visible corrosion products were present on CSC and WC specimens at all dose rates tested (1, 10 and 100 Gy h^{-1}), with a greater coverage at higher dose rates (see Figure 3-14). At a dose rate of 1 Gy h^{-1} (WC4-4 and CSC4-4) the patches of corrosion product consisted of small isolated black spots, with some specimens appearing pristine. At a dose rate of 10 Gy h^{-1} (WC4-6 and CSC4-6), all specimens exhibited large patches of black/brown corrosion product covering significant fractions of the specimens' surfaces. At 10 Gy h^{-1} there was a large variation in the amount of corrosion product present on the surface of repeat specimens, particularly for the WC. At a dose rate of 100 Gy h^{-1}, all specimens (WC4-8/CSC4-8) exhibited a green/brown corrosion product covering the entire specimen's surface with no areas appearing pristine. WC coupons appeared slightly greener than the CSC coupons, but noting the high variability observed between specimens at other dose rates, this could be attributable to random variation.

The only dose rate investigated in the tests run for a duration of 5000 hours was 0.2 Gy h^{-1} (WC3-5, CSC 3-5). At 0.2 Gy h^{-1} the specimens appeared largely pristine following 5000 hours of exposure, with two specimens exhibiting very small brown patches of corrosion (see Figure 3-15).

Following the longest exposure duration of 10000 hours, corrosion products were visible at all dose rates tested (0.1, 1 and 10 Gy h^{-1}) with a greater coverage at higher dose rate, as shown in Figure 3-16. Only WC coupons were tested for 10000 hours and after testing at a dose rate of 0.1 Gy h^{-1} small patches of dark brown corrosion products were visible on all specimens (WC6-2), which ranged from 0.5 mm to 2 mm in diameter. Between one and two patches appeared on each sample and the remainder of the surface appeared pristine. At a dose rate of 1 Gy h^{-1} (WC6-4) the dark brown patches had a more extensive surface coverage, but still had a patchy distribution across the surface. At a dose rate of 10 Gy h^{-1} the majority of the surface was covered in a dark brown/black material. Upon further inspection, one end of all specimens had some green material on the surface except for #1, which was completely covered with the dark brown/black corrosion product. The presence of the green material wasn't unique to the ends of the specimens and patches of green can be seen towards the centre of specimens #4 and #6. The greater amount of green corrosion product at the end of the specimens could coincide with the ends of the specimen which protruded from the bottom of the inner glass tube, as described in Section 2.4. However, this hypothesis could not be confirmed as the ends which protruded from the inner glass tube were not noted during dismantling.

EURAD (Deliverable n° 15.7) – Elucidation of critical irradiation parameter
Dissemination level: Public
Date of issue of this report: 06/02/2024

Page 44

Figure 3-11. Wrought copper samples exposed for 1 h at 0 Gy h⁻¹ (WC1-1). Note replica samples #1 - #6, as denoted in Section 2.4, are positioned from left to right.
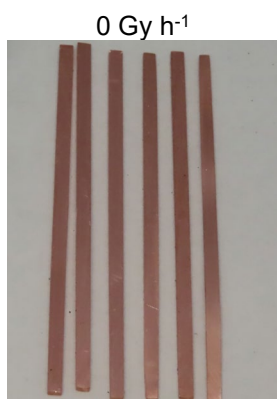
Figure 3-12. Wrought copper samples exposed for 10 h at 0 Gy h⁻¹ (WC2-1). Note replica samples #1 - #6, as denoted in Section 2.4, are positioned from left to right.
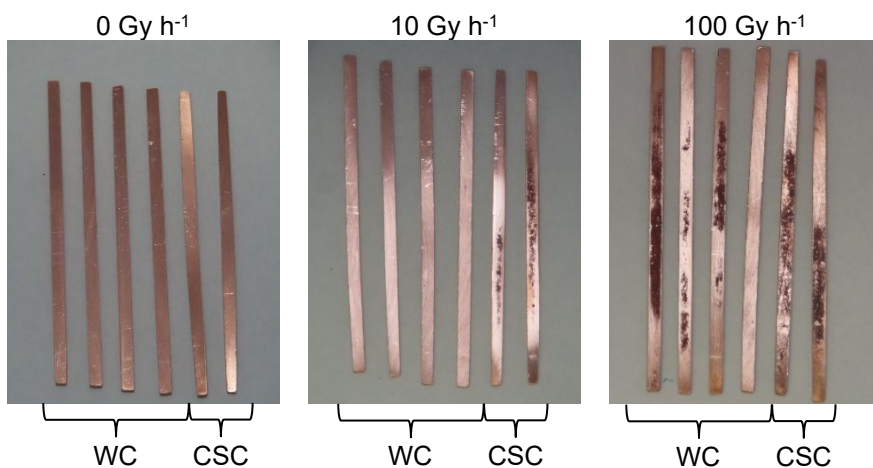
Figure 3-13. Wrought and cold-sprayed copper samples exposed for 100 h at 0 Gy h⁻¹ (WC3-1/CSC3-1), 10 Gy h⁻¹ (WC3-6/CSC3-6), and 100 Gy h⁻¹ (WC3-8/CSC3-8). Note replica wrought copper samples #1 - #4, as denoted in Section 2.4, are positioned from left to right in each image. Cold-sprayed copper samples #1 and #2 are positioned to the right of the wrought copper samples.

EURAD (Deliverable n° 15.7) – Elucidation of critical irradiation parameter
Dissemination level: Public
Date of issue of this report: 06/02/2024

Page 45
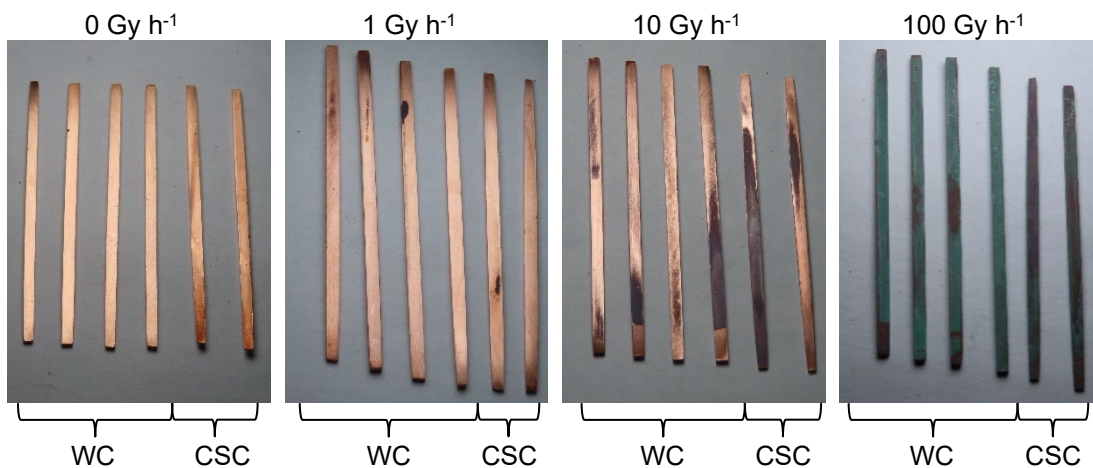
Figure 3-14. Wrought and cold-sprayed copper samples exposed for 1000 h at 0 Gy h⁻¹ (WC4-1/CSC4-1), 1 Gy h⁻¹ (WC4-4/CSC4-4), 10 Gy h⁻¹ (WC4-6/CSC4-6), and 100 Gy h⁻¹ (WC4-8/CSC4-8). Note replica wrought copper samples #1 - #4, as denoted in Section 2.4, are positioned from left to right in each image. Cold-sprayed copper samples #1 and #2 are positioned to the right of the wrought copper samples.
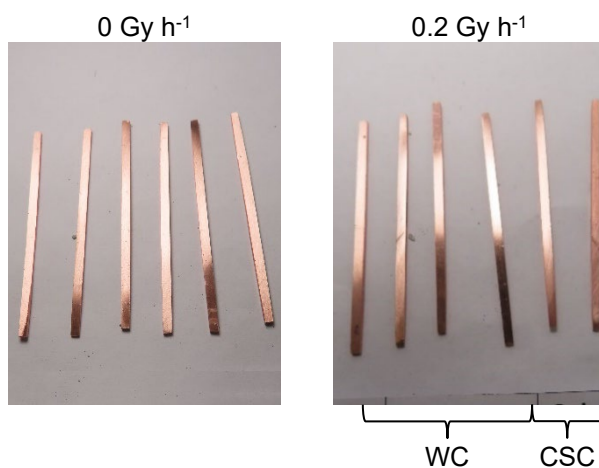
Figure 3-15. Wrought and cold-sprayed copper samples exposed for 5000 h at 0 Gy h⁻¹ (WC5-1) and 0.2 Gy h⁻¹ (WC5-3/CSC5-3). Note replica wrought copper samples #1 - #4, as denoted in Section 2.4, are positioned from left to right in each image. Cold-sprayed copper samples #1 and #2 are positioned to the right of the wrought copper samples.
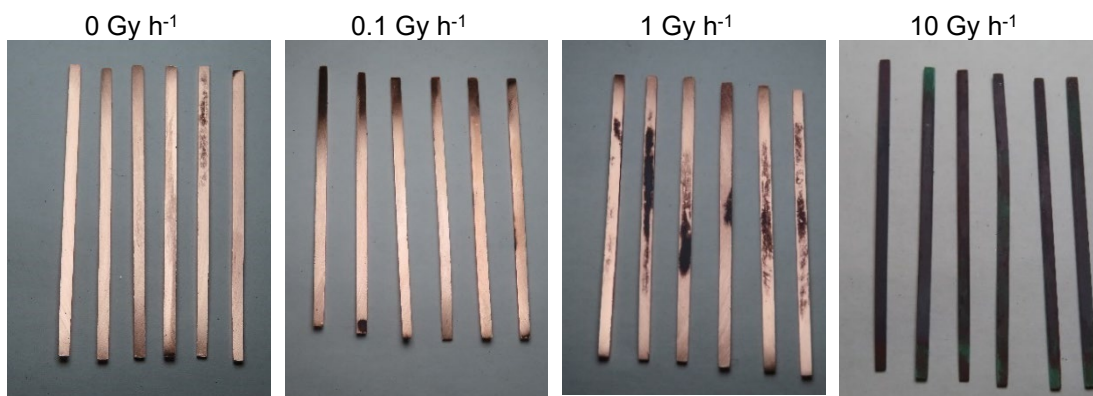
Figure 3-16. Wrought copper samples exposed for 10000 h at 0 Gy h⁻¹ (WC6-1), 0.1 Gy h⁻¹ (WC6-2), 1 Gy h⁻¹ (WC6-4), and 10 Gy h⁻¹ (WC6-6). Note replica samples #1 - #6, as denoted in Section 2.4, are positioned from left to right in each image.

EURAD (Deliverable n° 15.7) – Elucidation of critical irradiation parameter
Dissemination level: Public
Date of issue of this report: 06/02/2024

Page 46

3.4.2 Carbon steel

Images of the carbon steel specimens following testing are shown in Figure 3-17 to Figure 3-22. In general, the presence of radiation did not have a big impact on the visual appearance of the specimens. The appearance of corrosion product on the surface of the specimens appeared to be dominated by the test duration, with all specimens exhibiting a complete coverage of black corrosion product at durations exceeding 1000 hours irrespective of the degree of radiation exposure. At shorter durations the corrosion presented as either discontinuous patches of corrosion product or light tarnishing. Additionally, the extent of corrosion appeared to increase with increasing dose rate/total dose, but the effect was minimal as described below.

After just 1 hour of exposure, the control (CS1-1) samples tested at 0 Gy h^{-1}, appeared similar to the pristine samples with minimal tarnishing on their surfaces following exposure for one hour (see Figure 3-17). The samples tested at (1000 Gy h^{-1}) also showed minimal corrosion after radiation exposure with only one sample (CS1-9#5) exhibiting any evidence of tarnishing.

After exposure for 10 hours, the control sample CS2-1 (0 Gy h^{-1}) showed a small amount of tarnishing on the surface with a few black spots dotted across the surface (see Figure 3-18). CS2-8 (100 Gy h^{-1}) had a similar appearance to CS2-1 with a slightly tarnished appearance and a small number of black dots spread across the surface. Following exposure to 1000 Gy h^{-1} dose rate the surface of CS2-9 appeared more tarnished than the other 10 h samples and a brown discolouration appeared in patches across the surface of some samples (notably CS2-9#1, CS2-9#3 and CS2-9#5).

After a duration of 100 h the surface of the control specimen CS3-1 presented with a dark grey/black material covering the majority of the surface (see Figure 3-19). At a dose rate of 100 Gy h^{-1} more black patches were found covering the surface of CS3-8 and similar observations were found on CS3-9 (1000 Gy h^{-1}).

At exposure durations of 1000, 5000 and 10000 h (see Figure 3-20, Figure 3-21, and Figure 3-22), all carbon steel specimens were covered with a black corrosion product and no other distinctive features. There was no clear visual distinction between control specimens and those irradiated at any dose rate.
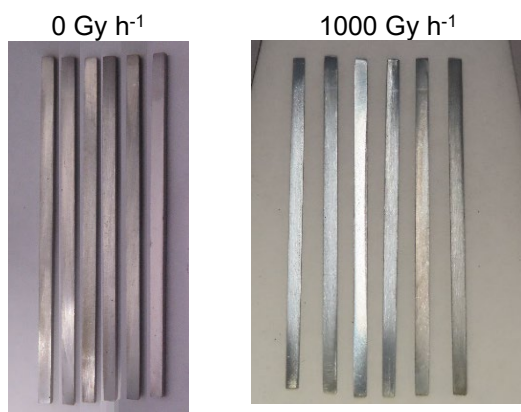
Figure 3-17. Carbon steel samples exposed for 1 h at 0 Gy h^{-1} (CS1-1) and 1000 Gy h^{-1} (CS1-9). Note replica samples #1 - #6, as denoted in Section 2.4, are positioned from left to right in each image.

EURAD (Deliverable n° 15.7) – Elucidation of critical irradiation parameter
Dissemination level: Public
Date of issue of this report: 06/02/2024

Page 47
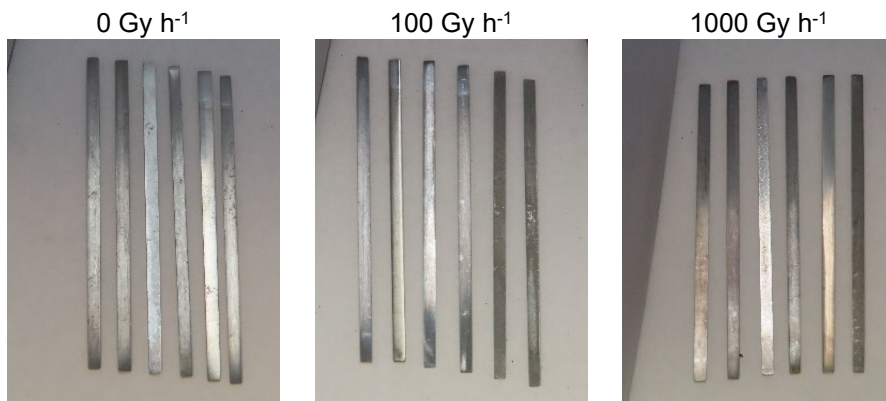
Figure 3-18. Carbon steel samples exposed for 10 h at 0 Gy h⁻¹ (CS2-1), 100 Gy h⁻¹ (CS2-8), and 1000 Gy h⁻¹ (CS2-9). Note replica samples #1 - #6, as denoted in Section 2.4, are positioned from left to right in each image.
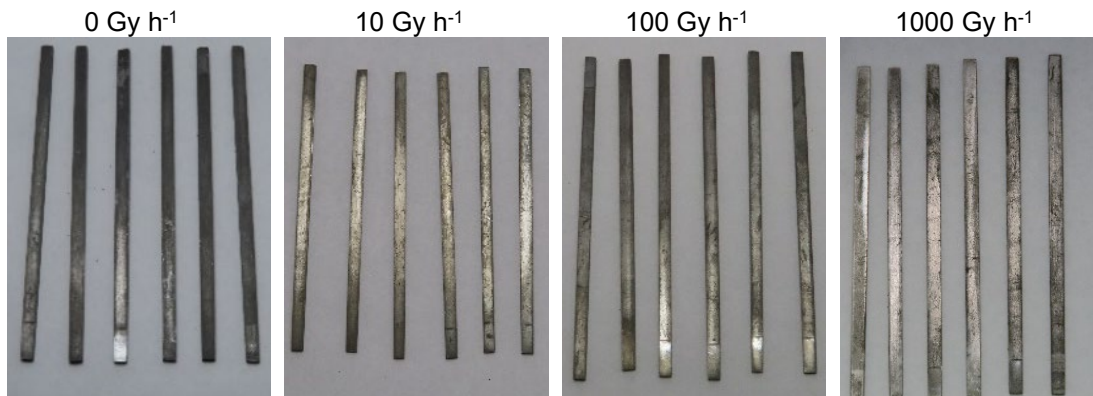
Figure 3-19. Carbon steel samples exposed for 100 h 0 Gy h⁻¹ (CS3-1), 10 Gy h⁻¹ (CS3-6), 100 Gy h⁻¹ (CS3-8), and 1000 Gy h⁻¹ (CS3-9). Note replica samples #1 - #6, as denoted in Section 2.4, are positioned from left to right in each image.
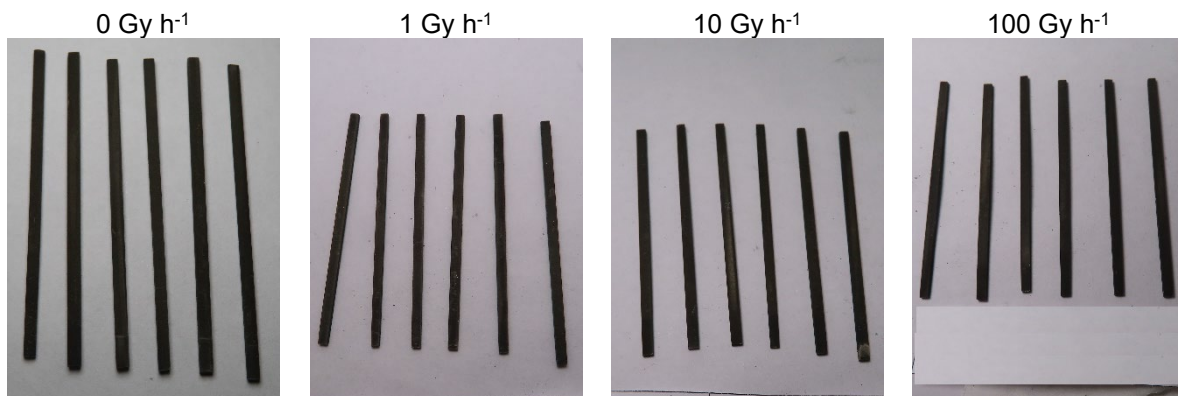
Figure 3-20. Carbon steel samples exposed for 1000 h at 0 Gy h⁻¹ (CS4-1), 1 Gy h⁻¹ (CS4-4), 10 Gy h⁻¹ (CS4-6), and 100 Gy h⁻¹ (CS4-8). Note replica samples #1 - #6, as denoted in Section 2.4, are positioned from left to right in each image.

EURAD (Deliverable n° 15.7) – Elucidation of critical irradiation parameter
Dissemination level: Public
Date of issue of this report: 06/02/2024

Page 48
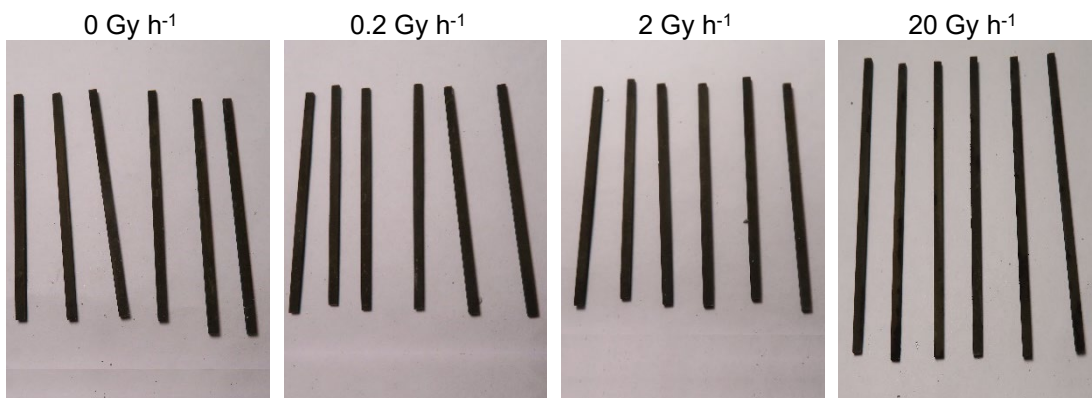
Figure 3-21. Carbon steel samples exposed for 5000 h at 0 Gy h^{-1} (CS5-1), 0.2 Gy h^{-1} (CS5-3), 2 Gy h^{-1} (CS5-5), and 20 Gy h^{-1} (CS5-7). Note replica samples #1 - #6, as denoted in Section 2.4, are positioned from left to right in each image.
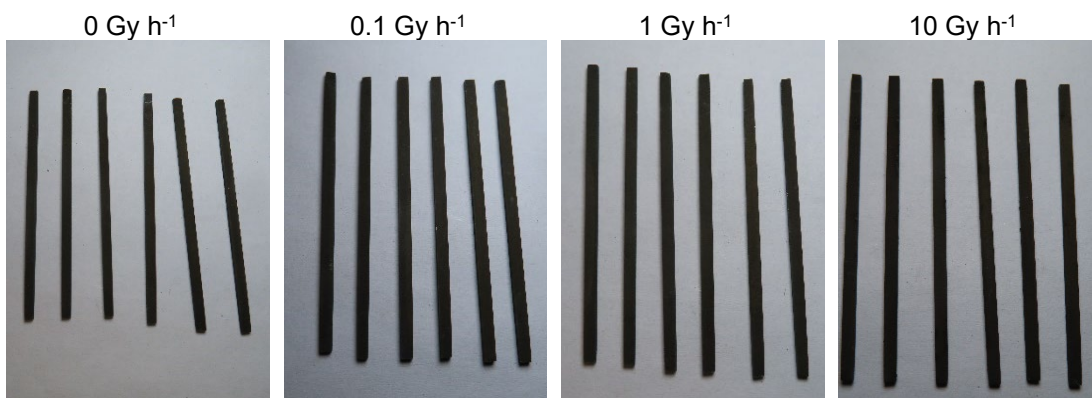
Figure 3-22. Carbon steel samples exposed for 10000 h at 0 Gy h^{-1} (CS6-1), 0.1 Gy h^{-1} (CS6-2), 1 Gy h^{-1} (CS6-4), and 10 Gy h^{-1} (CS6-6) Note replica samples #1 - #6, as denoted in Section 2.4, are positioned from left to right in each image.

3.5 Surface SEM-EDX

3.5.1 Copper

In the following section, SEM/EDX results are provided for the samples exposed for 100 hours at a dose rate of 10 Gy h^{-1} (WC3-6) and 5000 hours (WC5-3) at a dose rate of 0.2 Gy h^{-1}, i.e., both received a total dose of 1 kGy. Representative images as well as EDX spectra and maps for the samples are shown in Figure 3-23 to Figure 3-27.

The SEM image in Figure 3-23 (specimen WC3-6#2C) shows a seemingly pristine copper surface following 100 hours of testing at 10 Gy h^{-1}. Grinding lines from the sample preparation process (see Section 2.2) can be clearly seen in the SEM image and no signs of corrosion products are visible. The corresponding EDX spectra are dominated by the presence of copper. A small shoulder on the lower energy side of the Cu Lα peak at 0.9 keV can be seen in Figure 3-23 and could be characteristic of oxygen, although the intensity and spectral resolution are too low to resolve the peak. The elemental maps in Figure 3-24 also indicate a copper surface with trace amounts of oxygen and carbon.

An optical image of a sub-sample taken from a specimen that was tested for 5000 hours at a dose rate of 0.2 Gy h^{-1} (WC5-3) is shown in Figure 3-25, highlighting a dark spot that was present on the surface. It is worth noting, as described in Section 3.4, that these dark features were uncommon under these test conditions (WC5-3) and only four of them were identified across all 6 duplicate specimens. The exposed copper surface was more representative of the surface of all samples. SEM/EDX spectra and

![EURAD logo] European Joint Programme on Radioactive Waste Management

EURAD (Deliverable n° 15.7) – Elucidation of critical irradiation parameter
Dissemination level: Public
Date of issue of this report: 06/02/2024

Page 49

maps of the exposed copper surface (not presented here) showed a lack of oxygen and the same grinding lines as those observed on WC3-6.

The SEM image (Figure 3-26) of the dark feature shown in Figure 3-25 indicates the presence of a surface precipitate comprising crystallites of the order of a few microns in diameter. EDX spectra of these deposits indicated a small amount of oxygen as well as a predominance of copper, which probably indicates the presence of a thin copper oxide with a significant contribution to the EDX signal still coming from the copper substrate. The oxygen map shown in Figure 3-27 indicated a slightly higher intensity than that observed on the seemingly pristine surface, however it is still comparatively low compared to copper.
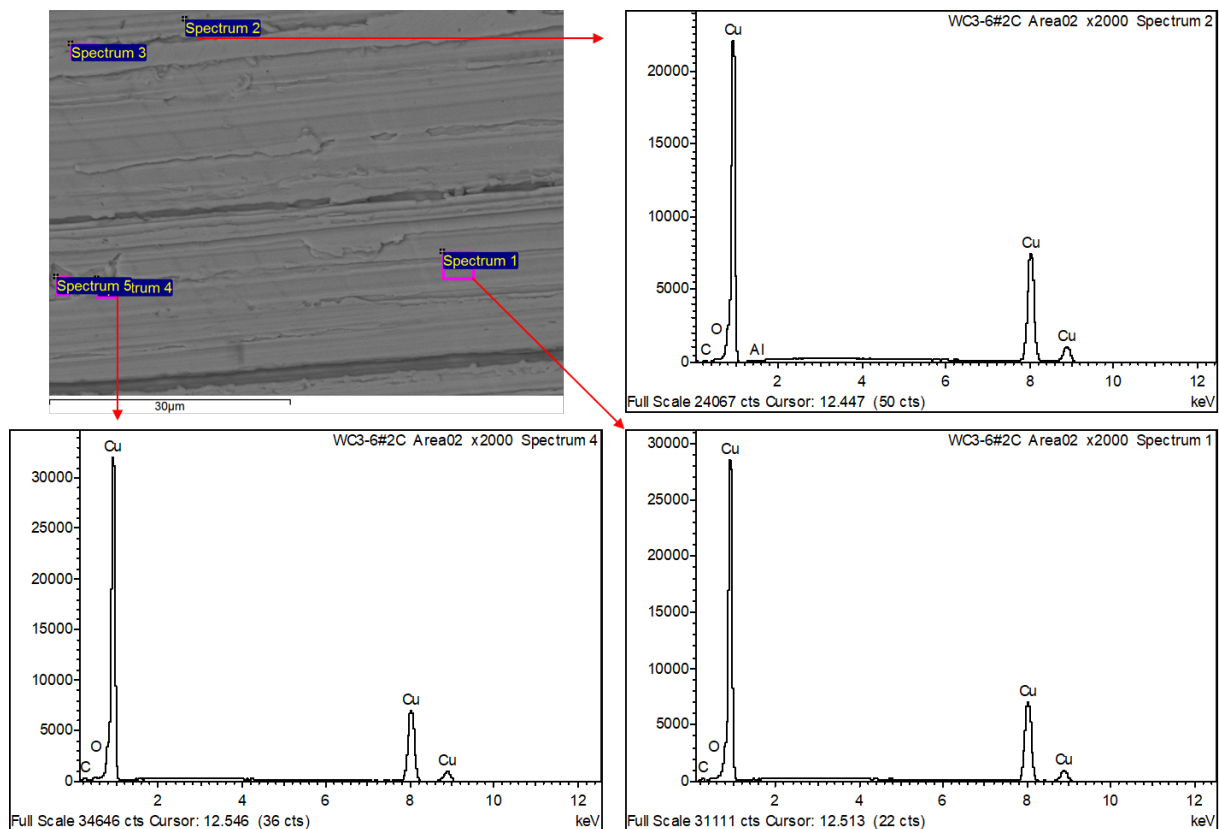
Figure 3-23. Backscattered electron micrograph, at x2000 magnification, of a wrought copper specimen (WC3-6#2C) exposed at a dose rate of 10 Gy h^{-1} for 100 hours with EDX analysis areas illustrated (top left) and corresponding EDX spectra (top right and bottom).

EURAD (Deliverable n° 15.7) – Elucidation of critical irradiation parameter
Dissemination level: Public
Date of issue of this report: 06/02/2024

Page 50
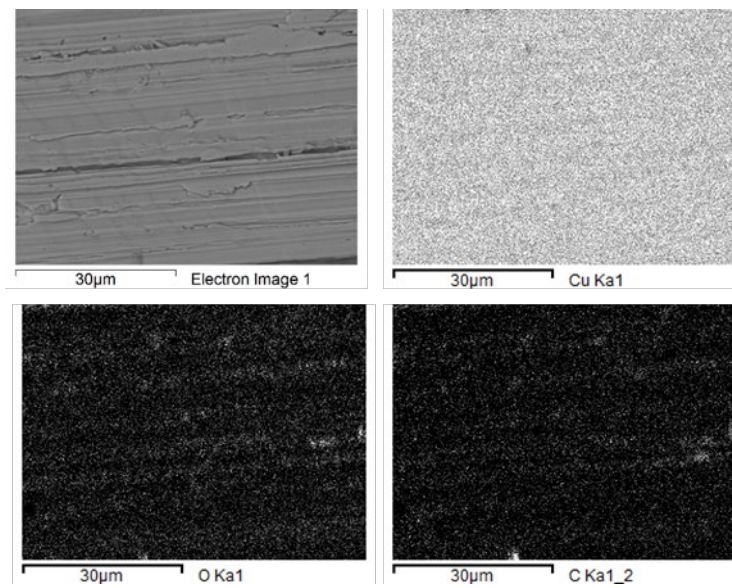
Figure 3-24. Backscattered electron micrograph (top left), at x2000 magnification, and elemental maps (Cu, O and C) of Area 2 of a wrought copper specimen exposed to a dose rate of 10 Gy h^{-1} for 100 hours (WC3-6#2C).

Figure 3-25. An optical image of a sample sub-section from a wrought copper sample exposed to a dose rate of 0.2 Gy h^{-1} for 5000 hours (WC5-3#1C) analysed with SEM/EDX and Raman spectroscopy.

EURAD (Deliverable n° 15.7) – Elucidation of critical irradiation parameter
Dissemination level: Public
Date of issue of this report: 06/02/2024

Page 51
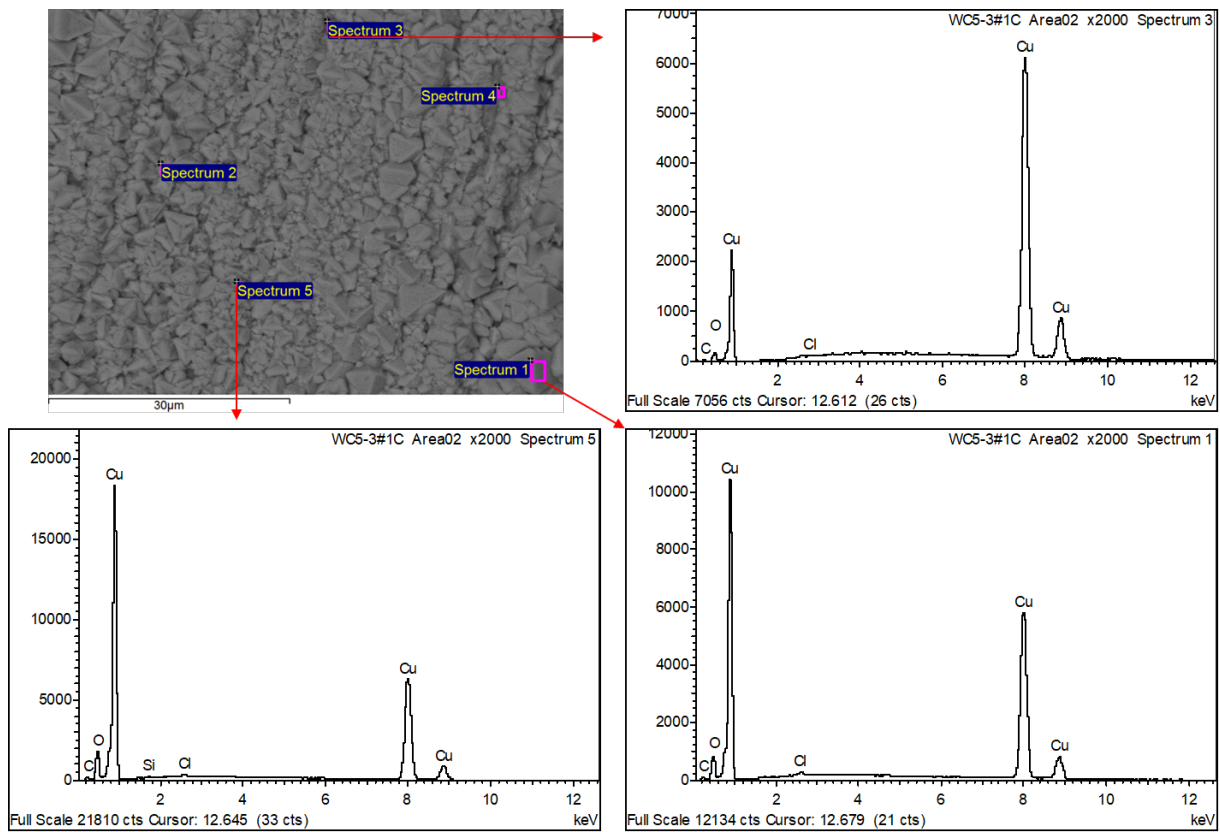
Figure 3-26. Backscattered electron micrograph, at x2000 magnification, of a wrought copper specimen (WC5-3#1C) exposed at a dose rate of 0.2 Gy h^{-1} for 5000 hours with EDX analysis areas illustrated (top left) and corresponding EDX spectra (top right and bottom).
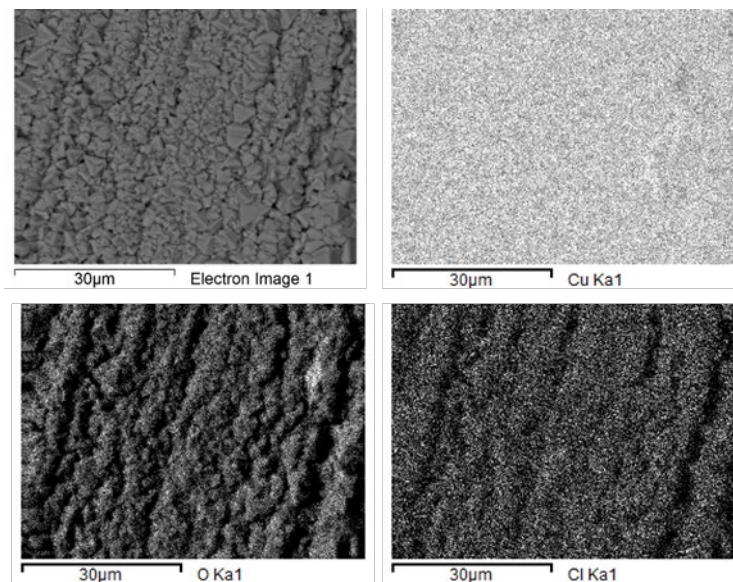
Figure 3-27. Backscattered electron micrograph (top left), at x2000 magnification, and elemental maps (Cu, O and C) of a wrought copper specimen exposed to a dose rate of 0.2 Gy h^{-1} for 5000 hours (WC5-3#1C).

3.5.2 Carbon steel

In the following section, SEM/EDX results are provided for carbon steel samples exposed for 100 hours at dose rates of 10, 100 and 1000 Gy h^{-1} (i.e., total doses of 1, 10, and 100 kGy), and for 5000 h at dose

EURAD (Deliverable n° 15.7) – Elucidation of critical irradiation parameter
Dissemination level: Public
Date of issue of this report: 06/02/2024

Page 52

rates of 0.2 and 2 Gy h^{-1} (i.e., 10 and 100 kGy). Representative SEM images as well as EDX spectra and maps taken from select test specimens are shown in Figure 3-29. to Figure 3-39.

Figure 3-28 shows low magnification images of carbon steel specimens exposed to dose rates of 10, 100 and 1000 Gy h^{-1} (a to c) for 100 hours (CS3-6). The images show each of the surfaces are inhomogeneous with no consistent correlation between dose rate and the degree of surface oxidation. At the highest dose rate, several dark black regions were observed that possibly indicate more extensive corrosion product precipitation. Figure 3-29 shows a higher resolution SEM image and corresponding EDX spectra of the specimen shown in Figure 3-28a, which was exposed to a dose rate of 10 Gy h^{-1} for 100 hours (CS3-6). The figure shows the steel surface was covered with a patchy distribution of seemingly cubic precipitates, roughly 2.5 to 3.0 μm in diameter and rich in iron, carbon, and oxygen. Figure 3-30 shows a SEM image and corresponding EDX maps taken from the same specimen as shown in Figure 3-29, the maps indicate that the carbon is not simply adventitious carbon and is associated with precipitates, although some more than others. The presence of carbon, oxygen and iron in the precipitated layer indicates the possibility of an iron carbonate. At a higher dose rate of 100 Gy h^{-1} (CS3-8), similar precipitates were observed on the surface, however they had a slightly smaller diameter and the surface coverage was less than that observed at 10 Gy h^{-1} (as shown in Figure 3-31). It was also noticed that the sample exposed to 100 Gy h^{-1} exhibited some copper and zinc contamination on the surface which is shown more clearly in Figure 3-32. There is no obvious source of either zinc or copper in the test, so it is assumed that the contamination occurred during specimen manufacture, possibly during EDM machining which uses a brass electrode. At the highest dose rate of 1000 Gy h^{-1} (CS3-9), the surface exhibited the densest coverage of precipitate observed for any of the tests performed for 100 hours (Figure 3-33 and Figure 3-34). The size, morphology and chemical composition of the surface precipitate formed at 1000 Gy h^{-1} closely resembled that observed at 10 Gy h^{-1}.

Following exposure to dose rates of 0.2 and 2 Gy h^{-1} for a duration of 5000 hours (CS5-3 and CS5-5, respectively), the coverage of the surface by corrosion products was considerably greater than observed after 100 hours following equivalent total radiation doses of 10 and 100 kGy. After 5000 hours of exposure, the specimens exhibited complete coverage of their surfaces in a dense precipitate, which can be seen in the low magnification SEM images shown in Figure 3-35. Figure 3-36 to Figure 3-29 show higher resolution SEM images of the surfaces and corresponding EDX spectra and mapping of the corrosion product observed after 5000 hours exposure to dose rates of 0.2 and 2 Gy h^{-1}. From the SEM images and EDX spectra, no distinction could be made between the surfaces exposed to a dose rate of 0.2 Gy h^{-1} and 2 Gy h^{-1}. At both dose rates, the surface precipitates produced after 5000 h had a different morphology, appearing generally larger and more irregular in both size and geometry to those produced after 100 h of exposure, even when the total dose was the same. The EDX data show that after 5000 h, the surface precipitate has a similar composition to that observed following 100 h, with the main constituents being iron and oxygen with small amounts of carbon and sodium. The presence of a particle rich in sodium and silicon was identified on the surface of the specimen exposed to a dose rate of 2 Gy h^{-1} for 5000 hours (CS5-5), but this was identified in isolation (see Figure 3-39) and similar features were not observed in any of the other analysis areas that are not shown.

EURAD (Deliverable n° 15.7) – Elucidation of critical irradiation parameter
Dissemination level: Public
Date of issue of this report: 06/02/2024

Page 53
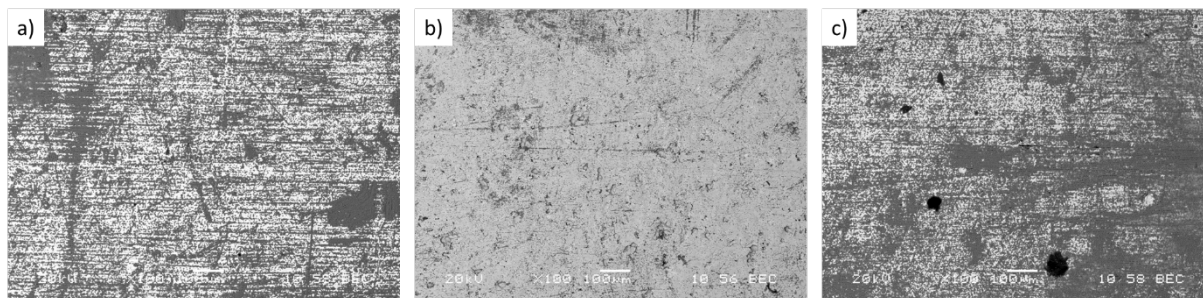
Figure 3-28. SEM backscattered electron images, at x100 magnification, of carbon steel specimens exposed to 100 hours of radiation at: a) 10 Gy h^{-1} (CS3-6#5C), b) 100 Gy h^{-1} (CS3-8#4C) and c) 1000 Gy h^{-1} (CS3-9#4C).
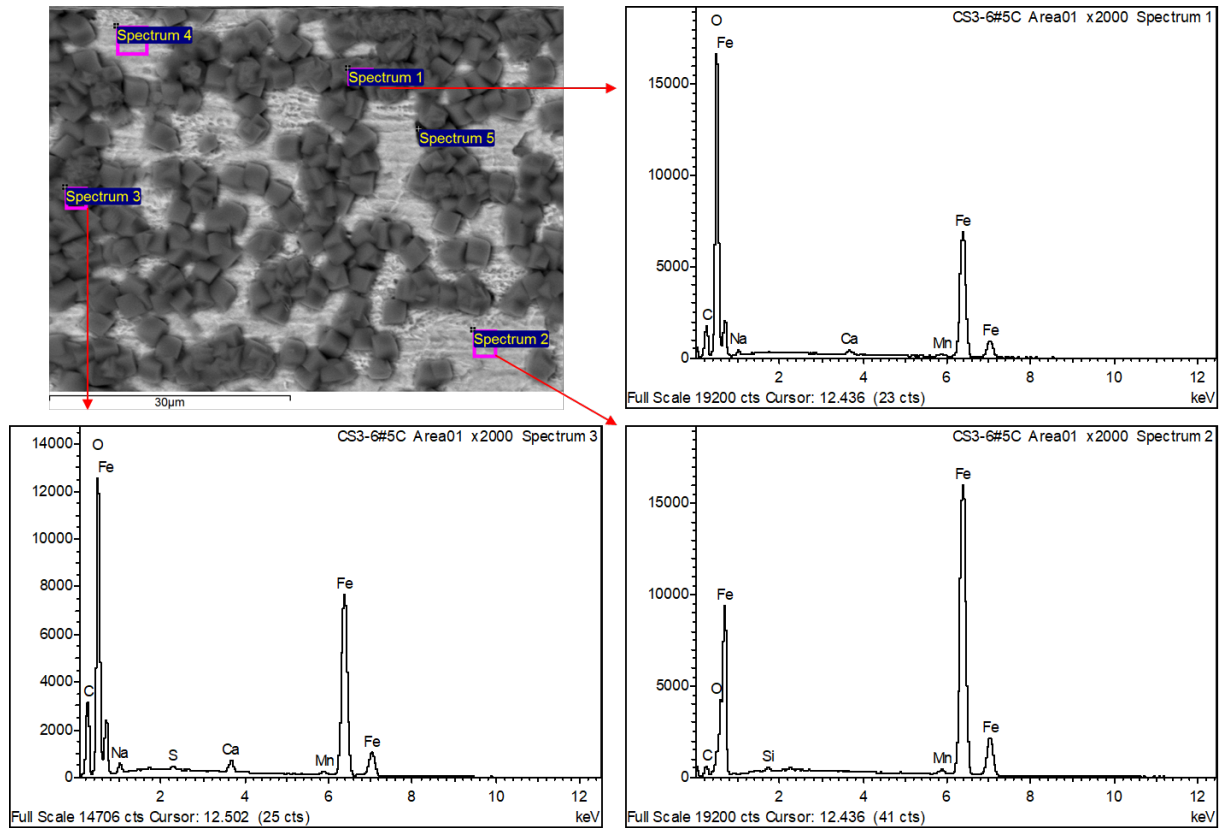
Figure 3-29. Backscattered electron micrograph, at x2000 magnification, of a carbon steel specimen (CS3-6#5C) exposed to a dose rate of 10 Gy h^{-1} for 100 hours with EDX analysis areas illustrated (top left) and corresponding EDX spectra (top right and bottom).

EURAD (Deliverable n° 15.7) – Elucidation of critical irradiation parameter
Dissemination level: Public
Date of issue of this report: 06/02/2024

Page 54
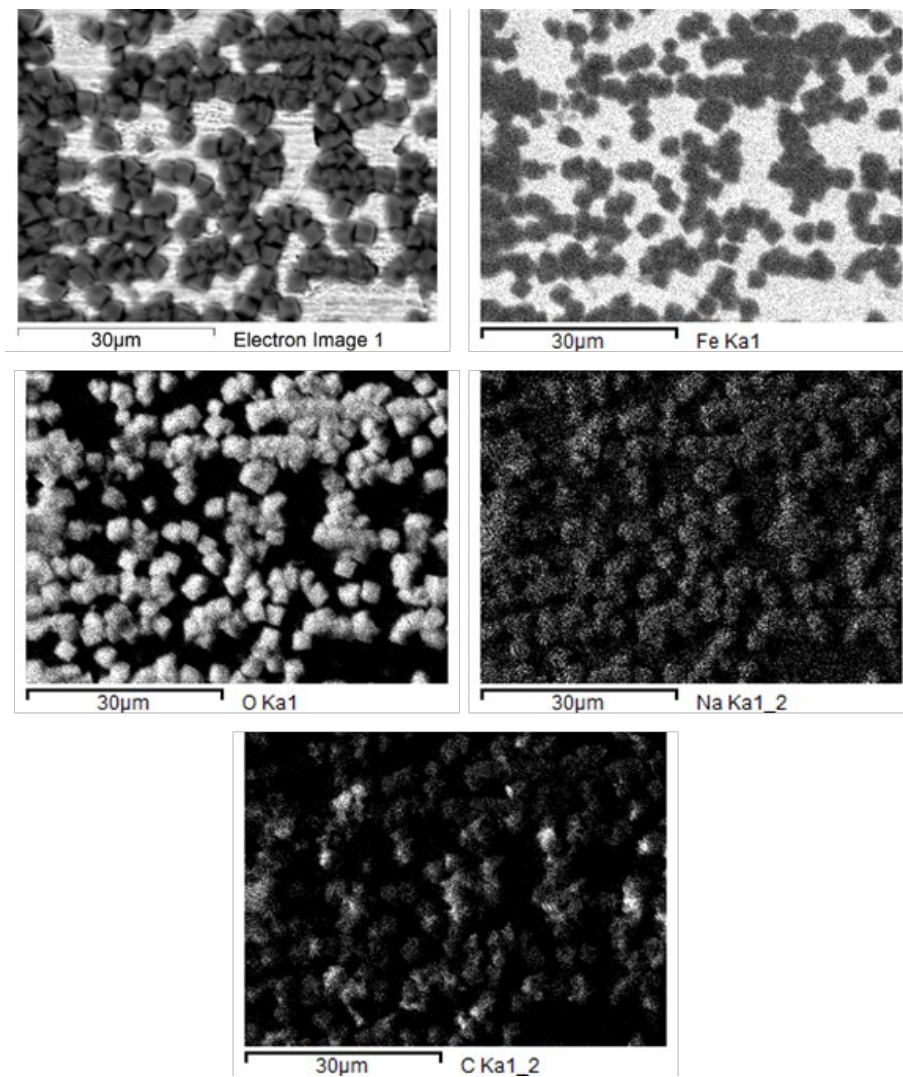
Figure 3-30. Backscattered electron micrograph (top left), at x2000 magnification, and elemental maps (Fe, O, Na, and C) of a carbon steel specimen exposed to a dose rate of 10 Gy h^{-1} for 100 hours (CS3-6#5C).

EURAD (Deliverable n° 15.7) – Elucidation of critical irradiation parameter
Dissemination level: Public
Date of issue of this report: 06/02/2024

Page 55
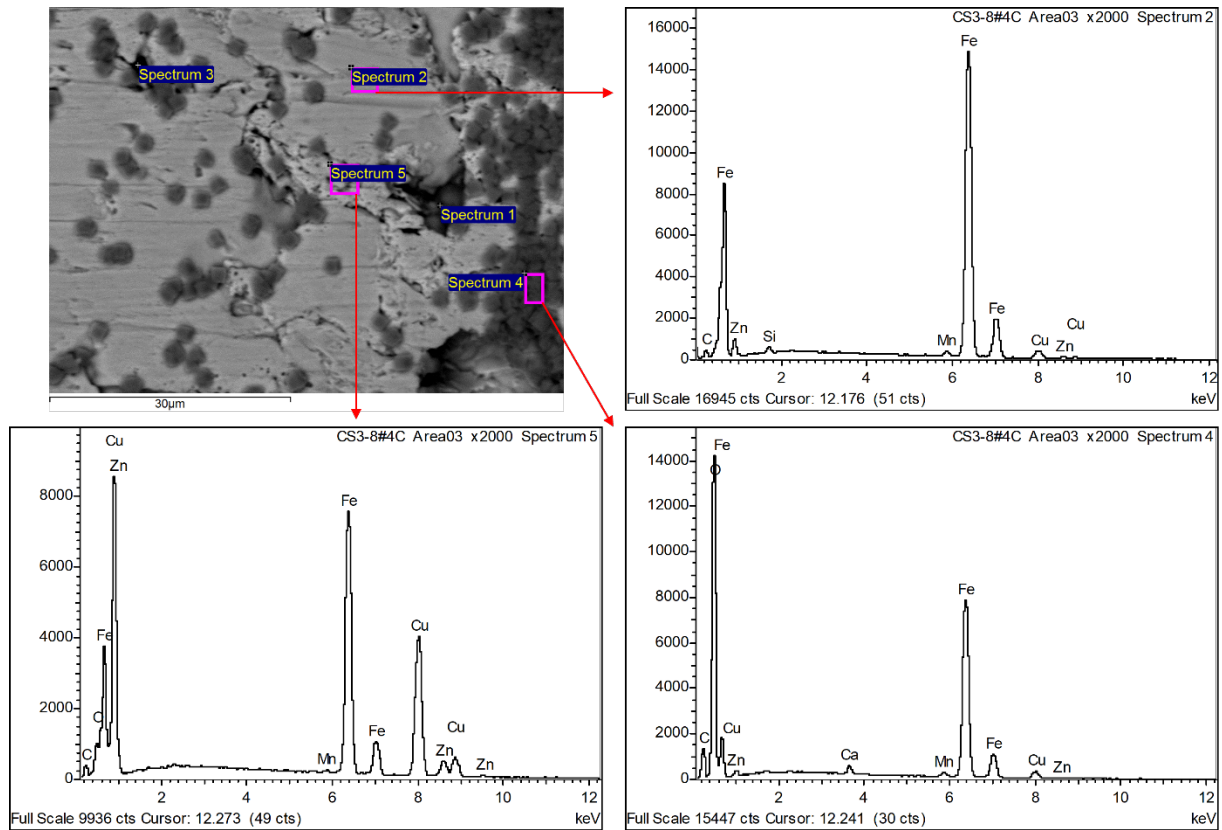
Figure 3-31. Backscattered electron micrograph, at x2000 magnification, of a carbon steel specimen (CS3-8#4C) exposed to a dose rate of 100 Gy h^{-1} for 100 hours with EDX analysis areas illustrated (top left) and corresponding EDX spectra (top right and bottom).

EURAD (Deliverable n° 15.7) – Elucidation of critical irradiation parameter
Dissemination level: Public
Date of issue of this report: 06/02/2024

Page 56
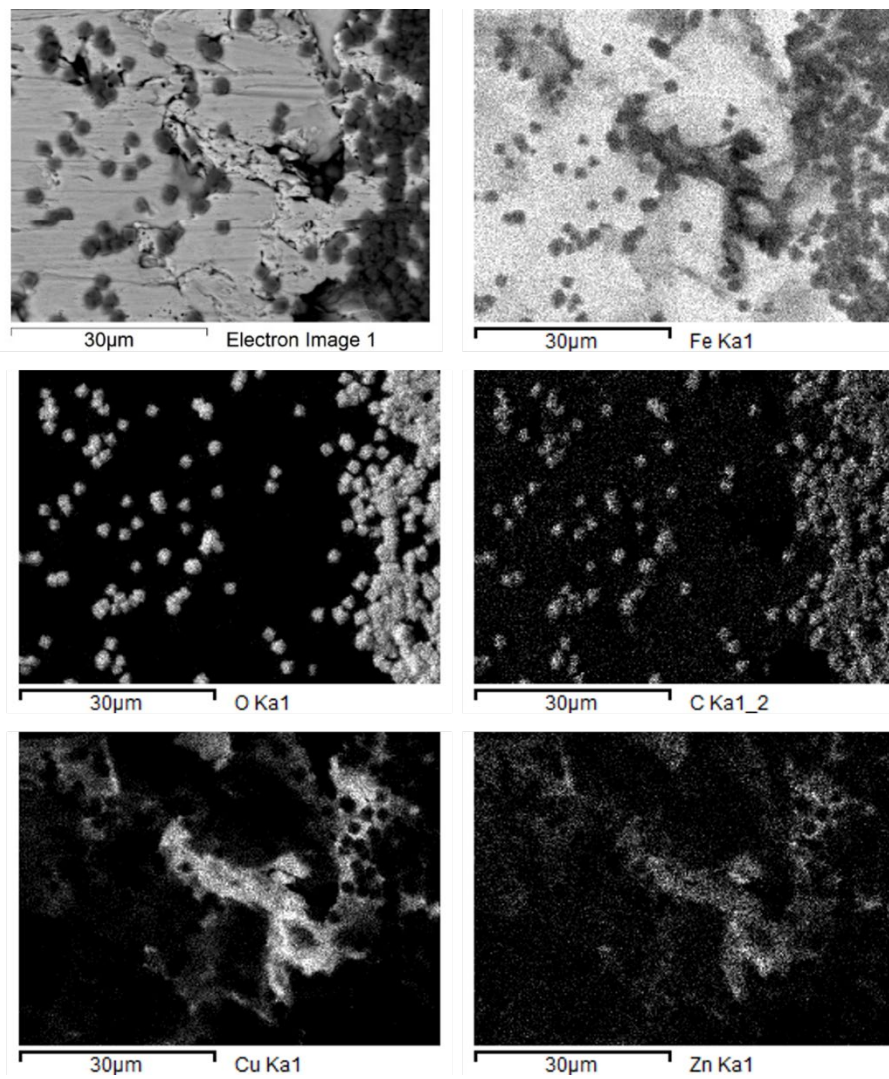
Figure 3-32. Backscattered electron micrograph (top left), at x2000 magnification, and elemental maps (Fe, O, C, Cu, and Zn) of a carbon steel specimen exposed to a dose rate of 100 Gy h^{-1} for 100 hours (CS3-8#4C).

EURAD (Deliverable n° 15.7) – Elucidation of critical irradiation parameter
Dissemination level: Public
Date of issue of this report: 06/02/2024

Page 57
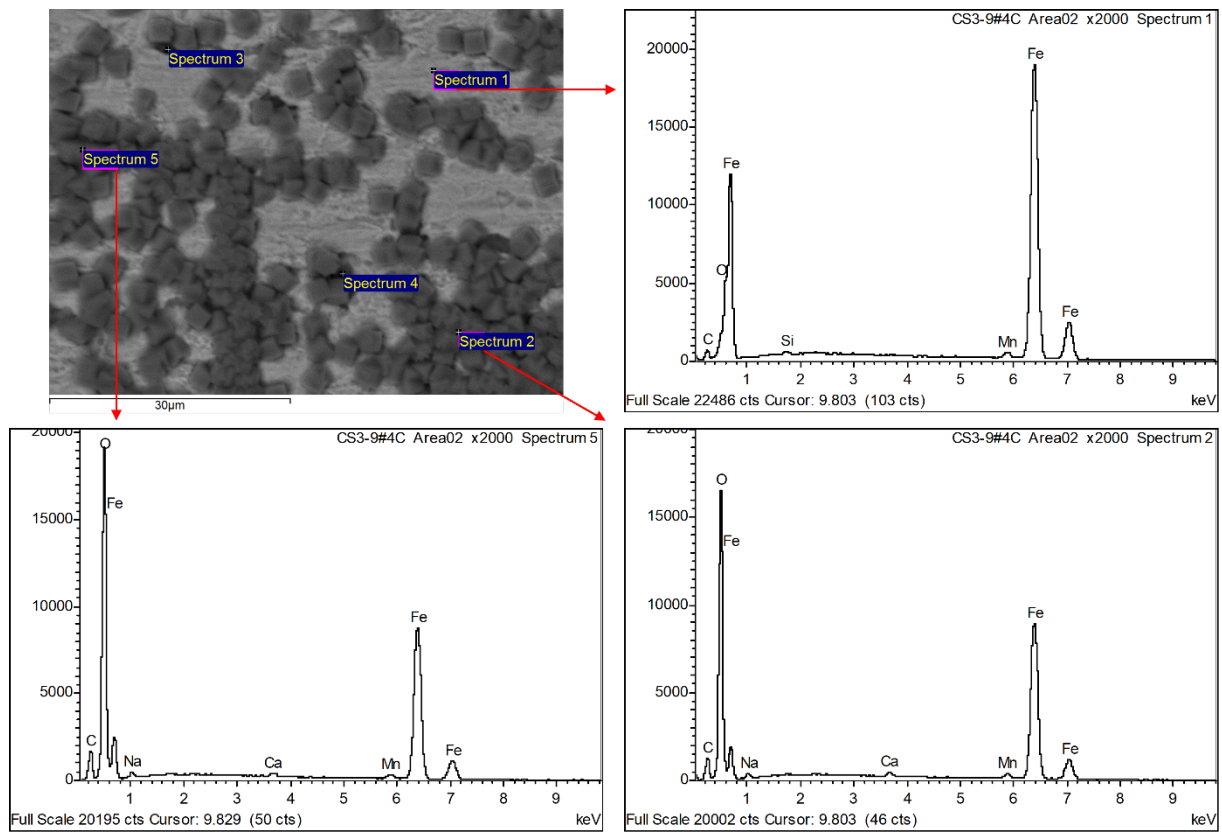
Figure 3-33. Backscattered electron micrograph, at x2000 magnification, of a carbon steel specimen (CS3-9#4C) exposed to a dose rate of 1000 Gy h^{-1} for 100 hours with EDX analysis areas illustrated (top left) and corresponding EDX spectra (top right and bottom).

EURAD (Deliverable n° 15.7) – Elucidation of critical irradiation parameter
Dissemination level: Public
Date of issue of this report: 06/02/2024

Page 58
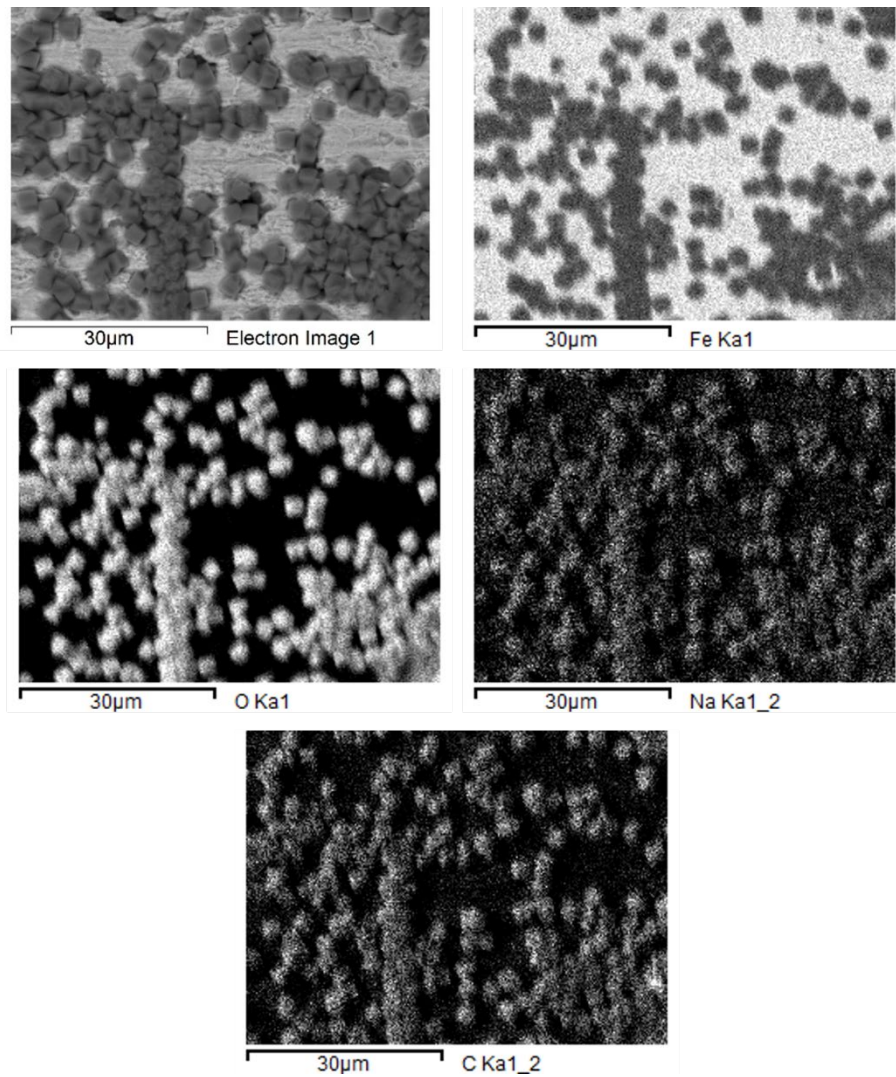
Figure 3-34. Backscattered electron micrograph (top left), at x2000 magnification, and elemental maps (Fe, O, Na, and C) of a carbon steel specimen exposed to a dose rate of 1000 Gy h^{-1} for 100 hours (CS3-9#4C).
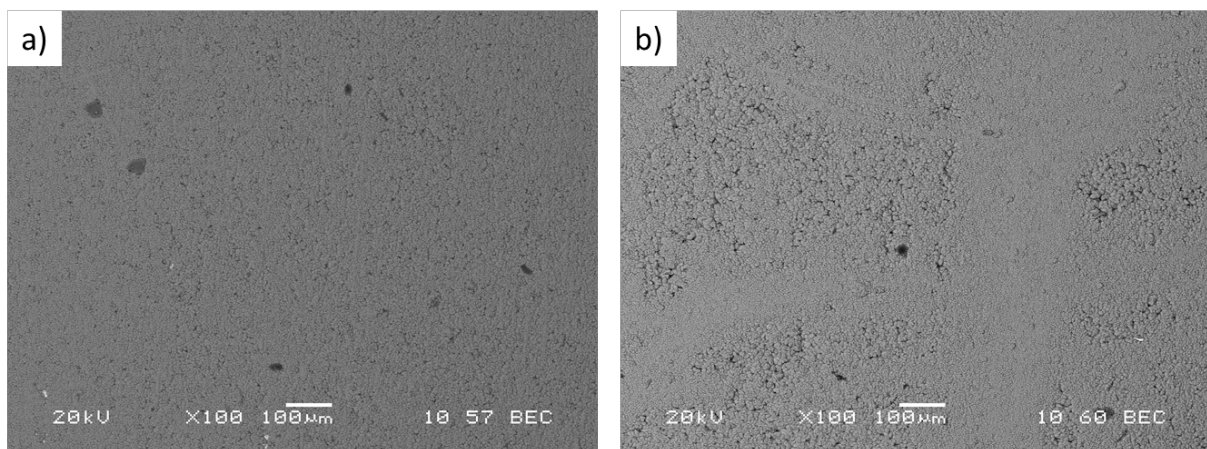
Figure 3-35. SEM-EDX backscattered electron image, at x100 magnification, of carbon steel specimens exposed to 5000 hours of radiation at: a) 0.2 Gy h^{-1} (CS5-3#2C) and b) 2 Gy h^{-1} (CS5-5#2).

EURAD (Deliverable n° 15.7) – Elucidation of critical irradiation parameter
Dissemination level: Public
Date of issue of this report: 06/02/2024

Page 59
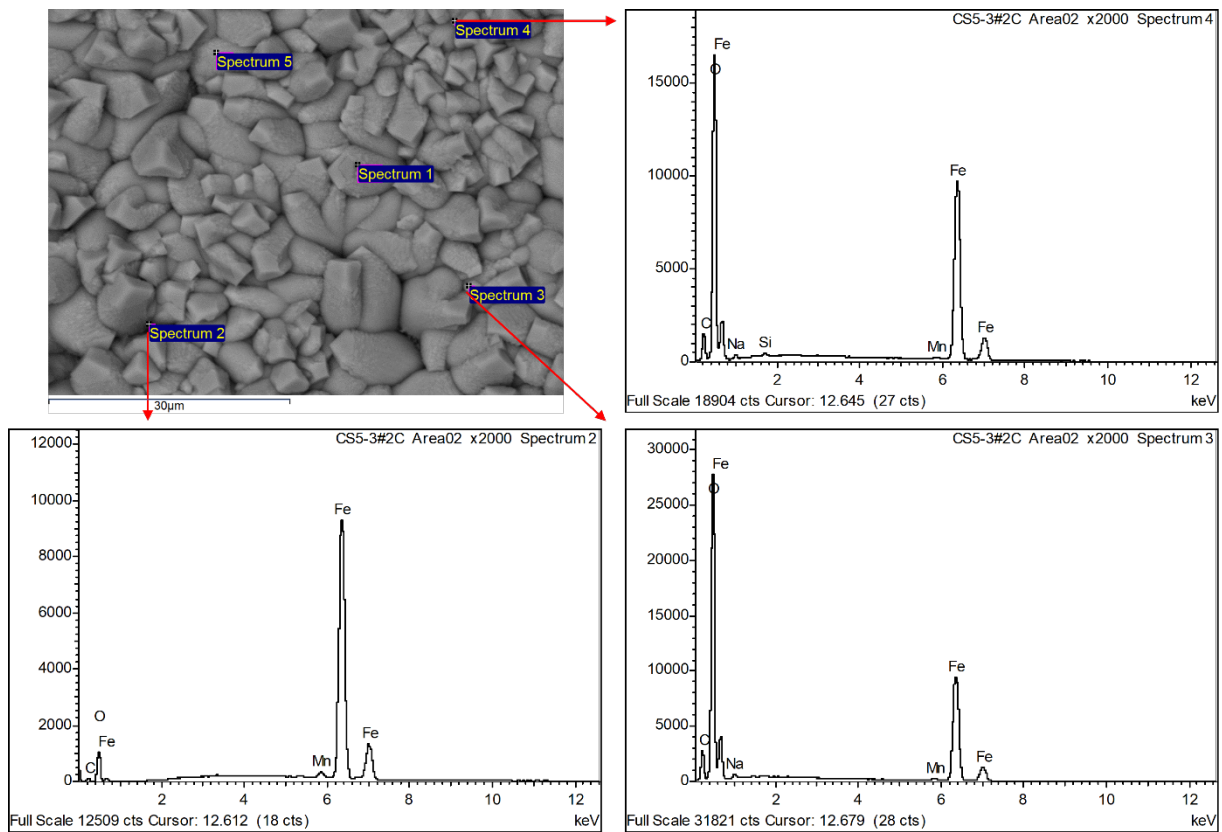
Figure 3-36. Backscattered electron micrograph, at x2000 magnification, of a carbon steel specimen (CS5-3#2C) exposed at a dose rate of 0.2 Gy h⁻¹ for 5000 hours with EDX analysis areas illustrated (top left) and corresponding EDX spectra (top right and bottom).

EURAD (Deliverable n° 15.7) – Elucidation of critical irradiation parameter
Dissemination level: Public
Date of issue of this report: 06/02/2024

Page 60
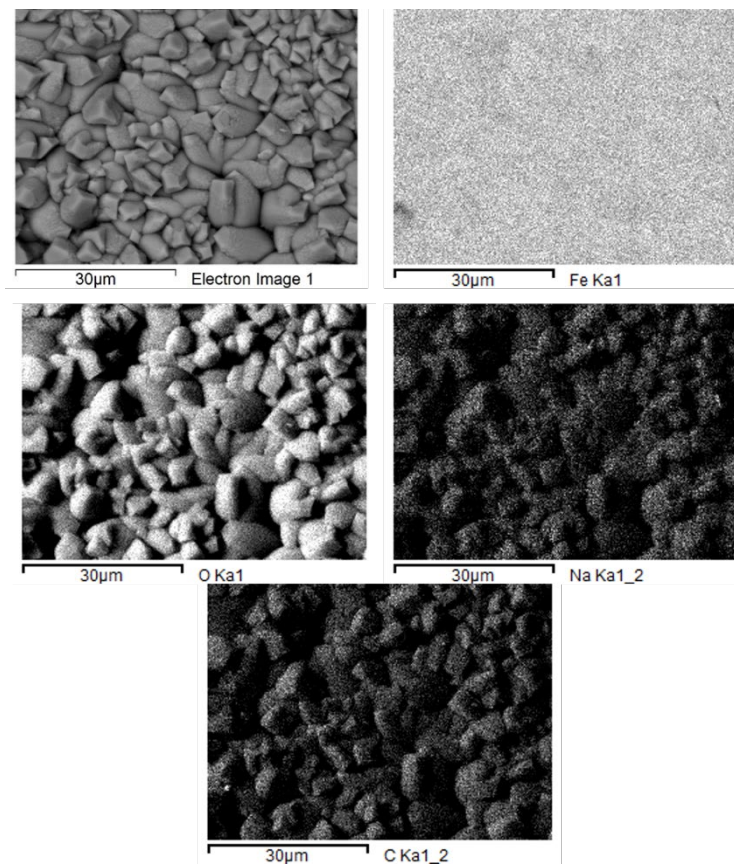
Figure 3-37. Backscattered electron micrograph (top left), at x2000 magnification, and elemental maps (Fe, O, Na, and C) of a carbon steel specimen exposed to a dose rate of 0.2 Gy h^{-1} for 5000 hours (CS5-3#2C).

EURAD (Deliverable n° 15.7) – Elucidation of critical irradiation parameter
Dissemination level: Public
Date of issue of this report: 06/02/2024

Page 61
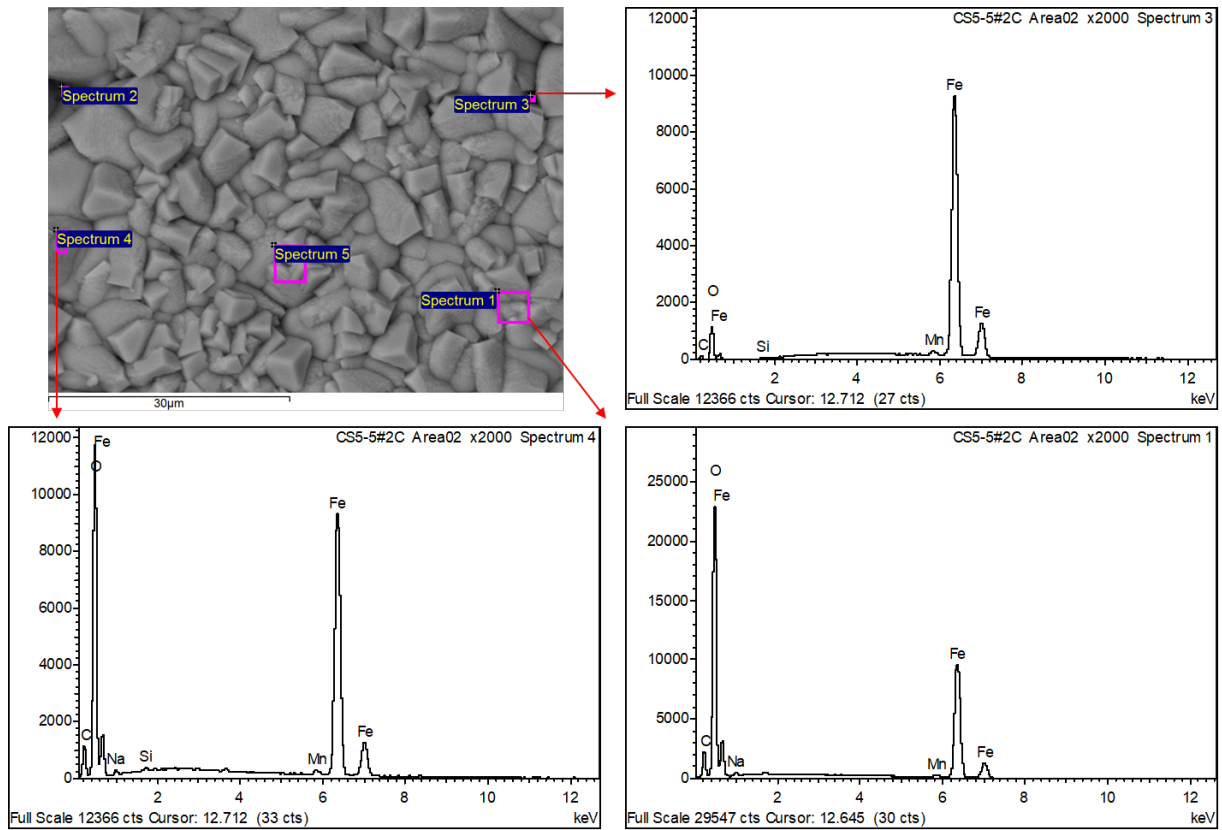
Figure 3-38. Backscattered electron micrograph, at x2000 magnification, of a carbon steel specimen (CS5-5#2C) exposed to a dose rate of 2 Gy h^{-1} for 5000 hours with EDX analysis areas illustrated (top left) and corresponding EDX spectra (top right and bottom).

EURAD (Deliverable n° 15.7) – Elucidation of critical irradiation parameter
Dissemination level: Public
Date of issue of this report: 06/02/2024

Page 62
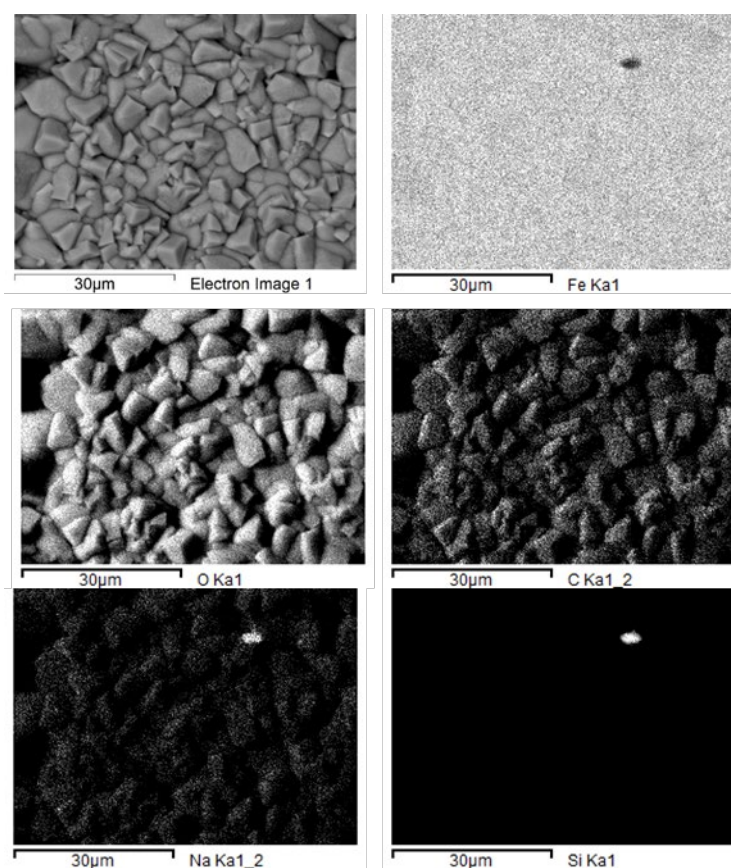
Figure 3-39. Backscattered electron micrograph (top left), at x2000 magnification, and elemental maps (Fe, O, C, Na, and Si) of a carbon steel specimen exposed to a dose rate of 2 Gy h^{-1} for 5000 hours (CS5-5#2C).

3.6 SEM-EDX in cross-section

3.6.1 Copper

In the following section cross-section SEM/EDX results are provided for wrought copper samples exposed for 100 h at dose rates of 0 and 10 Gy h^{-1} and 5000 h at dose rates of 0 and 0.2 Gy h^{-1}. Representative SEM images and EDX line scan elemental profiles for samples WC3-6 and WC5-3 are shown in Figure 3-40 to Figure 3-41. In summary all wrought copper specimens examined showed no evidence of corrosion products in cross-section. This is likely due to the sparce distribution of corrosion products as seen in the visual analysis in Section 3.4.1 not being captured in the cross-section.

After 100 h of exposure the unirradiated control and irradiated (10 Gy h^{-1}) wrought copper specimens (WC3-1 and WC3-6) showed no evidence of oxygen containing corrosion products when viewed in cross-section. A surface region approximately 1.4 μm deep was found to be enriched in carbon on the irradiated specimen. This region was not associated with any surface adhered corrosion product but embedded within the surface of the sample. It is believed this may be an artifact of the measurement of sample mounting procedure. This can be seen in the elemental profile line scan in Figure 3-40 where the carbon intensity peaks between 3 to 4 μm along the scan line.

Following 5000 hours of exposure, neither the unirradiated control specimen or the specimen exposed to a dose rate of 0.2 Gy h^{-1} (WC5-1 and WC5-3, respectively) exhibited any evidence of corrosion products on their surfaces. Both specimens had seemingly pristine copper surfaces with a sharp transition from the wrought copper metal to the epoxy resin as indicated by the elemental line scans of the irradiated sample WC5-3#1B (Figure 3-41). The irradiated sample (dose rate of 0.2 Gy h^{-1}) had a

EURAD (Deliverable n° 15.7) – Elucidation of critical irradiation parameter
Dissemination level: Public
Date of issue of this report: 06/02/2024

Page 63

small number of dark brown/black deposits on the surface, as described in Section 3.4.1. However, the cross-section that was prepared did not intersect any of the surface deposits, which is why it showed only a pristine copper surface.
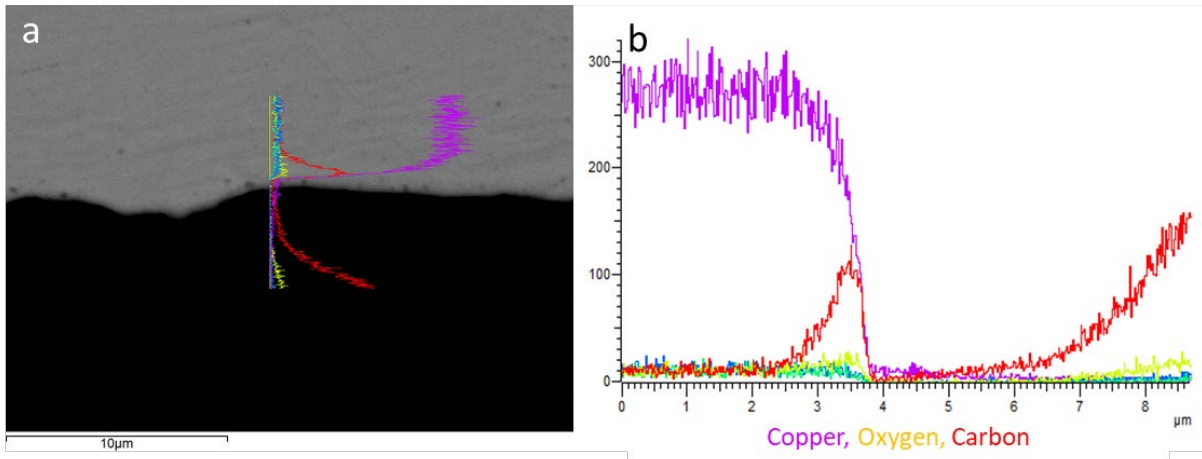
Figure 3-40. SEM backscattered electron image of a wrought copper specimen (WC3-6#2A) following exposure at a dose rate of 10 Gy h^{-1} for 100 hours, shown at x5000 magnification with a) EDX elemental line scan overlaid on scan path and b) same elemental line scan shown separately.
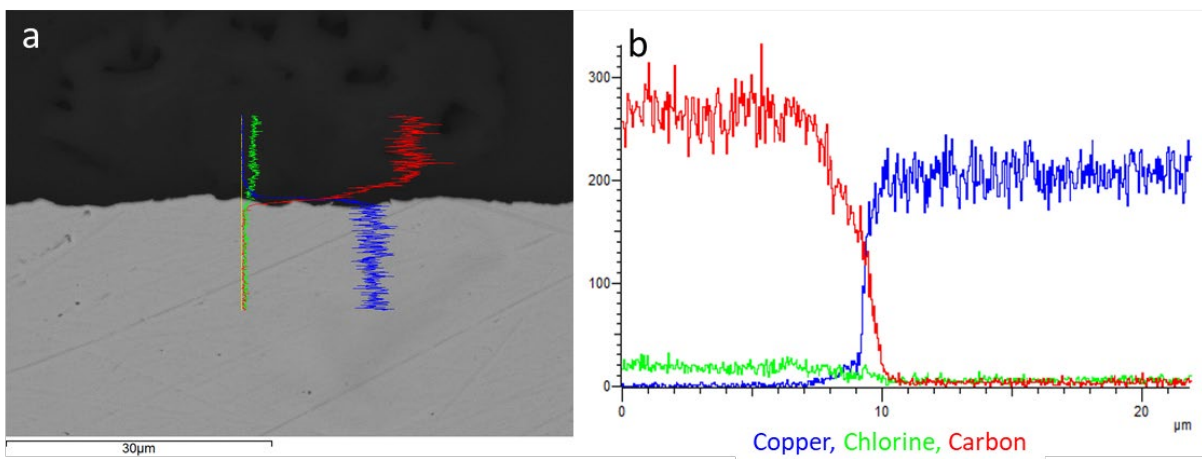
Figure 3-41. SEM backscattered electron image of a wrought copper specimen (WC5-3#1B) following exposure at a dose rate of 0.2 Gy h^{-1} for 5000 hours, shown at x5000 magnification with a) EDX elemental line scan overlaid on scan path and b) same elemental line scan shown separately.

3.6.2 Carbon steel

Cross-section SEM/EDX results for carbon steel samples are presented for unirradiated specimens and specimens exposed to either 1 kGy or 10 kGy total dose. A summary of observations made can be found in Table 3-7. Representative SEM images and line scan elemental profiles for carbon steel samples exposed for 10 h at 1000 Gy h^{-1}, 100 h at 0 and 10 Gy h^{-1}, and 5000 h at 0, 0.2, and 0.2 Gy h^{-1} are presented in Figure 3-42 to Figure 3-48.

EURAD (Deliverable n° 15.7) – Elucidation of critical irradiation parameter
Dissemination level: Public
Date of issue of this report: 06/02/2024

Page 64

Table 3-7. Summary of results from cross-section SEM/EDX analysis spectroscopy analysis of carbon steel samples analysed. The total dose received in each condition is highlighted in bold.

Exposure Duration (h)	Dose Rate (Gy h⁻¹)								
	0	0.1	0.2	1	2	10	20	100	1000
1									**1 kGy** No oxide
14								**1 kGy** No oxide.	**10 kGy** One oxide particle observed on one analysis area.
100	**0 kGy** ~ 1 µm thick patchy oxide. Carbon found in corrosion layer.					**1 kGy** ~ 2 µm thick patchy oxide. Carbon found in corrosion layer.		**10 kGy** ~ 2 µm thick patchy oxide. Carbon found in corrosion layer.	**100 kGy** No oxide
1000									
5000	**0 kGy** ~ 6 µm thick continuous oxide layer.		**1 kGy** ~ 6 µm thick continuous oxide layer.		**10 kGy** ~ 6 µm thick continuous oxide layer.		**100 kGy** ~ 6 µm thick continuous oxide layer.		
10000									

After the shortest exposure durations of 1 and 10 h little or no evidence of corrosion were observed in cross-section. No corrosion products were observed after one hour exposure at a dose rate of 1000 Gy h^{-1} (CS1-9). Similarly, no corrosion products were observed after 10 h exposure at 100 Gy h^{-1} (CS2-8). After 10 h exposure at the highest dose rate of 1000 Gy h^{-1} one scan area presented with tentative evidence of oxygen containing corrosion species on the surface (Figure 3-42). A small peak in oxygen and iron intensity occurred between 2.5 – 3.5 μm along the line scan in Figure 3-43 coinciding with a small particle separated from the sample surface observed in the SEM image in Figure 3-42.

More significant amounts of corrosion products start to become observable after 100 h of exposure. The SEM image and line scans of the unirradiated CS3-1 (Figure 3-44) shows oxygen and iron co-locating with particles on the surface, indicative of oxygen containing corrosion products. These corrosion products had a patchy distribution across the surface with an average thickness of 1.4 μm. Although lower in intensity compared to the mounting epoxy resin, carbon is also found in the cross-section of these corrosion products, corroborating the identification of carbon within the corrosion products from the surface SEM/EDX analysis in section 3.5.2. As discussed in the aforementioned section, the exact form carbon takes within the corrosion product region will require additional chemical analysis from XPS and Raman spectroscopy before its state can be confidently identified.

At 10 Gy h^{-1} similar corrosion products are observed (see CS3-6#5A in Figure 3-45), however with a higher surface coverage compared to the 0 Gy h^{-1} control sample (CS3-1#1A). Oxygen, iron, and carbon were again found to co-locate across these particles and measurements from SEM images showed these particles to be on average 2.0 μm thick. Increasing the dose rate to 100 Gy h^{-1} after 100 h exposure did not significantly increase the coverage or thickness of the corrosion product. The corrosion product layer of CS3-8 was also composed of iron, oxygen, and carbon. The SEM cross-section of carbon steel exposed to a dose rate of 1000 Gy h^{-1}, interestingly, showed no corrosion product on the surface; however, surface SEM/EDX analysis in Section 3.5.2 of the same sample showed corrosion products covering the surface with a patchy distribution. It is assumed that the cross-section taken happened to be devoid of any corrosion products.

All cross-section SEM images of 5000 h exposure samples (Figure 3-46 to Figure 3-48) show a continuous corrosion product layer and line scans showed corrosion products were composed of iron, oxygen and carbon on all samples. Interestingly, the intensity of carbon relative to iron and oxygen in the corrosion product was lower on the 5000 h samples compared to the 100 h samples, indicating proportionately less integration of these carbon species in the corrosion product layer at longer durations. The corrosion product layers also appeared to be thicker on the 5000 h samples compared to 100 h samples. It is difficult to consistently measure the thickness of the corrosion layer where the height of the steel surface changes due to the rough surface; however, the control sample appeared notably thinner at 6.5 μm on average compared to the irradiated samples which ranged from 7.0 – 8.0 μm on average.

Corrosion appeared to increase the roughness of steel samples exposed for 5000 h at a dose rate of 0 Gy h^{-1} with local thickness losses in the range of 1.9 to 6.2 μm in depth across all thee different scan areas. When exposed to a dose rate of 0.2 Gy h^{-1} the depth localised material loss increased on average and the steel surface appeared visually rougher. This can be seen on sample CS5-3#2A in Figure 3-47 where the cross-section of a region of local material loss of 7.5 μm can be seen accompanied by a rougher surface. Similarly features were also seen when exposed to dose rates of 2 Gy h^{-1} (see Figure 3-48) and 20 Gy h^{-1} (data not presented in this report). The presence of corrosion product in the regions around these features suggests that they are not corrosion pits but are more likely to be uneven general corrosion.

EURAD (Deliverable n° 15.7) – Elucidation of critical irradiation parameter
Dissemination level: Public
Date of issue of this report: 06/02/2024

Page 66
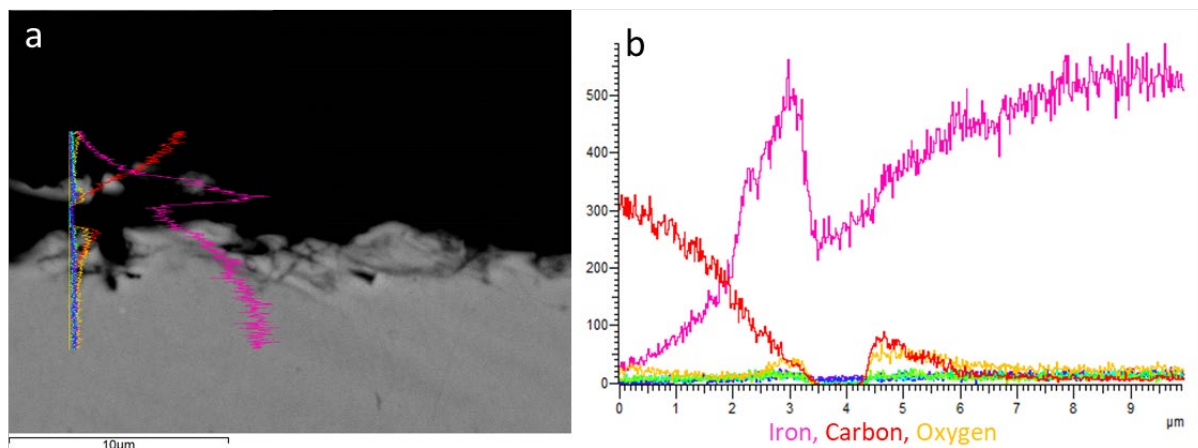
Figure 3-42. SEM backscattered electron image of a carbon steel specimen (CS2-9#2C) following exposure at a dose rate of 1000 Gy h^{-1} for 10 hours, shown at x5000 magnification with a) EDX elemental line scan overlaid on scan path and b) same elemental line scan shown separately.
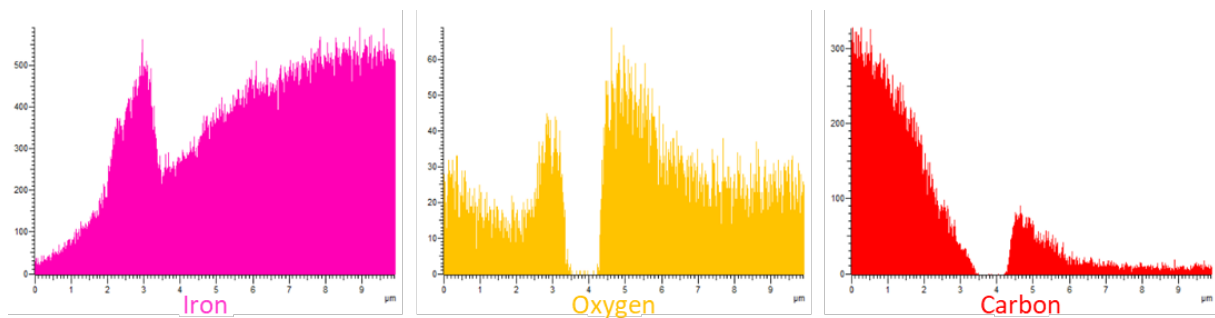
Figure 3-43. Individual elemental line scans of iron, oxygen and carbon for a carbon steel specimen (CS2-9#2C) following exposure to a dose rate of 1000 Gy h^{-1} for 10 h.

EURAD (Deliverable n° 15.7) – Elucidation of critical irradiation parameter
Dissemination level: Public
Date of issue of this report: 06/02/2024

Page 67
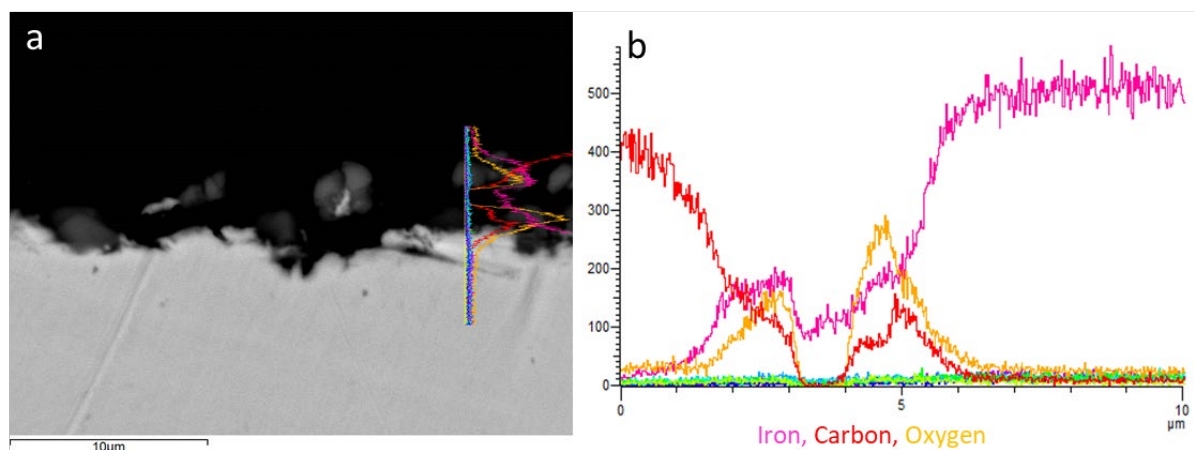
Figure 3-44. SEM backscattered electron image of a carbon steel specimen (CS3-1#1A) following exposure at a dose rate of 0 Gy h^{-1} for 100 hours, shown at x5000 magnification with a) EDX elemental line scan overlaid on scan path and b) same elemental line scan shown separately.
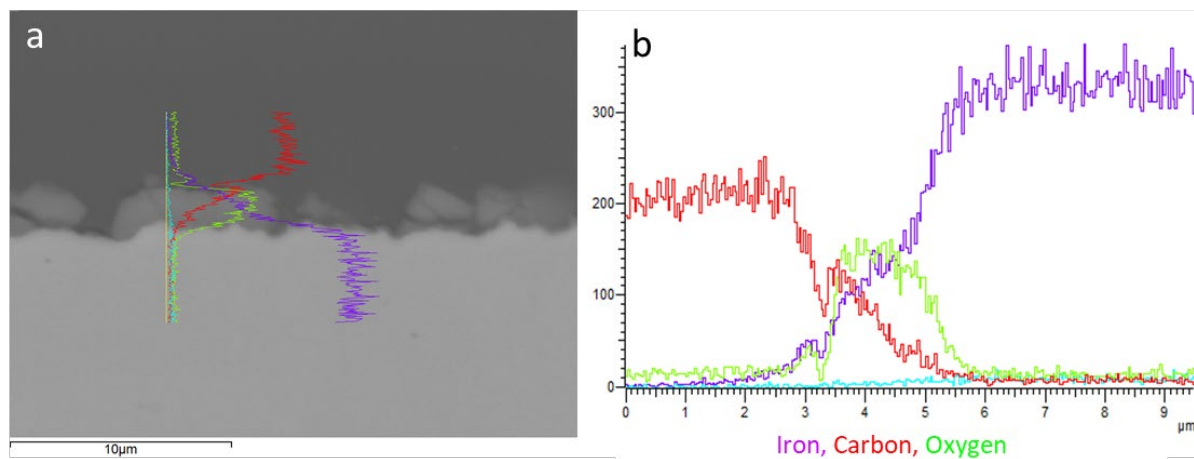
Figure 3-45. SEM backscattered electron image of a carbon steel specimen (CS3-6#5A) following exposure at a dose rate of 10 Gy h^{-1} for 100 hours, shown at x5000 magnification with a) EDX elemental line scan overlaid on scan path and b) same elemental line scan shown separately.

EURAD (Deliverable n° 15.7) – Elucidation of critical irradiation parameter
Dissemination level: Public
Date of issue of this report: 06/02/2024

Page 68
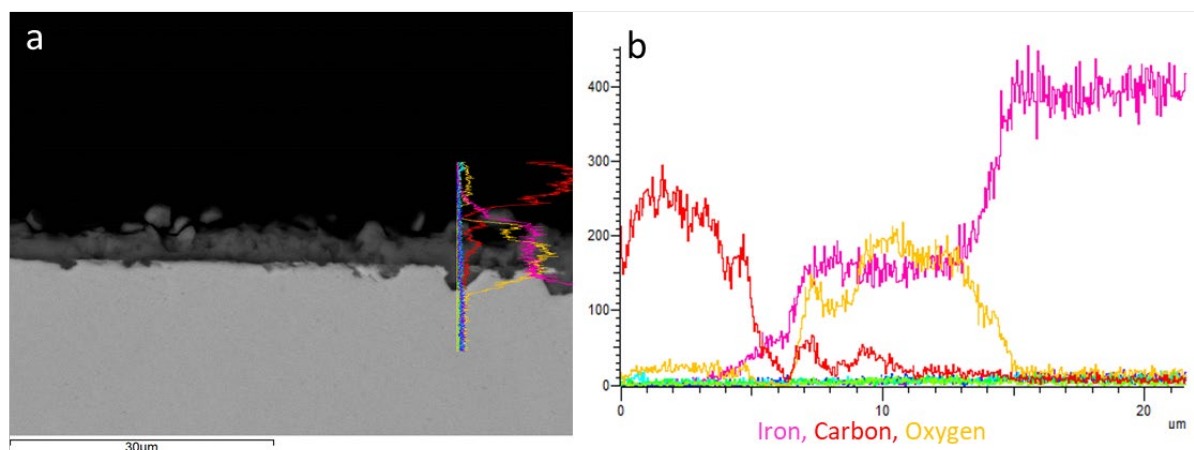
Figure 3-46. SEM backscattered electron image of a carbon steel specimen (CS5-1#4A) following exposure at a dose rate of 0 Gy h^{-1} for 5000 hours, shown at x5000 magnification with a) EDX elemental line scan overlaid on scan path and b) same elemental line scan shown separately.
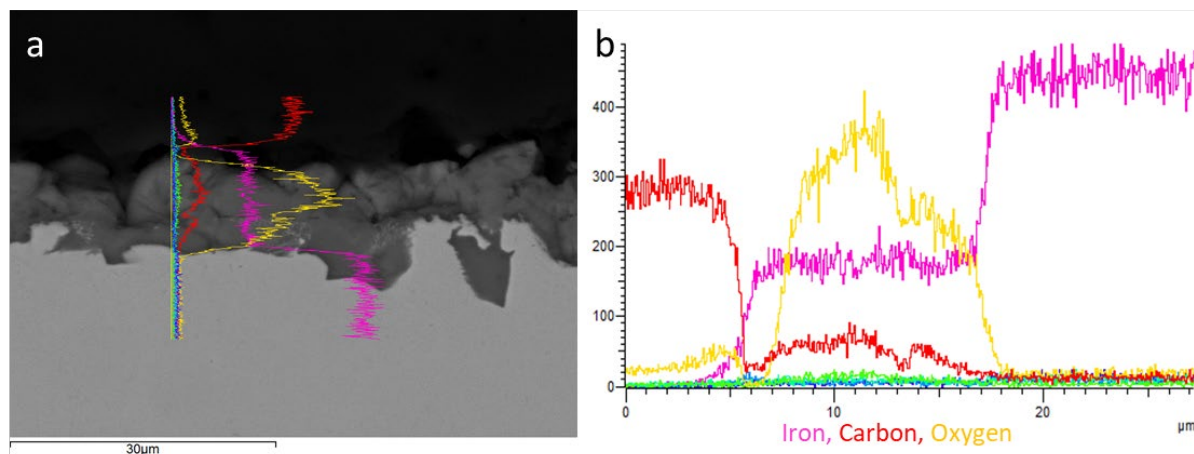
Figure 3-47. SEM backscattered electron image of a carbon steel specimen (CS5-3#2A) following exposure at a dose rate of 0.2 Gy h^{-1} for 5000 hours, shown at x2000 magnification with a) EDX elemental line scan overlaid on scan path and b) same elemental line scan shown separately.

EURAD (Deliverable n° 15.7) – Elucidation of critical irradiation parameter
Dissemination level: Public
Date of issue of this report: 06/02/2024

Page 69
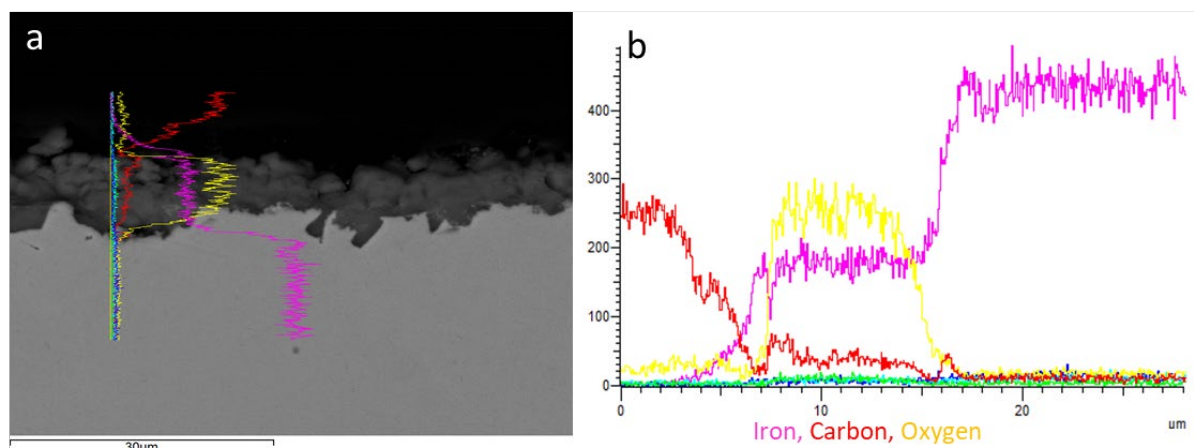
Figure 3-48. SEM backscattered electron image of a carbon steel specimen (CS5-5#2A) following exposure at a dose rate of 2 Gy h⁻¹ for 5000 hours, shown at x2000 magnification with a) EDX elemental line scan overlaid on scan path and b) same elemental line scan shown separately.

3.7 Raman spectroscopy

3.7.1 Copper

Raman spectroscopy was conducted on two wrought copper samples, one exposed for 100 h at a dose rate of 10 Gy h⁻¹ and another for 5000 h at 0.2 Gy h⁻¹. Both samples were exposed to a total dose of 1 kGy and Raman spectra of the 5000 h sample can be found in Figure 3-49. All Raman peaks identified in the spectra of wrought copper samples are tabulated in Table 3-8 with peak assignment and confidence values listed. A summary of what corrosion products were identified on each sample analysed is given in Table 3-9.

The Raman spectra of wrought copper samples irradiated at 10 Gy h⁻¹ for 100 h were dominated by a fluorescent background with very little or no Raman scattered bands apparent (spectra not presented here). Only one scan area presented with broad Raman scattering bands, but these could not be assigned to any specific corrosion product. After 5000 h exposure at a dose rate of 0.2 Gy h⁻¹ the majority of the copper surface appeared pristine with a small number of dark brown/black spots which were included in the Raman analysis. Spectra taken from the pristine surface shown in Figure 3-49b are similar to that taken of samples exposed at 100 h with a broad rising fluorescence background with no distinctive Raman scattering bands. A small peak was observed at 1080 cm⁻¹ and could be ascribed to trace amounts of carbonate species on the surface. Another small peak at 325 cm⁻¹ was also observed but this could not be assigned to any specific species. Raman spectra of the dark spot on the same sample (WC5-3#1C, 5000 h, 0.2 Gy h⁻¹ dose rate) in Figure 3-49a had well defined Raman bands at 145, 200, 220, 415, 530 and 625 cm⁻¹, all characteristic of cuprite (Cu_2O) and were assigned as so. In addition to the cuprite characteristic peaks, a low intensity peak at 1080 cm⁻¹ was also observed and is characteristic of carbonate species, potentially sodium bicarbonate from the buffer solution.

EURAD (Deliverable n° 15.7) – Elucidation of critical irradiation parameter
Dissemination level: Public
Date of issue of this report: 06/02/2024

Page 70
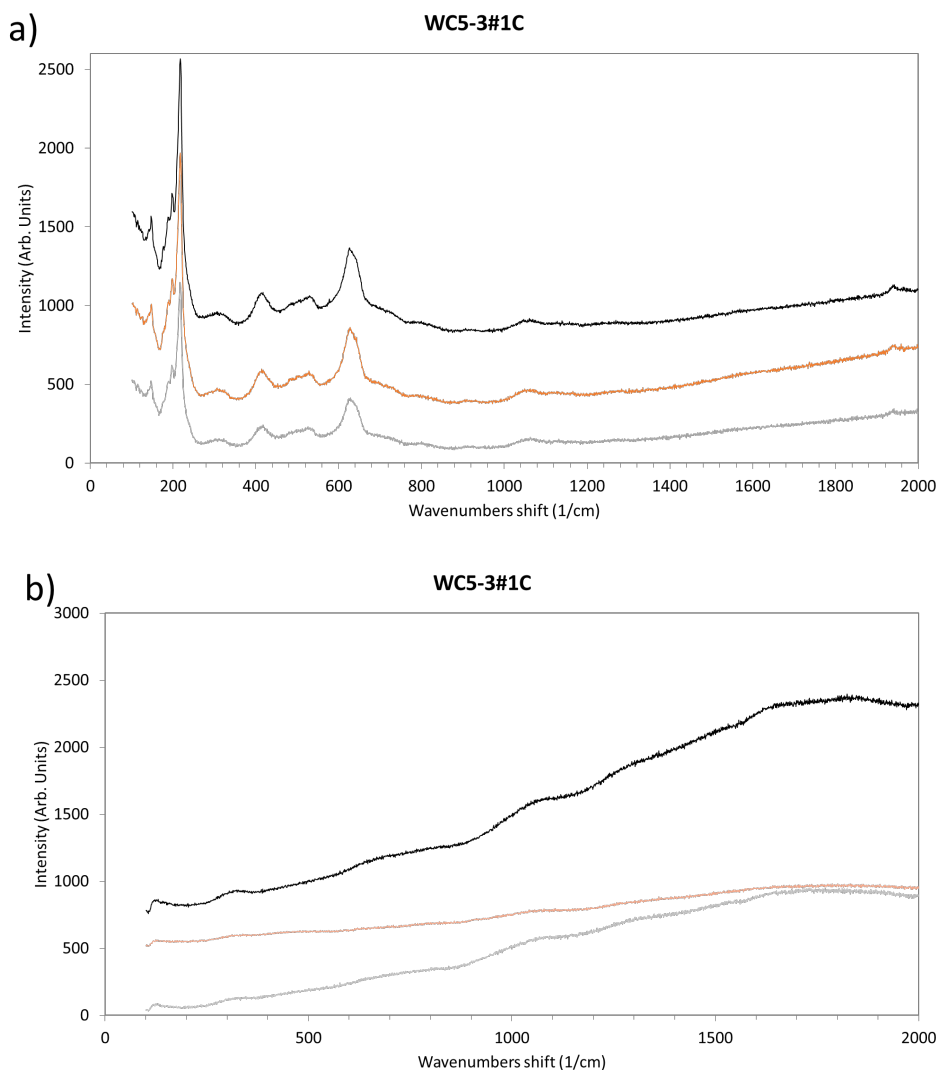
Figure 3-49. Raman spectra obtained from wrought copper sample exposed to a dose rate of 0.2 Gy h^{-1} for 5000 hours (WC5-3#1C). a) spectrum taken of the dark spot and b) spectrum of the pristine area shown in Figure 3-25.

EURAD (Deliverable n° 15.7) – Elucidation of critical irradiation parameter
Dissemination level: Public
Date of issue of this report: 06/02/2024

Page 71

Table 3-8. A list of identified peaks and corresponding Raman active compounds on wrought copper samples exposed for 100 and 5000 h with the confidence in peak assignment listed (L = low, M = medium, H = high). Unidentifiable peaks have been omitted from the table.

Peak cm^{-1}	Assignment	Confidence
145	Cuprite (Cu_2O)	H
200	Cuprite (Cu_2O)	H
220	Cuprite (Cu_2O)	H
415	Cuprite (Cu_2O)	H
530	Cuprite (Cu_2O)	H
625	Cuprite (Cu_2O)	H

EURAD (Deliverable n° 15.7) – Elucidation of critical irradiation parameter
Dissemination level: Public
Date of issue of this report: 06/02/2024

Page 72

Table 3-9. Summary of compounds identified from Raman spectroscopy analysis of wrought copper samples analysed. The total dose received in each condition is highlighted in bold.

Exposure Duration (h)	Dose Rate (Gy h^{-1})								
	0.0	0.1	0.2	1	2	10	20	100	1000
1									
10									
100						**1 kGy** None			
1000									
5000			**1 kGy** Cuprite						
10000									

3.7.2 Carbon steel

The following section includes the Raman spectra for samples exposed for 100 h to a dose rate of 10, 100, and 1000 Gy h^{-1} (total doses of 1 kGy, 10 kGy, and 100 kGy respectively) in addition to 5000 h exposure samples exposed to 0.2 and 2 Gy h^{-1} (1 kGy and 10 kGy respectively). Table 3-10 summarises the compounds identified by Raman spectroscopy for the different test conditions of the specimens that were analysed. Raman spectra for 100 h samples can be found in Figure 3-50 and 5000 h samples in Figure 3-51. Table 3-11 lists the Raman peaks identified and their assignment.

Peaks at 185, 285, 740, 1080, and 1440 cm^{-1} were found on all irradiated carbon steel samples examined and were characteristic of siderite. The peak at 1080 cm^{-1} is specifically characteristic of carbonate and therefore could also include contribution from other carbonate species such as sodium bicarbonate from the buffer solution. Goethite was also found on the surface of the irradiated carbon steel samples with characteristic peaks found at 285, 380, 480, and 560 cm^{-1}. Both siderite and goethite were assigned with high confidence considering that the majority of expected peaks were observed were well defined and at the expected wavenumber. Maghemite was tentatively identified on carbon steel exposed to a dose rate of 1000 Gy h^{-1} for 100 h (CS3-9#4C).

EURAD (Deliverable n° 15.7) – Elucidation of critical irradiation parameter
Dissemination level: Public
Date of issue of this report: 06/02/2024

Page 74

Table 3-10. Summary of compounds identified from Raman spectroscopy analysis of carbon steel samples analysed. The total dose received in each condition is highlighted in bold.

Exposure Duration (h)	Dose Rate (Gy h⁻¹)								
	0.0	0.1	0.2	1	2	10	20	100	1000
1									
10									
100						**1 kGy** siderite goethite		**10 kGy** siderite goethite	**100 kGy** siderite goethite maghemite
1000									
5000			**1 kGy** siderite goethite		**10 kGy** siderite goethite				
10000									

Figure 3-50. Raman spectra obtained from carbon steel samples exposed for 100 h to a dose rate of a) 10 Gy h^{-1} (CS3-6#5C), b) 100 Gy h^{-1} (CS3-8#4C), and 1000 Gy h^{-1} (CS3-9#4C).

EURAD (Deliverable n° 15.7) – Elucidation of critical irradiation parameter
Dissemination level: Public
Date of issue of this report: 06/02/2024

Page 76
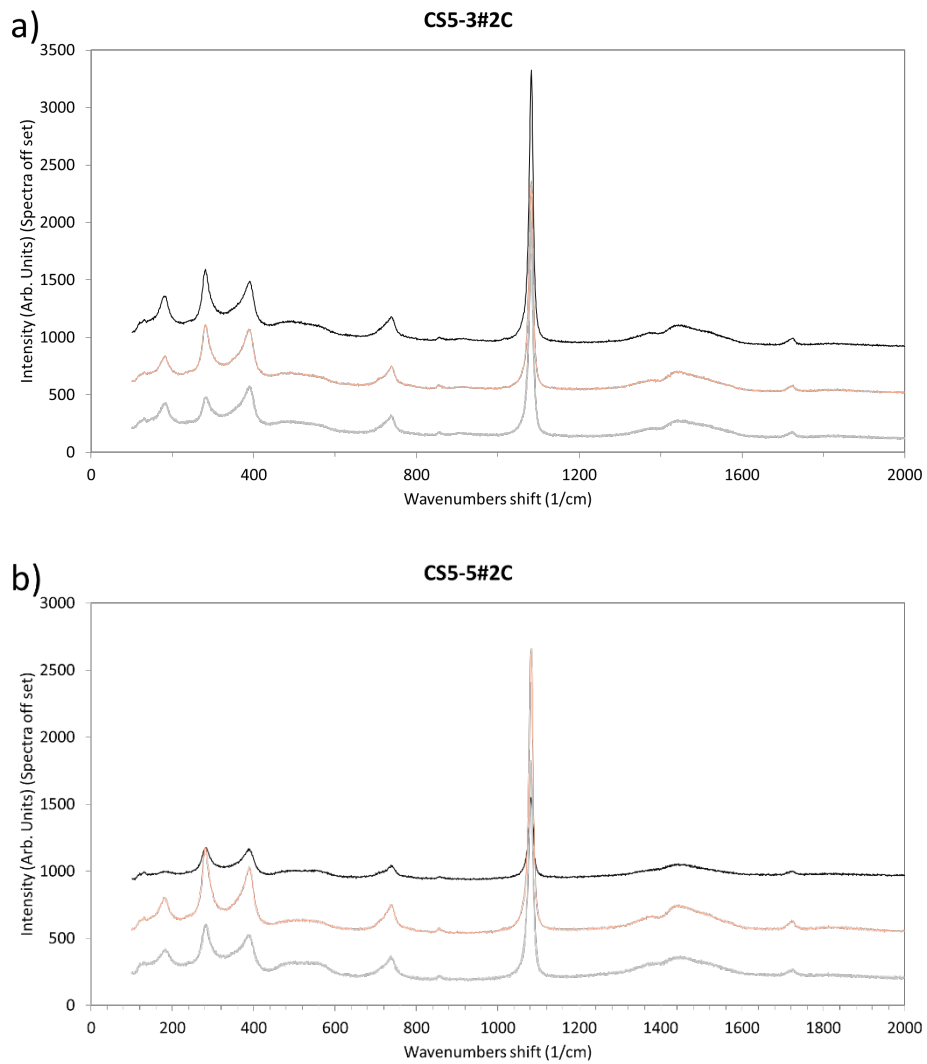
Figure 3-51. Raman spectra obtained from carbon steel samples exposed for 5000 h to a dose rate of a) 0.2 Gy h^{-1} (CS5-3#2C) and b) 2 Gy h^{-1} (CS5-5#2C).

EURAD (Deliverable n° 15.7) – Elucidation of critical irradiation parameter
Dissemination level: Public
Date of issue of this report: 06/02/2024

Page 77

Table 3-11. A list of identified peaks and corresponding Raman active compounds on carbon steel samples exposed for 100 and 5000 h with the confidence in peak assignment listed (L = low, M = medium, H = high). Unidentifiable peaks have been omitted from the table.

Peak cm-1	Coupon number and analysis area	Assignment	Confidence
180	CS3-6#5C (Left)	Siderite	H
	CS3-8#4C (Left)	Siderite	H
	CS3-9#4C (Left)	Siderite	H
210	CS3-9#4C (Right)	Maghemite	M
285	CS3-6#5C (Left)	Siderite/Goethite	H
	CS3-8#4C (Left)	Siderite/Goethite	H
	CS3-9#4C (Left)	Siderite/Goethite	H
	CS3-9#4C (Right)	Maghemite	M
380	CS3-6#5C (Left)	Goethite	H
	CS3-8#4C (Left)	Goethite	H
	CS3-9#4C (Left)	Goethite	H
390	CS3-9#4C (Right)	Maghemite	M
480	CS3-6#5C (Left)	Goethite	H
	CS3-8#4C (Left)	Goethite	H
	CS3-9#4C (Left)	Goethite	H
560	CS3-6#5C (Left)	Goethite	H
	CS3-8#4C (Left)	Goethite	H
	CS3-9#4C (Left)	Goethite	H
740	CS3-6#5C (Left)	Siderite	H
	CS3-8#4C (Left)	Siderite	H
	CS3-9#4C (Left)	Siderite	H
1080	CS3-6#5C (Left)	Siderite/Carbonate	H
	CS3-8#4C (Left)	Siderite/Carbonate	H
	CS3-9#4C (Left)	Siderite/Carbonate	H
1325	CS3-9#4C (Right)	Maghemite	L
1440	CS3-6#5C (Left)	Siderite	L
	CS3-8#4C (Left)	Siderite	L
	CS3-9#4C (Left)	Siderite	L

3.8 XPS

The XPS analysis was focused on wrought copper and carbon steel samples exposed for 100 h. Wrought copper was only exposed to a dose rate of 10 Gy h^{-1} at this duration and a mixture of copper metal and Cu_2O were identified on the surface indicating a thin copper (I) oxide film on the surface in the region of nanometres thick. A mixture of Fe(II) and Fe(III) oxidation state species were identified on all carbon steel samples. Fe_3O_4 was identified as the likely source of Fe(II) species however it could not be determined whether Fe_2O_3 or $Fe(O)OH$ was the main source of Fe(III) species. Comparison of the Fe(III):Fe(II) ratios found Fe(III) species increased in proportion to Fe(II) species at higher dose rates.

EURAD (Deliverable n° 15.7) – Elucidation of critical irradiation parameter
Dissemination level: Public
Date of issue of this report: 06/02/2024

Page 78

3.8.1 Copper

The following section examines the XPS analysis of wrought copper exposed for 100 h at a dose rate of 10 Gy h^{-1} (WC3-6). The Cu2p and CuL$_3$M$_{45}$M$_{45}$ XPS spectra for WC3-6#2B are presented in Figure 3-52, C1s and O1s spectra in Figure 3-53, and snapshot spectra of CuL$_3$M$_{45}$M$_{45}$ taken during depth profiling are shown in Figure 3-54. Table 3-12 presents the surface composition of the sample before and after depth profiling.

Pre-depth profile the majority of the surface is composed of carbon, oxygen, and copper with small contributions of sulphur and chlorine. Inspection of the C1s spectrum (see Figure 3-53) indicates the carbon species present are adventitious in nature. The Cu2p spectrum in Figure 3-52 indicated either Cu(I) or Cu(0) species were the only copper species present and the CuL$_3$M$_{45}$M$_{45}$ Auger spectrum identified the copper species as a mixture of Cu$_2$O and Cu(0). Considering the amount of Cu(0) (> 50 % of copper species) detected within the inherent 10 nm analysis depth of XPS, one could infer that the Cu$_2$O is present as a thin film in the region of nanometres thick on top of the copper metal. This nanometre thin copper oxide could originate from the corrosion processes taking place during exposure or it could have been a pre-existing oxide present on the pristine sample. One cannot definitively state whether the oxide was pre-existing or formed during exposure, however the tendency for the corrosion products to form thick, isolated regions as seen in the visual analysis in section 3.4 would suggest it was pre-existing.

Results from the depth profile support this hypothesis where the snapshot spectrum of the CuL$_3$M$_{45}$M$_{45}$ Auger peak pre-depth profile was composed of equal amounts of Cu$_2$O and Cu(0). However, after the first etch cycle the Cu$_2$O component rapidly decreased, contributing 16 % and indicating it was only present in the top few nanometres of the sample surface. The sulphur concentration was 3.2 at.% prior to depth profiling and its binding energy was consistent with sulphide species. Chlorine was present in trace concentrations and was tentatively assigned as a metal chlorine due to the low peak intensity and uncertainty in peak binding energy.

Table 3-12 Surface composition for wrought copper specimen WC3-6#2B (100 h exposure, 10 Gy h^{-1} dose rate), pre- and post-depth profile (DP).

Sample		Concentration at.%				
		C	O	Cu	S	Cl
WC3-6#2B	Pre-DP	51.4	23.0	22.0	3.2	0.3
	Post-DP	2.5	2.5	95.1	-	-

EURAD (Deliverable n° 15.7) – Elucidation of critical irradiation parameter
Dissemination level: Public
Date of issue of this report: 06/02/2024

Page 79
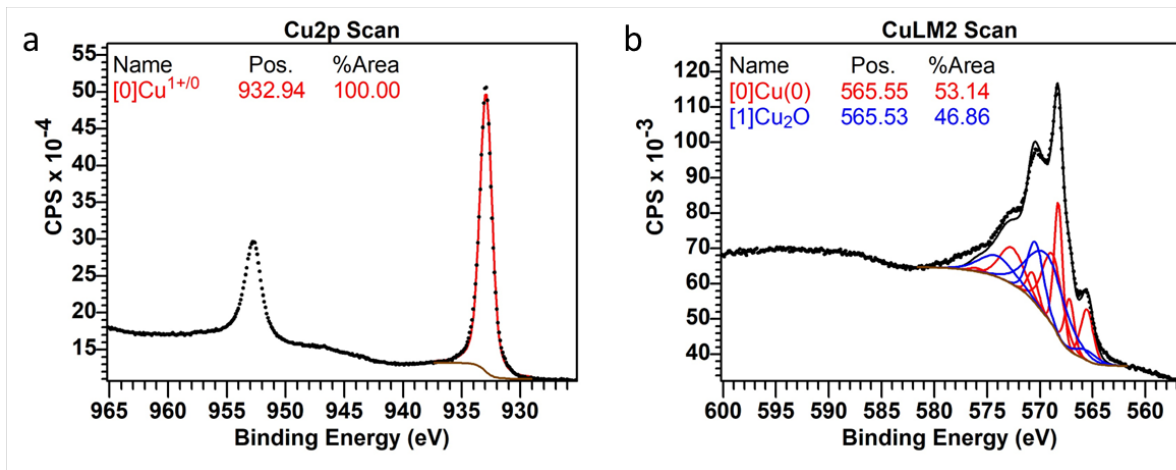
Figure 3-52. a) Cu2p and b) $CuL_3M_{45}M_{45}$ XPS spectra pre-depth profile of wrought copper sample exposed for 100 h at 10 Gy h^{-1} (WC3-6#2B).
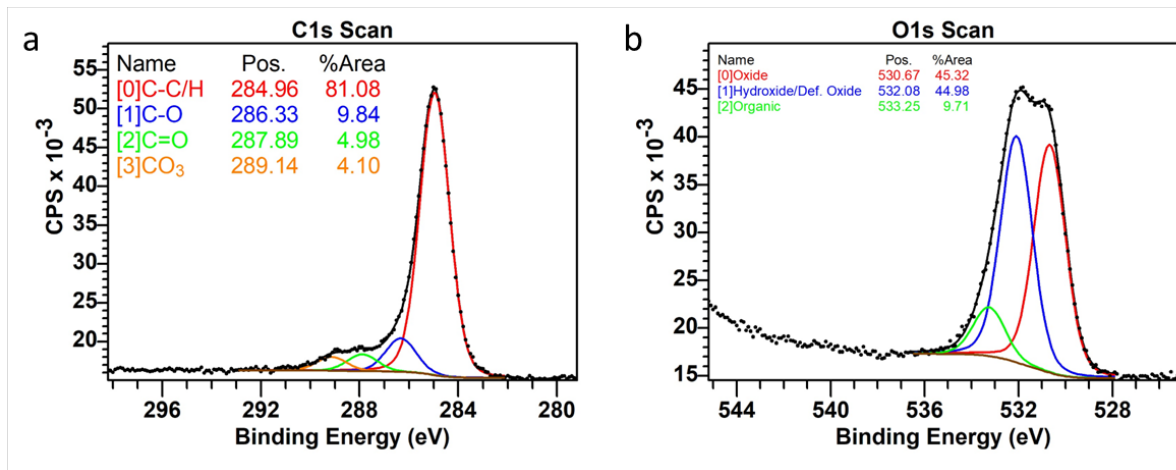
Figure 3-53. a) C1s and b) O1s XPS spectra pre-depth profile of wrought copper sample exposed for 100 h at 10 Gy h^{-1} (WC3-6#2B).
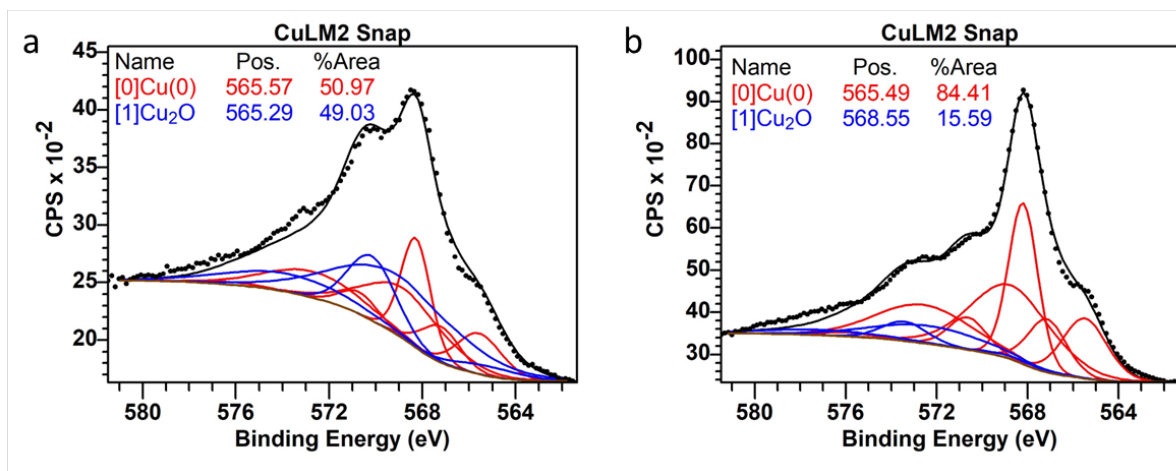
Figure 3-54. $CuL_3M_{45}M_{45}$ XPS snapshot spectra captured during depth profiling of wrought copper sample exposed for 100 h at 10 Gy h^{-1} (WC3-6#2B). a) snapshot spectrum before first etch cycle and b) snapshot spectrum after first etch cycle (20s of etching).

EURAD (Deliverable n° 15.7) – Elucidation of critical irradiation parameter
Dissemination level: Public
Date of issue of this report: 06/02/2024

Page 80

3.8.2 Carbon steel

Carbon steel samples exposed for 100 h at 10 (CS3-6), 100 (CS3-8) and 1000 (CS3-9) Gy h^{-1} were analysed with XPS including depth profiling. Table 3-13 shows the elemental composition of the samples' surface before and after depth profiling.

The Fe2p spectra were fitted based on peak fitting parameters determined from reference materials in a number of published articles [32-34]. A mixture of Fe_3O_4 and either Fe_2O_3 or $Fe(O)OH$ were the dominant components in the Fe2p spectra of samples exposed to 10 Gy h^{-1} (CS3-6#5B, Figure 3-55) and 1000 Gy h^{-1} (CS3-9#4B, Figure 3-57). The Fe(III):Fe(II) ratios of 10 Gy h^{-1} and 1000 Gy h^{-1} samples were 1.4 and 3.3 respectively, indicating proportionately more Fe(III) species were formed at 1000 Gy h^{-1} compared to 10 Gy h^{-1}. It was not possible to reliably distinguish between Fe_2O_3 and $Fe(O)OH$ in the Fe2p peak fitting procedure due to similar peak fitting parameters for these species. Although there was an element of uncertainty in the assignment of Fe(III) species, there was still a high confidence in the peak fits of Fe(II) and Fe(III) species and their relative intensities. In addition to these iron oxides and/or oxyhydroxides, Fe(0) and $FeCO_3$ were also identified in the Fe2p spectra. The sample exposed to a dose rate of 100 Gy h^{-1} showed a particularly high amount of $FeCO_3$ as seen in both Fe2p and C1s spectra (see CS3-8#4B in Figure 3-56).

EURAD (Deliverable n° 15.7) – Elucidation of critical irradiation parameter
Dissemination level: Public
Date of issue of this report: 06/02/2024

Page 81

Table 3-13. Surface composition for carbon steel specimens CS3-6#5B (100 h exposure, 10 Gy h^{-1} dose rate), CS3-8#4B (100 h exposure, 100 Gy h^{-1} dose rate), and CS3-9#4B (100 h exposure, 1000 Gy h^{-1} dose rate), pre- and post-depth profile (DP).

Sample		Concentration at.%										
		C	O	Fe	Cu	N	Cl	Mn	Na	S	Ca	Ni
CS3-6#5B	Pre-DP	70.3	23.1	3.2	1.2	1.6	0.3	0.1	0.1	0.1	0.1	-
	Post-DP	19.2	47.0	31.6	0.3	0.1	-	0.6	0.7	0.1	0.3	0.1
CS3-8#4B	Pre-DP	49.9	41.2	6.3	1.3	0.1	0.1	0.1	0.2	0.4	0.3	-
	Post-DP	8.3	54.0	35.4	0.7	-	-	0.2	0.8	-	0.6	-
CS3-9#4B	Pre-DP	56.0	32.1	5.6	3.6	1.1	-	0.3	-	1.0	0.1	0.1
	Post-DP	13.9	34.6	49.8	1.2	-	-	0.4	-	-	0.1	-
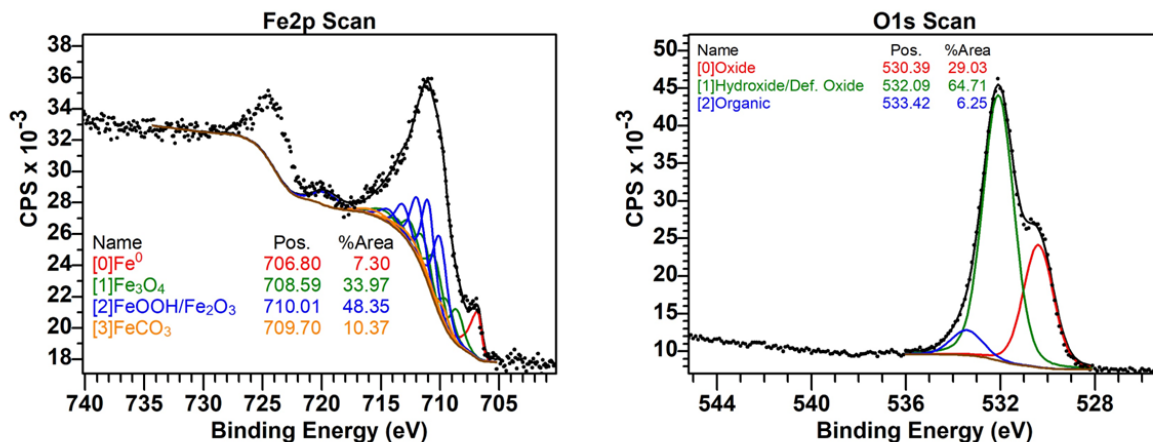
Figure 3-55 Fe2p and O1s XPS spectra pre-depth profile of carbon steel sample exposed for 100 h exposure at 10 Gy h^{-1} dose rate (CS3-6#5B).
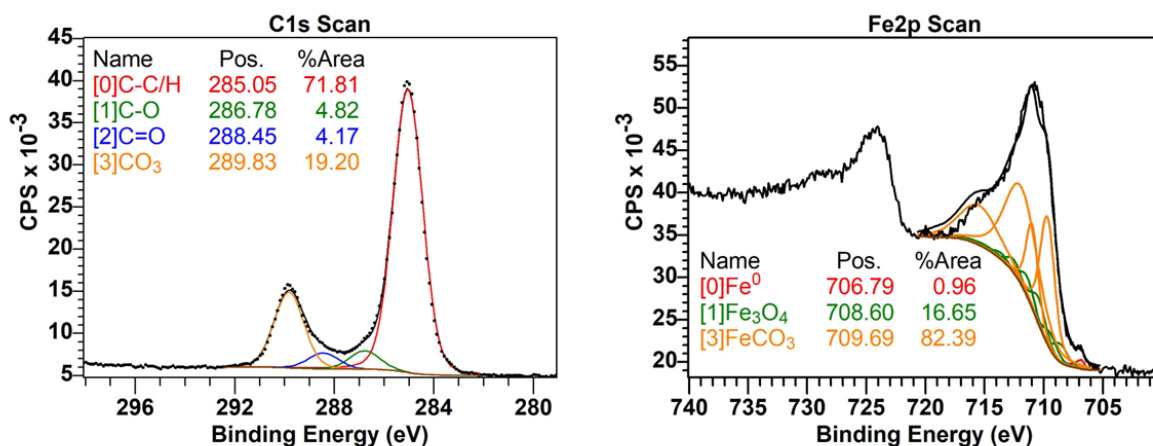
Figure 3-56. C1s and Fe2p XPS spectra pre-depth profile of carbon steel sample exposed for 100 h exposure at 1000 Gy h^{-1} dose rate (CS3-9#4B)
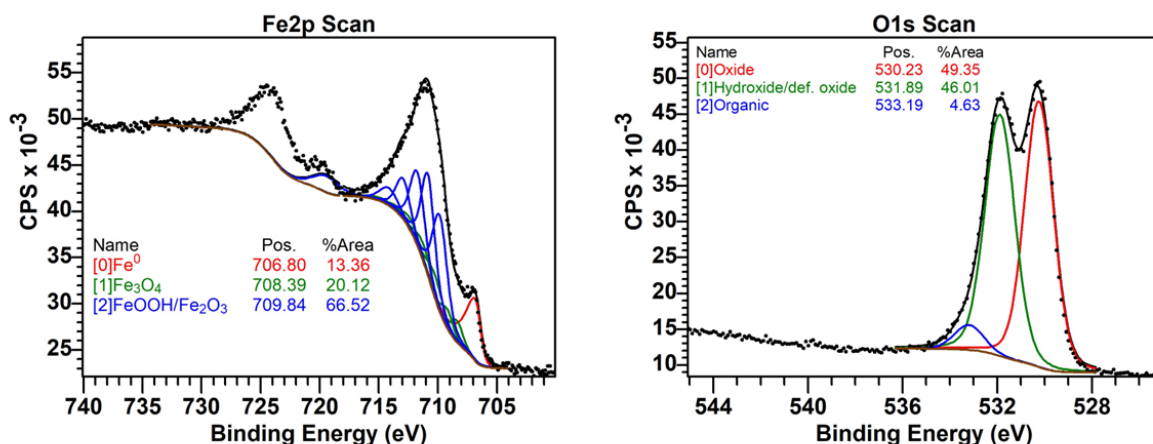
Figure 3-57. Fe2p and O1s XPS spectra pre-depth profile of carbon steel sample exposed for 100 h exposure at 1000 Gy h^{-1} dose rate (CS3-9#4B)

EURAD (Deliverable n° 15.7) – Elucidation of critical irradiation parameter
Dissemination level: Public
Date of issue of this report: 06/02/2024

Page 83

4. **Discussion of Jacobs results**

4.1 **Impact of radiation on corrosion rate**

4.1.1 Overview

Addressing the relevant impact of radiation dose and radiation dose rate on corrosion processes is inherently difficult as the two are inextricably linked. Over a given duration of exposure the two parameters are linearly proportional to one another. Therefore, decoupling their effects can only be done by making comparisons over different durations, whereby an equal radiation dose can be given at different dose rates for different durations. However, this approach brings with it a new set of challenges owing to the attenuation in corrosion rate that typically occurs over time, and has been observed in the present study and elsewhere for several candidate canister materials in simulated repository environments [35-37]. To address these challenges, it is more beneficial to develop a mechanistic understanding of the influence of radiation on corrosion rather than to simply quantify it over a range of idealised or simulated conditions, as this will help to determine how both dose rate and total dose need to be considered for each combination of material and environment.

In anoxic simulated porewater solution at near neutral pH, carbon steel corrosion is supported by water reduction leading to hydrogen evolution. The standard reduction potential for water is below that for copper, so copper is often considered to be thermodynamically stable in near neutral pH water in the absence of other oxidants. However, this perspective has been the subject of some debate [38, 39]. The half equation for water reduction is described below.

$$2H_2O + 2e^- \rightarrow H_2 + 2OH^-$$
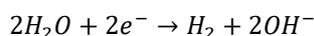
The presence of gamma radiation leads to radiolysis of the solution which forms a range of chemical species, both oxidising and reducing, including short lived species such as radicals and longer lived species such as O_2 and H_2O_2. The formation of additional species via radiolysis provides additional oxidants that can be reduced at the canister surface enabling corrosion to occur at a higher rate than when water is the primary oxidant. Whilst certain radicals (e.g., $OH^\bullet$) are more oxidising than either O_2 or H_2O_2, they are much shorter lived and only those produced at the metal interface are reduced at the surface, whereas more stable species that are produced further from the surface can be transported towards it where they can be reduced [40]. For O_2 at slightly alkaline pH, reduction is considered to occur via the following half reaction:

$$O_2 + 2H_2O + 4e^- \rightarrow 4OH^-$$
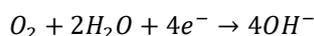
H_2O_2 can interact with the surface in two ways, either by direct reduction, or by catalytic decomposition, which is proposed to occur via the general multistep reaction shown below [13, 40]. It has been demonstrated for copper corrosion in the presence of H_2O_2, oxidation occurs via the reduction of catalytically produced O_2, rather than direct reduction of H_2O_2, or reduction of the surface bound hydroxyl radical [13] as is observed for the oxidation of UO_2 [41].

$$H_2O_2 \rightarrow 2OH^\bullet_{(ads)}$$

$$OH^\bullet_{(ads)} + H_2O_2 \rightarrow H_2O + HO^\bullet_2$$

$$HO^\bullet_2 + HO^\bullet_2 \rightarrow H_2O_2 + O_2$$
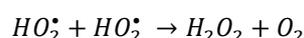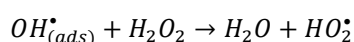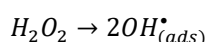
One method of evaluating the impact of radiolytically produced oxidants in the experiment, which is a closed system, is to consider a mass balance whereby it is assumed that all radiolytically generated oxidants contribute to metal oxidation. However, since oxidising and reducing species can react with each other and with other species in solution without leading to corrosion, this would lead to an over

EURAD (Deliverable n° 15.7) – Elucidation of critical irradiation parameter
Dissemination level: Public
Date of issue of this report: 06/02/2024

Page 84

estimation of the extent of corrosion. A further consideration is that this approach does not assume any limitations due to mass transport or reaction kinetics. For the experimental setup adopted here, at the end of the experiment there will inevitably be unreacted radiolytic species present, which would further enhance the overestimate of the amount of corrosion calculated from mass balance alone. This estimate can be somewhat refined by considering the transport limitation of radiolytically produced oxidants towards the corroding surface. If the corrosion reaction is transport limited, then the flux of reactant towards the surface will be proportional to its steady state concentration, according to Ficks first law of diffusion (Equation 1).

$$J = -D \frac{\partial C}{\partial x} \qquad\qquad 1$$

Where

J is the diffusive flux

D is the diffusion coefficient

C is the concentration

x is the diffusion length

For shorter duration tests the solution may not reach a steady state within the duration of the test, which could lead to complex trends in the time dependence of the corrosion rate. Furthermore, if the radiolytic yield is very high or a very stable protective oxide is formed, then the reaction may cease to be transport limited. A further point for consideration is if the presence of oxidants raises the corrosion potential enough to change the chemistry of the oxide film and its morphology changes to that of a porous or unprotective oxide, then the corrosion rate could increase by more than that caused by reduction of the radiolytic species, owing to an increase in the rate of corrosion caused by water reduction too. Conversely, more oxidising conditions could lead to the formation of more protective oxides e.g. maghemite or hematite, which could reduce the corrosion rate compared to unirradiated conditions [2, 5]. The total rate of RIC (C_T) can be expressed by Equation 2.

$$C_T = C_w + C_r \qquad\qquad 2$$

Where

C_w is the amount of corrosion that occurs in the absence of radiation owing to water reduction.

C_r is the change in amount of corrosion that occurs due to presence of radiation and can be positive or negative.

C_r is influenced by the formation of radiolytically generated species. This can affect the corrosion rate by acting as additional oxidants or reductants in the system and can influence the chemistry and/or morphology of the corrosion product.

When interpreting the impact of radiation in the context of a performance assessment, it is useful to quantify the impact of radiation in relative terms, as this can be informative when estimating the impact on the design life of a canister. This can be done by expressing the influence of radiation on corrosion

EURAD (Deliverable n° 15.7) – Elucidation of critical irradiation parameter
Dissemination level: Public
Date of issue of this report: 06/02/2024

Page 85

rate as an enhancement[5] factor (E), which expresses the corrosion rate in the presence of radiation relative to the corrosion rate in the absence of radiation over the same duration as shown in Equation 3.

$$E = \frac{C_w + C_r}{C_w}$$

3

4.1.2 Interpretation of radiolysis modelling

The test cells had 45 or 60 mL of test solution per test vessel and had a ullage volume of 37.5 or 50 mL, giving a ratio of solution to ullage of 1.2 in both cases. In the absence of consuming reactions such as corrosion, the steady state concentration of O_2 determined after 1000 hours was calculated as being between 2.7 µM[6] and 6.1 µM[7], and the steady state concentration of H_2O_2 was calculated as being between 0.3 µM[6] and 3.7 µM over the 1 to 1000 Gy h^{-1} dose rates, as shown in Table 3-5. However, given that each test specimen was placed within a thin glass tube with an internal volume of just 0.9 mL (see Figure 2-4), leaving roughly 0.8 mL volume available for solution, the transport of radiolytically generated oxidants from the bulk of the solution in the vessel to the test specimens is expected to be significantly hindered. A key question that arises is whether the increase in corrosion that occurs due to a high dose rate of radiation can be sustained by the formation of radiolytic oxidants from within the capillary tubes containing each specimen, or whether corrosion is sustained by the diffusion of radiolytically generated oxidants into each end of the tube from the bulk solution environment.

A bounding estimate of the extent to which radiolysis within the capillary tube could support corrosion was made by consideration of the mass balance of oxidants within the tube. This was achieved by calculating the rate of formation of O_2 and H_2O_2 in a volume of solution equal to that of the capillary tube, which is greatest at short durations[8] and hence low concentrations. The rate of formation of oxidant was then converted into an equivalent corrosion rate by making the pessimistic assumption that all radiolytic oxidants within the capillary tube are consumed by corrosion reactions immediately, with a reaction stoichiometry based on direct reduction of O_2 and catalytic formation of O_2 from H_2O_2 (i.e., 1 mole of O_2 corrodes 2 mole of steel or 4 mole of copper and 2 mole of H_2O_2 produces 1 mole of O_2). By assuming that oxidants are consumed as soon as they are formed, the concentration in solution is assumed to not increase, and hence the rate of formation can be assumed to persist at the highest rate, i.e., it does not attenuate at longer durations as the concentration increases. Whilst not representative of the real environment, these assumptions provide a pessimistic bounding corrosion rate from the model, given that in a real system oxidants would have to transport towards the corroding surface to be consumed leading to a concentration gradient away from the surface.

Under the aforementioned assumptions, a pessimistic estimate of the maximum corrosion rate that could be sustained by radiolysis within the capillary tube was determined for steel and copper, based on the formation of Fe^{2+} and Cu^+, as presented in Table 4-1.

---

[5] The word 'enhancement' is used even though there may be an inhibiting effect.
[6] At 0.1 Gy h^{-1} the concentration approached steady state but had not quite reached it.
[7] For reference, fully aerated water has a dissolved oxygen concentration of roughly 253 µM under standard conditions.
[8] The shortest timestep used in the modelling was 0.01 hour, hence the rate of formation of radiolytic oxidants was based on the concentration calculated at 0.01 hour.

EURAD (Deliverable n° 15.7) – Elucidation of critical irradiation parameter
Dissemination level: Public
Date of issue of this report: 06/02/2024

Page 86

Table 4-1.　　　Maximum rate of radiolytic oxidant formation within capillary tube expressed as an equivalent corrosion rate, assuming 1 mole of O_2 corrodes 2 mole of steel, or 4 mole of copper, and 2 mole of H_2O_2 produces 1M of O_2 with no kinetic limitation.

Dose Rate (Gy h^{-1})	Steel corrosion rate (μm yr^{-1})	Copper corrosion rate (μm yr^{-1})
0.1	0.0027	0.0047
1	0.026	0.044
10	0.26	0.44
100	2.6	4.3
1000	22	36

4.1.3 Copper

The impact of radiolysis on the corrosion of copper was evident at all dose rates investigated indicated by the higher corrosion rate observed in the presence of radiation than in the unirradiated control tests. This is probably due to the extremely low corrosion rate of copper in anoxic simulated porewater solution, which means even a slight increase in corrosion rate due to radiation effects can be easily detected. This is indicated in Figure 4-1, which shows the increase in corrosion due to radiation, C_r (see Equation 2), as a function of dose rate/total dose. Due to the very low corrosion rate observed in the absence of radiation, Figure 4-1 exhibits a very similar trend to Figure 3-1, but with the x-axis expressed on the log scale[9] to allow for comparison with the results of the tests on carbon steel that were performed over a wider range of dose rates. Figure 4-2 expresses the copper corrosion rates as an enhancement factor, E (see Equation 3). Figure 4-2 exhibits a similar trend to Figure 4-1, but the uncertainty is dominated by the relative magnitude of the repeatability of the results obtained in the absence of radiation. In the unirradiated control tests, the magnitude of the corrosion was only 0.02 μm yr^{-1} so the relative uncertainty was higher than for the irradiated tests that exhibited significantly higher corrosion rates. Nevertheless, the mean values of enhancement factor indicates that at representative dose rates/total doses the corrosion rate is anticipated to increase by over an order of magnitude compared to unirradiated conditions at a dose rate of just 1 Gy h^{-1} and a total dose of 10 kGy, with further increases at higher dose rates/total doses.

Comparison of the values indicated in Figure 4-1 with those expressed in Table 4-1, shows that the increase in corrosion rate of copper due to the presence of radiation was around double the estimated maximum amount of corrosion that could be supported by reduction of O_2 and H_2O_2 in the capillary tube at a given dose rate. Furthermore, since copper is largely thermodynamically stable under anoxic unirradiated conditions (indicated by the very low corrosion rate observed under these conditions), it is assumed for copper that the increase in corrosion rate of copper observed under radiation is being primarily driven by diffusion of oxidants towards the surface, as opposed to a reduction in the barrier properties of a surface oxide. If oxidant transport is driving copper corrosion in irradiated conditions, then it is expected that the corrosion rate would exhibit a similar dependence on dose rate as the combined steady state concentration of O_2 plus H_2O_2. However, when compared with the values shown

---

[9] The x-axis of Figure 3-1 could not be expressed on the log scale due to the presence of results obtained from tests at zero dose rate.

EURAD (Deliverable n° 15.7) – Elucidation of critical irradiation parameter
Dissemination level: Public
Date of issue of this report: 06/02/2024

Page 87

in Figure 3-8, Figure 3-9 and Table 3-5, the combined concentration of oxidants at steady state exhibits a much weaker dependence on dose rate than the C_r does. This is primarily due to the weak dose rate dependence of O_2 concentration in the model at steady state, which dominates because of its higher concentration compared to H_2O_2. Elsewhere, modelling of the radiolysis at dose rates above 3.6 kGy h^{-1} was performed for water at a pH 6 and 10.6, which predicted that the steady state concentration of molecular species (i.e., H_2, O_2 and H_2O_2) could be approximated by a square root dependence on dose rate [42]. The present authors fitted the data presented in [42] to provide a more accurate estimate of the dependence of oxidant concentration on dose rate, which was dose rate$^{0.34}$ at pH 6 and dose rate$^{0.43}$ at pH 10.6. The Amphos21 model reported on here predicts the combined steady state concentration of $O_2 + H_2O_2$ to exhibit a roughly dose rate$^{0.11}$ relationship between 0.1 to 10 Gy h^{-1} for a solution of 0.1 M NaCl. In the present work, the increase in copper corrosion due to radiation, C_r, followed a near linear dose rate dependence between 0.1 to 10 Gy h^{-1} (dose rate$^{0.94}$) and a slightly weaker dependence between 1 to 10 Gy h^{-1} (dose rate$^{0.66}$). The discontinuity between the modelled dose dependence of the steady state concentrations of the stable oxidants suggests one of two things: i) that the radiolytic yield or the subsequent speciation that is predicted by the modelling is different to that experienced in the experiment, and may be due to differences between the test solution and the solution that was assumed in the radiolysis models or possibly due to uncertainty in the radiolysis model; ii) that the conceptual model of RIC of copper being driven by diffusion of stable radiolytically generated oxidants from the bulk solution is wrong, or incomplete. In the former case, comparison against the measured corrosion rates would imply that the steady state concentration of stable oxidising species in the test solution should exhibit a much greater dose dependence than was predicted for either water radiolysis or water and chloride radiolysis. In the case of the latter, it could imply a greater importance of radical oxidants, which were completely omitted from the conceptual model under the assumption that, although they may be more oxidising, their net flux to the surface would be low owing to their comparatively short lifetimes. Alternatively, it could imply a greater importance between the coupling between interfacial reactions and radiolysis, which was omitted from the conceptual model on the assumption that corrosion was largely driven by the formation of oxidants far from the corroding surface.
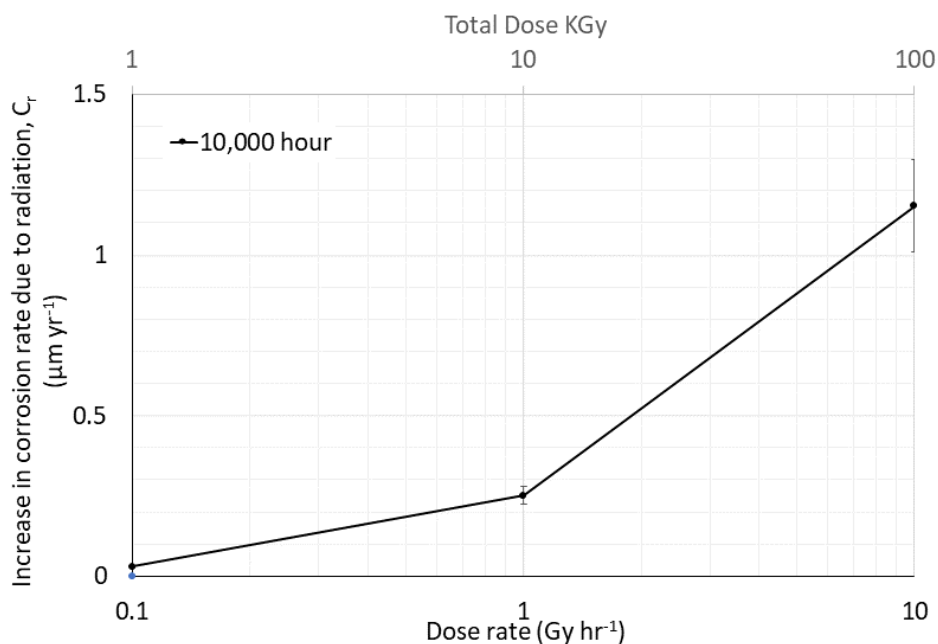
Figure 4-1. Influence of dose rate/total dose on the change in corrosion rate of wrought copper due to radiation (C_r). Error bars reflect the combined standard deviation of C_T measured in the absence and in the presence of radiation.

EURAD (Deliverable n° 15.7) – Elucidation of critical irradiation parameter
Dissemination level: Public
Date of issue of this report: 06/02/2024

Page 88
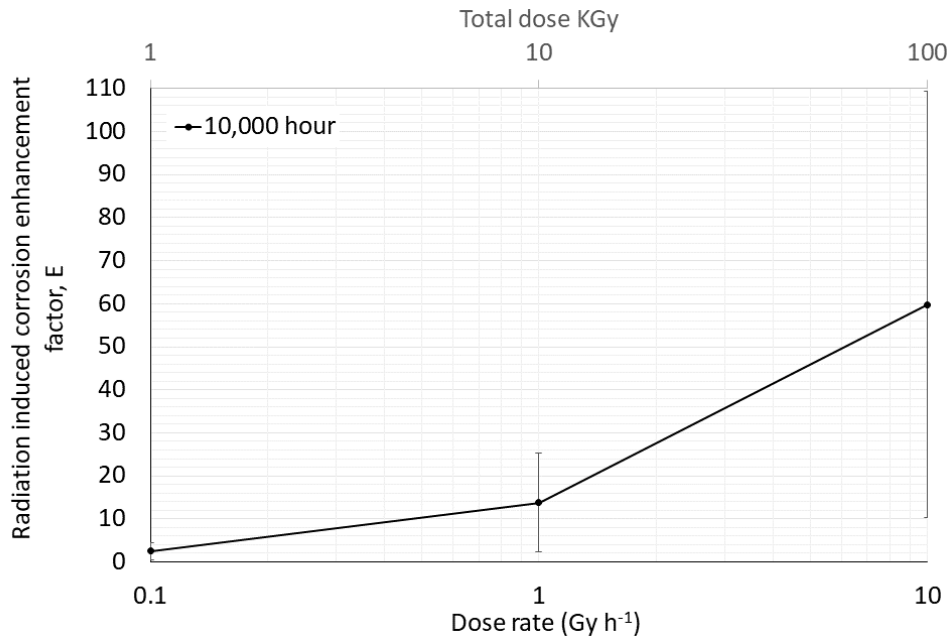
Figure 4-2. Influence of dose rate/total dose on the radiation induced corrosion enhancement factor for wrought copper, E, for tests performed for 10000 hours. Error bars reflect the combined relative standard deviation of C_T measured in the absence and in the presence of radiation.
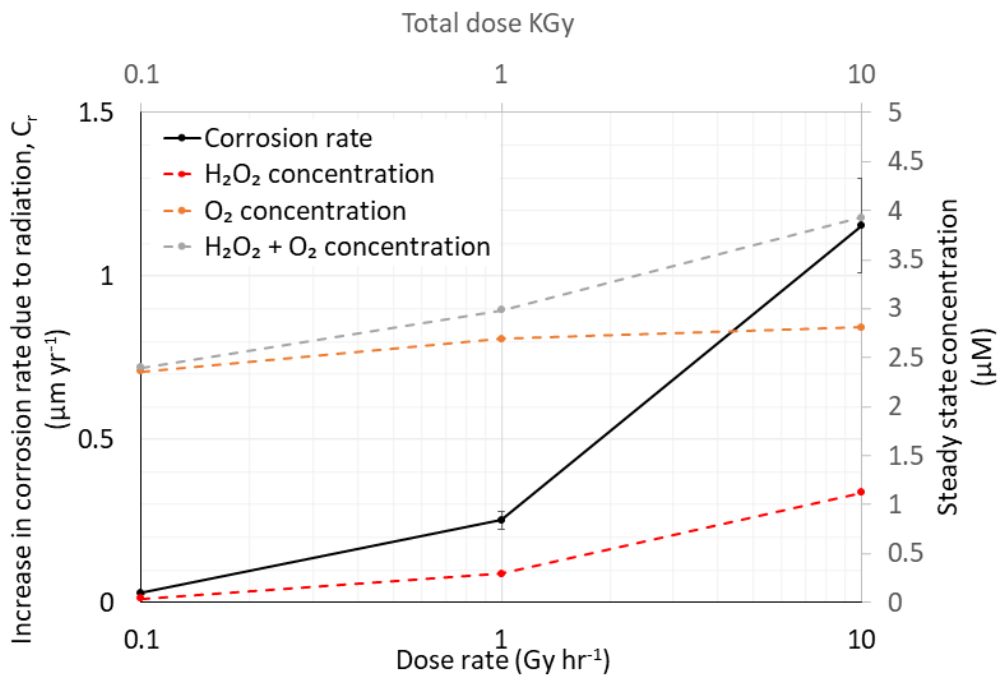
Figure 4-3. Influence of dose rate/total dose on the change in corrosion rate of wrought copper due to radiation (C_r) and the modelled steady state concentration of O_2, H_2O_2 and $O_2 + H_2O_2$. Error bars reflect the combined standard deviation of C_T measured in the absence and in the presence of radiation.

EURAD (Deliverable n° 15.7) – Elucidation of critical irradiation parameter
Dissemination level: Public
Date of issue of this report: 06/02/2024

Page 89

If the conceptual model for RIC is largely correct and the discrepancy with modelling is due to the reasons described previously it would be expected that, assuming no attenuation in corrosion rate due to oxide formation, at the same dose rates but for longer durations (i.e., greater total doses), the magnitude of C_r (when expressed as a rate) would remain similar to that indicated in Figure 4-1. However, an increasing total dose would still be expected to result in an increase in the total material loss, as at a fixed dose rate this would result in a longer duration. Visual inspection of the specimens is consistent with this hypothesis as it was observed that the extent of corrosion on copper specimens correlated broadly with the total radiation dose, indicating that there was little or no attenuation in the corrosion rate with time. Hence, for the copper specimens exposed to a fixed dose rate, the corrosion rate would be expected to broadly correlate with the total dose provided the corrosion rate remains steady. However, for a fixed duration, where the total dose is varied by altering the dose rate, a greater corrosion loss per Gy of radiation exposure is obtained at lower dose rates due to the sublinear relationship between dose rate and the increase in corrosion due to radiation, C_r.

The general observation of a strong influence of radiation on the corrosion rate of copper differs from previously published literature on the corrosion of copper under similar test conditions [17]. It was reported that in 0.1 M NaCl, and a range of other solutions, gamma radiation at a dose rate of ~12.7 Gy h^{-1} resulted in either minimal influence on the corrosion of copper, or an inhibiting effect [1, 17]. A key reason for this discrepancy with the present results may be the very high corrosion rates reported in [17]. The actual corrosion rates were not reported but calculation from the data presented implies they were approximately 41 μm yr^{-1} in deaerated 0.1M NaCl in the absence of radiation, which is considerably higher than those observed in the present study. It is not clear why such different corrosion rates were observed both in the presence and absence of radiation as the main difference in the test conditions is the addition of 0.2 M NaHCO$_3$ to the solution in the work presented here and a slight difference in the maximum dose rate applied in the irradiated tests. It has been reported that the presence of carbonate will reduce passivity in alkaline environments above pH 8.5 [43, 44], but will enhance passivity at pH values closer to neutral [45]. However, the presence of Cl$^-$ destabilises the passive film of copper, and corrosion proceeds though the formation of CuCl$_2^-$ [45] with passivation at a pH around 8 occurring via formation of a protective film comprising Cu$_2$O and CuCl [46]. Visual observation of the copper specimens indicated the widespread formation of a corrosion product following total doses of 100 kGy, although there is no indication that these films were protective. Raman spectroscopy and XPS of the surfaces of copper samples exposed to total doses of 1 kGy indicated the presence of a thin (nanoscale) Cu$_2$O film and thicker macroscopically visible precipitates of Cu$_2$O. It is not thought that these films were passivating, owing to the progressive coverage in visible corrosion products that increased with both duration and dose rate (and therefore total dose). However, for specimens that exhibited visible corrosion product over the whole surface following an exposure to a total dose of 100 kGy, there was no comparison with specimens exposed for longer durations so it is impossible to determine whether corrosion would have continued at the same rate, or whether the corrosion product was protective. Nor have the surfaces of specimens that were exposed to the highest total doses been analysed spectroscopically to determine the chemistry of the surface film, and based on differences in the colour of the oxide there did appear to be an influence of dose rate on corrosion product chemistry.

4.1.4 Carbon steel

From the data shown in Figure 3-4, in the absence of radiation, carbon steel exhibits a substantial decrease in average corrosion rate over time, from 182 μm yr^{-1} after 1 hour of exposure to 1.60 μm yr^{-1} after 10000 hours of exposure. Similar trends in long-term corrosion rate have been previously reported for carbon steel exposed to bentonite saturated with simulated porewater solution and for carbon steel

EURAD (Deliverable n° 15.7) – Elucidation of critical irradiation parameter
Dissemination level: Public
Date of issue of this report: 06/02/2024

Page 90

exposed to simulated porewater solution in the absence of bentonite [35, 47]. Notably, the average corrosion rate of 1.60 μm yr⁻¹ after 10000 hours is very close to carbon steel corrosion rates reported following in-situ testing in compacted bentonite for ~9300 hours (1.06 years) as part of the Mont Terri program, which were between 1.57 to 1.60 μm yr⁻¹ [35, 47]. Previously, the attenuation in corrosion rate of carbon steel in simulated repository conditions was shown to exhibit a power law decay in the long-term [27]. The current data can be loosely approximated with a power law relationship, but this does not produce a good fit owing to the larger decay constant observed at longer durations, implying a more complex expression to describe the trend in the data. The reduction in corrosion rate is most likely attributable to the formation of a compact corrosion product that acts as a kinetic barrier to dissolution, in which case the more rapid decay in corrosion rate observed at longer timescales could indicate a relative increase in the barrier properties of the surface layer as it ages. The substantial decrease in corrosion rate over time is an important parameter to consider when attempting to discern the impact of radiation on corrosion rate, as the duration of exposure will be the dominant factor influencing the corrosion rate that is measured. This is demonstrated in the comparison of the corrosion losses between 5000 and 10000 hours, which indicate no measurable increase in corrosion between these durations. Rather than indicating a cessation of corrosion altogether, this probably indicates that the instantaneous corrosion rate had reduced to below the uncertainty of the measurement. This perspective is consistent with the results of long-term respirometric[10] corrosion rate measurements, that show the corrosion of carbon steel in similar environments to persist after many years, as indicated by the continuous evolution of cathodically generated hydrogen gas [35, 47].

Figure 4-4 and Figure 4-5 shows the increase in corrosion due to radiation, C_r (from Equation 2), expressed as corrosion rate against radiation dose rate, which exhibits two key trends. Firstly, for a given duration of exposure, the corrosion rate associated with the presence of radiation (C_r) tends to increase with dose rate, with a greater dependence observed at shorter durations as indicated by the steeper gradient. At lower dose rates, which were only tested for longer durations, the gradient is close to zero indicating little or no influence of radiation on the corrosion rate. The only exceptions to this were the results measured for 14 hours, which showed a decrease in the corrosion rate associated with increasing radiation dose rate from 100 to 1000 Gy h⁻¹ and the results from the single test that was run for just 1 hour. The results of shorter duration tests are inherently less reliable due to the lower amount of total material loss compared to longer tests. From inspection of Figure 3-8 and Figure 3-9, it can be seen that the dependence of concentration on dose rate is greater at shorter durations. Whereas, at longer durations approaching steady state, the dependence of concentration on dose rate is significantly weaker, as shown in Table 3-5. Another key observation is that the increase in corrosion rate associated with radiation is typically smaller than the corrosion rate associated with water reduction in the absence of radiation, the only exception being the results obtained at 100 Gy h⁻¹ in the tests that were run for 14 hours. However, the large error bars on the 14 hour tests, as shown in Figure 4-4, make this trend more uncertain. Furthermore, in some instances, the magnitude of the impact of radiation on corrosion was negative (see Figure 4-5), indicating a lower corrosion rate when compared to the unirradiated control test. A slight inhibition in corrosion rate under the influence of radiation has been reported previously for carbon steel [2] and to a greater extent for copper [16, 17], but typically carbon steel either exhibits no influence, or an increase in corrosion rate when exposed to gamma radiation [10, 19-24, 26]. Furthermore, the apparent inhibition in corrosion rate was only observed in tests operated for 100 or 1000 hours. Whereas, at longer durations, at the same dose rates no such effect was observed. This implies that the observation is either a transient effect or is attributable to measurement error. Given that

---

[10] Monitoring corrosion via the formation and or consumption of gas.

EURAD (Deliverable n° 15.7) – Elucidation of critical irradiation parameter
Dissemination level: Public
Date of issue of this report: 06/02/2024

Page 91

the repeatability of tests performed at shorter durations was poorer than for longer durations (indicated by the relative size of the error bars), the latter explanation seems more feasible.

Analysis of the surfaces of carbon steel coupons following 100 h of exposure by XPS indicated the presence of Fe_3O_4 and either $FeOOH$ or Fe_2O_3 [11]. It was found that at increasing dose rate from 10 Gy h^{-1} to 1000 Gy h^{-1} the oxide had a greater ratio of Fe(III) to Fe(II), which is consistent with a higher dose rate leading to a higher steady state concentration of stable oxidants and thus a higher potential [5]. Raman spectroscopy also indicated the presence of $FeCO_3$ on all specimens, which has been found to form more readily on carbon steel exposed to groundwater and gamma radiation at a dose rate of ~3 kGy h^{-1} [2]. The formation of $FeCO_3$ scales can improve corrosion resistance of carbon steel [48], and may be partly attributable to the attenuation in corrosion rate observed with increasing exposure duration. In long-term corrosion tests performed in bentonite and in simulated groundwater, a continuous attenuation in corrosion rate has been observed over many years [36]. Under anaerobic borehole conditions, the predominant corrosion products that have been identified at the corroding steel /bentonite interface are magnetite, hematite and other iron-sulphur compounds [49, 50]. Whereas, under 'mixed' conditions where there is some oxygen exposure, siderite, lepidocrocite and maghemite were also formed [51-54]. SEM imaging of the surface indicates that the morphology of the corrosion product is different for tests operated for a longer duration, despite being irradiated to the same total dose. Where the dose was achieved via a lower dose rate for a longer duration, the oxide layer exhibited a denser coverage and the individual crystallites were less regular in shape and size.

For the longest duration tests, a significant increase in corrosion rate of 0.6 and 0.9 μm yr^{-1} was observed for 5000 h at 20 Gy h^{-1} and 10000 h at 10 Gy h^{-1}, respectively. Whilst this increase in corrosion rate may appear small in absolute terms, because it was measured following fairly long durations of exposure, it is a significant fraction of the total corrosion loss, owing to the large attenuation in corrosion rate observed over the duration of the test. This can be visualised by plotting the influence of radiation as an enhancement factor (described in Equation 3) as shown in Figure 4-6. From Figure 4-6, it can be seen that there is a significant enhancement factor at dose rates of 10 Gy h^{-1} and greater, for tests operated for 1000 hours and longer. At dose rates of 100 Gy h^{-1} and greater a significant increase in the enhancement factor was observed following tests operated for 14 hours and longer, indicating that at higher dose rates the influence of radiation is larger than the experimental uncertainty, even for short duration tests that exhibit an inherently high uncertainty. It is anticipated that higher dose rates than investigated here would be required to observe a significant increase in enhancement factor following a 1 hour test. This trend in the data is explained by the attenuation in corrosion rate with time. At short durations, the corrosion rate is very high and hence the absolute magnitude of the uncertainty in corrosion rate is also high. For radiation to exhibit a significant influence on the measured corrosion rate it has to result in a large increase in the absolute corrosion rate, whereas at longer durations when the corrosion rate decays to very low levels even a small influence of radiation e.g., less than 1 μm yr^{-1}, will lead to a significant change in the enhancement factor. The enhancement factor gives an indication of the relative increase in canister thickness loss over the period of radiation, hence from Figure 4-6, at dose rates in the range anticipated at the canister outer wall in a GDF (i.e., ≤25 Gy h^{-1} [15, 16]) the mean enhancement factor is less than 1.5. An enhancement factor of 1.5 would indicate an increase in thickness loss by 50% during the period of exposure to the associated dose rate. With the exception of the seemingly anomalous results measured at 14 hours and 100 Gy h^{-1}, the enhancement factor observed at a given dose rate increases with duration. This is explained by the attenuation in unirradiated corrosion rate, which means that for a fixed rate of corrosion due to radiation (C_r), the enhancement factor will continuously increase as the corrosion rate decreases. Therefore, directly

---

[11] The two species could not be distinguished from each other.

EURAD (Deliverable n° 15.7) – Elucidation of critical irradiation parameter
Dissemination level: Public
Date of issue of this report: 06/02/2024

Page 92

comparing enhancement factors between studies performed under different environmental conditions is complex and can easily lead to erroneous conclusions about the influence of radiation. In very un-corrosive environments such as deaerated, deionised water at neutral pH, a very small corrosion rate under radiation could still result in a large enhancement factor and conversely, in corrosive environments such as concentrated brines, a small enhancement factor could be observed despite a large absolute increase in corrosion due to radiation. Therefore, it is key to establish to what extent the corrosion that is directly attributable to radiation, C_r, attenuates, as the relative rate of attenuation of C_r and C_w will enable determination of the long term enhancement factor.
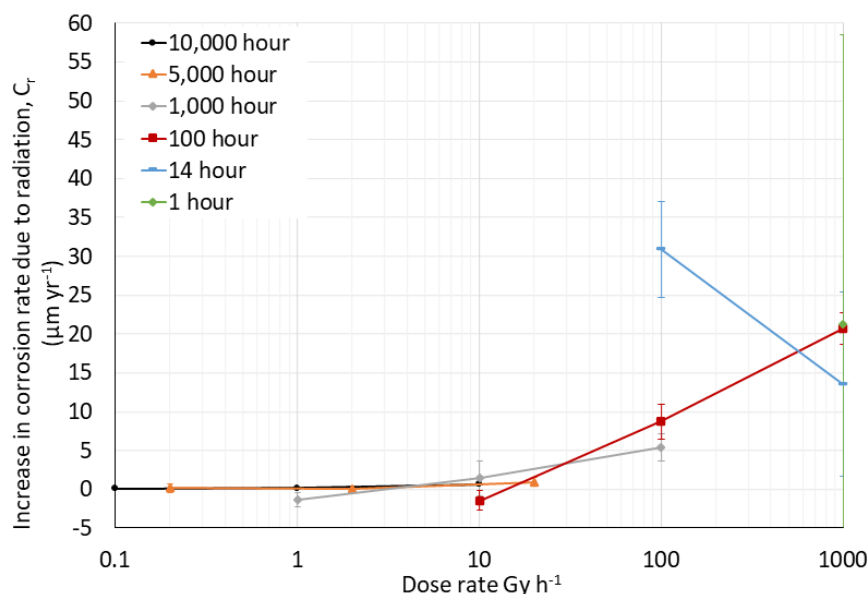
Figure 4-4. Influence of dose rate on the change in corrosion rate due to radiation (C_r), plotted for different durations. Error bars reflect the combined standard deviation of C_T measured in the absence and in the presence of radiation.

EURAD (Deliverable n° 15.7) – Elucidation of critical irradiation parameter
Dissemination level: Public
Date of issue of this report: 06/02/2024

Page 93
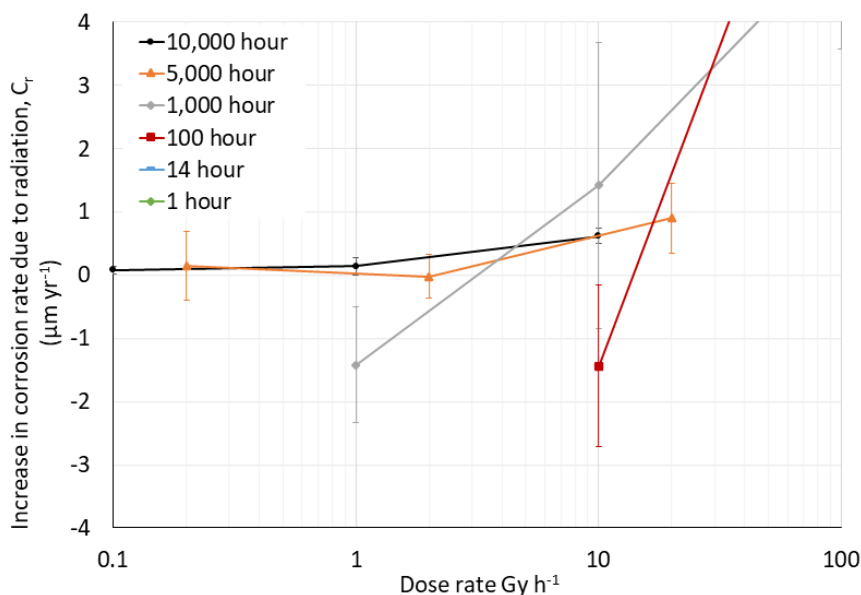
Figure 4-5. Influence of dose rate on the change in corrosion rate due to radiation (C_r), plotted for different durations. Error bars reflect the combined standard deviation of C_T measured in the absence and in the presence of radiation. This is the same data shown in Figure 4-4, but over a reduced range to better show the trends observed in the longer duration tests.
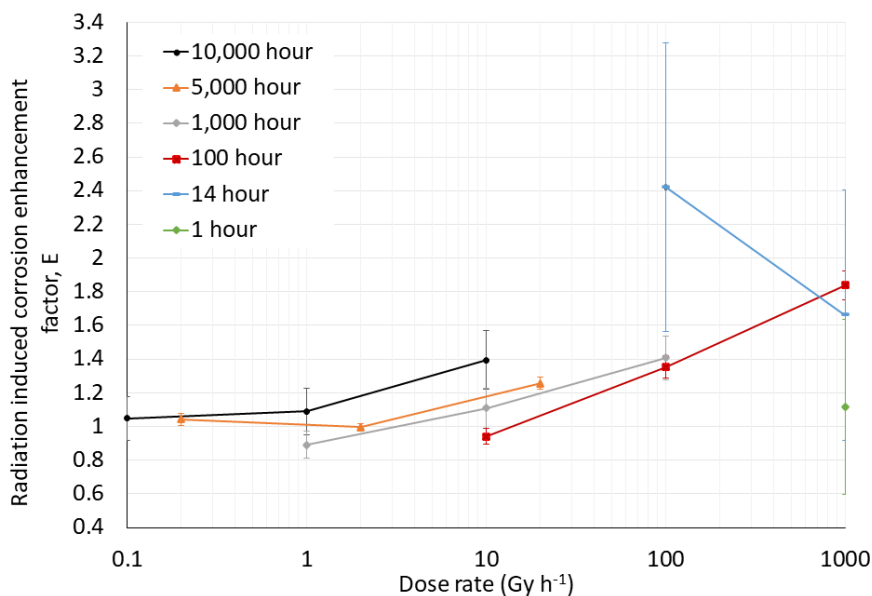
Figure 4-6. Influence of dose rate on the radiation induced corrosion enhancement factor, E, plotted for different durations. Error bars reflect the combined relative standard deviation of C_T measured in the absence and in the presence of radiation.

At dose rates greater than or equal to 10 Gy h^{-1}, the increase in corrosion rate due to radiation shown in Figure 4-4 and Figure 4-5 is higher than the estimated maximum rate of corrosion that could be supported by reduction of the oxidants produced in the capillary tube, shown in Table 4-1. If the results of the modelling are accurate, this would imply that either the increase in corrosion is being supported by diffusion of radiolytic oxidants from the bulk solution into the capillary tube, or the increase in corrosion rate is partly attributable to a radiation-induced increase in the rate of corrosion associated with water reduction, possibly because of a reduction in corrosion resistance owing to changes in the chemistry of

EURAD (Deliverable n° 15.7) – Elucidation of critical irradiation parameter
Dissemination level: Public
Date of issue of this report: 06/02/2024

Page 94

the surface oxide. Of these two mechanisms, if diffusion from the bulk solution is a key contributor to the increase in corrosion observed under radiation, then in the current experimental configuration the presence of the capillary tube probably reduces the impact of radiation on corrosion compared with experiments in which there is no barrier to mass transport with the bulk solution. Furthermore, this would also suggest that the chemistry of the aqueous environment is different towards the centre of the capillary tube compared to the two open ends.

Comparing the magnitude of C_r at a dose rate of 10 Gy h^{-1} (see Figure 4-5) for different durations and hence different total doses, shows that there is no clear correlation between either duration or total dose. At longer durations the corrosion rate decreases seemingly due to oxide formation/aging, however the total amount of oxidant also increases due to the increase in total dose. Hence the two influences may oppose each other. This is indicated in Figure 4-6, where it can be seen that at 10 Gy h^{-1} the enhancement factor E increases with duration, which is driven by the decrease in corrosion rate with time. However, it should be noted that, based on the radiolysis modelling, the concentration of radiolytically generated oxidants is only expected to increase with total dose until steady state conditions are reached. Once steady state is reached, there is not expected to be any significant change in solution chemistry with increasing dose for a given dose rate.

4.2 Summary and conclusions of Jacobs testing

4.2.1 General overview

For copper, which is typically immune (or very close to immunity) to corrosion under anoxic conditions due to its thermodynamic stability, the corrosion rate was significantly enhanced by gamma radiation even at low dose rates. When comparing the corrosion rate under radiation to the values obtained in unirradiated control tests (after 10000 h), gamma radiation led to an increase in corrosion rate from around 2 to 60 times when the dose rate was increased from 0.1 to 10 Gy h^{-1}. Considering the range of dose rates anticipated for copper canisters of 0.2 to 0.8 Gy h^{-1} in a GDF, the present data showed that corrosion rate depends on dose rate$^{0.94}$ in this range. However, it is anticipated that this dependence could differ significantly when the buffer material is present and for different geometries i.e., that of a canister in a repository. When converted into an absolute rate, the increase in corrosion rate due to radiation was approximately 0.03 to 1.15 μm yr^{-1} for dose rates of 0.1 to 10 Gy h^{-1}. Based on the relationship between dose rate and corrosion rate, if the corrosion rate in the presence of radiation does not attenuate appreciably with time then it is expected that for a given total dose, a greater amount of RIC will occur if the dose is applied at a lower dose rate, within the range of dose rates investigated.

For carbon steel, an increase in the corrosion rate due to radiation could only be observed above a dose rate of 10 Gy h^{-1} in the current test configuration. There may be an effect at lower dose rates that can't be resolved from the present data, owing to the higher corrosion rates and larger relative uncertainty of the carbon steel corrosion rates compared to copper. At a dose rate of 10 Gy h^{-1} and an equivalent exposure duration, the increase in corrosion rate of carbon steel due to radiation was similar to that observed for copper, 0.90 μm yr^{-1} compared to 1.15 μm yr^{-1}, respectively. However, since carbon steel exhibits a considerably higher corrosion rate in unirradiated conditions compared to copper, the relative increase in corrosion rate due to radiation is much smaller, hence the lower enhancement factor observed for carbon steel. A further consideration is that the corrosion rate of carbon steel exhibits a high rate of attenuation that did not appear to occur for copper. The impact of longer exposure durations (leading to substantially lower average corrosion rates) is that it severely hinders the ability to directly compare the effect of applying the same dose at different dose rates on the corrosion rate.

EURAD (Deliverable n° 15.7) – Elucidation of critical irradiation parameter
Dissemination level: Public
Date of issue of this report: 06/02/2024

Page 95

4.2.2 Limitations of the study

This work was designed to act as a model study to help better understand the influence of gamma radiation on the corrosion of copper and carbon steel to support future performance assessments for radioactive waste canisters in a GDF. As a consequence, the experimental conditions selected were not intended to exactly replicate those anticipated in a GDF but were focussed towards better understanding of the underpinning trends in corrosion rate with different radiation parameters (specifically dose rate and total dose). As a consequence, when attempting to use these results to predict how radiation may influence corrosion of a canister under disposal conditions it is important to consider several key factors that may cause the behaviour to differ from that reported on here.

- The present study investigated the corrosion behaviour in a model solution at pH 8, rather than in a bentonite or cement buffer. The availability of water for radiolysis within a given volume will be lower in a buffer of the types described above, hence the rate of formation of radiolytic oxidants within a given volume is expected to be lower. However, the presence of the buffer, and differences in the associated porewater chemistry, are also anticipated to influence the radiolytic yield and subsequent speciation compared to the model solution investigated here. The buffer is also expected to hinder the transport of radiolytic species generated further from the corroding interface, which is anticipated to reduce the rate of corrosion associated with radiation compared to that observed in solution. A further impact of the buffer is the influence of the chemistry at the corroding interface, which could influence the protective properties of the corrosion product film.

- The experimental design used in the current work is a closed system[12], in which stable oxidants increase in concentration in the solution and ullage volume over time. In a repository, radiolytically generated oxidants will be free to diffuse away from the canister towards the far field. Outward diffusion is anticipated to reduce the steady state concentrations of stable oxidants that are reached at a given dose rate, which could reduce the corrosion rate associated with radiation compared to the tests reported on here.

- The geometry of the corrosion test specimens in relation to the surrounding solution is considerably different to the geometry of a canister in a GDF. In the test environment, corrosion specimens are surrounded by solution. Hence, the volume of irradiated solution that can supply oxidants to the corroding surface is greater for a given surface area in the test environment than would be for a canister in a GDF. This is expected to result in a greater corrosion rate due to radiation in the test environment owing to the higher total flux of stable oxidants towards the surface. Conversely, the use of small diameter tubes surrounding test specimens may have partly attenuated corrosion rates by restricting the transport of corrosive species.

- Corrosion specimens were prepared for testing by grinding the surface and pickling in HCl to remove any air formed oxides, they were then stored under argon prior to exposure to the anoxic test solution. In the repository, canisters will be exposed to a wide range of environments prior to emplacement then, following emplacement, there will be a short-lived period of unsaturated oxic conditions. This exposure history will result in the surface of the canisters developing a corrosion product layer, which may impact the corrosion resistance once saturation occurs.

---

[12] It is acknowledged that in some radiolysis literature this system would be referred to as an open system because the presence of a headspace allows O2 and H2 to partition.

EURAD (Deliverable n° 15.7) – Elucidation of critical irradiation parameter
Dissemination level: Public
Date of issue of this report: 06/02/2024

Page 96

4.2.3 Implications for performance assessment

The observation that dose rates as low as 0.1 Gy h^{-1}, and possibly lower, cause a significant increase in the corrosion rate of copper in the conditions tested implies that the total radiation dose may be relevant when estimating the corrosion of canister materials in certain disposal systems. However, in the testing conditions used in this study, the amount of radiation-induced corrosion (C_r) was lower at higher dose rates. This implies that, if the corrosion rate is steady, delivering a fixed total dose at a lower dose rate will result in a greater total corrosion loss than if the dose is delivered at a higher dose rate (within the 0.1 to 10 Gy h^{-1} range investigated). The implication of this would be that radiation could impact corrosion for a long duration of time, or possibly even the entire design life. However, beyond the important limitations described in the previous section (e.g. testing environment), it should be noted that the current study only looked at corrosion rates up to 10000 hours, and did not evaluate the change in corrosion rate over time (which would indicate whether there was a gradual attenuation in corrosion rate at longer durations).

For the copper mass loss data, at the lowest dose rate of 0.1 Gy h^{-1} the loss of copper per unit of received dose was ~0.03 μm kGy^{-1}. Since the dose rate dependence on the increase in corrosion due to radiation was close to linear at lower dose rates, an estimate can be made for the loss of thickness due to corrosion following identification of a total dose equivalent to that anticipated for a copper canister over its estimated lifetime. For example, considering a Canadian Used Fuel Container, starting with 30 year old fuel, the total received dose over a 1 million year lifetime is estimated to be approximately 1.6 MGy [55]. Under the assumptions described above, 1.6 MGy would be expected to result in an increase in copper loss of roughly 50 μm for the current experimental configuration.

For carbon steel canisters, the absolute increase in corrosion rate was similar to that observed for copper at a dose rate of 10 Gy h^{-1}. However, due to the higher corrosion rate of carbon steel in the absence of radiation, the relative impact of radiation on the total corrosion rate was substantially less than for copper, leading to enhancement factors that were generally less than 1.5. A significant impact of radiation was only observed for carbon steel at a dose rate of 10 Gy h^{-1} and greater, but it is possible that there was an impact of radiation at lower dose rates that could not be observed above the experimental uncertainty. In the latter case, although the accumulation of oxidants due to low dose rate may increase the corrosion of carbon steel, the impact of this additional corrosion loss may not be significant, owing to high baseline corrosion rate that it exhibits in the absence of radiation. The impact of radiation on the performance assessment of carbon steel canisters could become more important if credit was taken for a continuous attenuation in corrosion rate, leading to very low corrosion rates over time. In this case the corrosion rate in the absence of radiation (C_w) could become small in relation to the expected corrosion rate associated with radiation (C_r). However, carbon steel waste canisters generally have a shorter target design life than copper canisters, so the potential for low dose rates to increase the corrosion rate over very long durations is inherently less for carbon steel containers than copper containers.

4.2.4 Implications for accelerated testing

Testing the corrosion resistance of candidate canister materials in simulated repository environments is a complex issue. Due to the inherently long design life of the various canister designs, testing either has to be performed under realistic conditions for a duration that comprises a very small fraction of the design life, or under accelerated conditions in an attempt to capture the impact of processes that act over a longer timescale. A key facet of this is the impact of radiation on corrosion processes, namely the impact of radiation dose and dose rate. A strategy to attempt to simulate the influence of radiation-induced corrosion is to irradiate test specimens to a total dose that is close to the dose that would be received by a canister over its design life, but delivered at a greatly increased dose rate to enable the total dose

EURAD (Deliverable n° 15.7) – Elucidation of critical irradiation parameter
Dissemination level: Public
Date of issue of this report: 06/02/2024

Page 97

to be delivered over a practical timeline. This approach invites a number of critical questions that must be answered in order to make use of these data when making corrosion assessments for canister materials in a GDF, namely:

- Will altering the dose rate at which a total dose is delivered alter the amount of radiation-induced corrosion that takes place, and if so in what way?
- Will altering the dose rate at which a total dose is delivered have an influence on other corrosion processes, e.g., oxide formation, water reduction etc.?

Based on the experimental results obtained in the present study, it is clear that the influence of dose rate on the magnitude of both the corrosion rate and the magnitude of the increase in corrosion rate that occurs in the presence of radiation is sub-linear over the range of conditions investigated. A minimum value of the dose rate at which an increase in corrosion rate was observed was 0.1 Gy h^{-1} for copper and 10 Gy h^{-1} for steel, respectively. If we consider a system where the corrosion rate is at a steady state, then there are several direct implications of this. Firstly, if the dose rate of interest is one in which no effect of radiation on corrosion is observed, or there is an inhibiting effect, then performing a test at a higher dose rate that accelerates corrosion will produce an exaggeration in the extent of radiation-induced corrosion, even if the dose rates are applied to the same total dose. Secondly, if the dose rate of interest is at a level where an increase in corrosion is observed, then performing a test at a higher dose rate will diminish the increase in corrosion than is observed under radiation for a fixed dose. However, it should be noted that at dose rates higher than those studied here (i.e. 10 Gy h^{-1} for copper), this trend may not hold due to other effects not considered i.e the influence of short-lived highly oxidising radicals at the metal surface. For a system that is not at steady state, such as for carbon steel, the situation is more complex and the influence of radiation on the rate of attenuation of corrosion must also be considered. If radiation does not influence the rate of attenuation in corrosion then the above statements are also true for an unsteady system. However, if the presence of radiation increases or decreases the rate of attenuation in corrosion rate, then it is impossible to determine what the effect of accelerating the dose rate would be without detailed knowledge of how that influences the subsequent change in corrosion rate and or the chemistry of the system. From the surface analysis presented here, and elsewhere, there is evidence that the dose rate influences the chemistry of the corrosion product, particularly for carbon steel. If the latter was true, since in this system the corrosion resistance is partly derived by formation of a protective or semi-protective film, varying the dose rate will impact the corrosion rate in a complex way.

5. Methodology of tests performed by UJV

5.1 Overview

The aim of this work was to investigate the influence of dose rate and temperature on the corrosion of carbon steel under simulated repository conditions. The experimental configuration consisted of bentonite with embedded carbon steel samples that were compacted and saturated in modules. The modules were inserted in to sealed chambers (mounted in an anaerobic box), irradiated (^{60}Co source) and constantly heated to 150 °C for durations of 6, 9, 12 and 18 months.

The dose rate (0.4 Gy h^{-1}) was calculated to simulate conditions anticipated to be experienced by the fuel assembly at the defined experimental temperature of 150 °C [56]. Prior to testing, modules were sealed to maintain an internal anaerobic environment. The non-irradiated reference modules were placed in an anaerobic box at the same temperature as their corresponding irradiated counterparts, and were tested for comparable durations to enable direct comparison of the influence of radiation

EURAD (Deliverable n° 15.7) – Elucidation of critical irradiation parameter
Dissemination level: Public
Date of issue of this report: 06/02/2024

Page 98

Additional, complementary modules were used for an estimation of microbial survivability after exposure at given conditions.

5.2 Test specimens

5.2.1 Carbon steel samples

Discs (10 mm in diameter, 1 mm thick) composed of carbon steel S355J2H (supplied by Škoda, Figure 5-1 were obtained by cutting a tube, which serves as the outer casing for the Czech canister concept seen in Figure 5-1[56]. The steel discs were prepared out of the steel by steel crosscutting and grinding using a grinding wheel with 46K grit. The initial masses of samples were weighed using Presica 240A analytical balances (Precisa Gravimetrics AG, Switzerland) with 0.1 mg resolution.

Figure 5-1. Left – carbon steel disks, right – outer case of the canister in the Czech concept.

5.2.2 Bentonite samples

Two types of bentonite were used in the corrosion experiment: a calcium-magnesium bentonite (BCV) from the Czech Republic (provided by KERAMOST, Plc., Czech Republic) and a sodium bentonite (MX-80) that served as a reference material (provided by CIEMAT).

5.2.3 Saturation solution

A synthetic granitic water (SGW3, Table 5-1) was used as a saturation medium in all experiments. The chemical composition of SGW3 was calculated to represent waters typical of the Rožná mine formation (the Bohemian Massif) layers located 1000 to 1200 m below the surface [57].

Table 5-1. Chemical composition of synthetic granitic water [57]

c (mg/l)	Na^+	K^+	Ca^{2+}	Mg^{2+}	F^-	Cl^-	NO_3^-	SO_4^{2-}	HCO_3^-
SGW3	89.4	0.7	1.3	0.1	9.9	18.7	-	10.5	163.5

EURAD (Deliverable n° 15.7) – Elucidation of critical irradiation parameter
Dissemination level: Public
Date of issue of this report: 06/02/2024

Page 99

5.3 Experimental design, irradiation and loading conditions

The experiment consisted of 23 cells, each containing carbon steel coupons embedded in compacted bentonite (Figure 5-2). According to the deep geological repository (same as GDF) concept [56] initial bentonite moisture content was adjusted to 15 % (cells heated to 150 °C) and 20 % (cells heated to 90 °C). The dry density of compacted bentonite was 1600 kg m^{-3}. In each corrosion cell, there were 12 carbon steel samples that are divided into three layers, each layer containing four steel samples. The cells were compacted using hydraulic press machine MEGA 11-300 DM1S (Form+Test Seidner+Co GmbH, Germany).
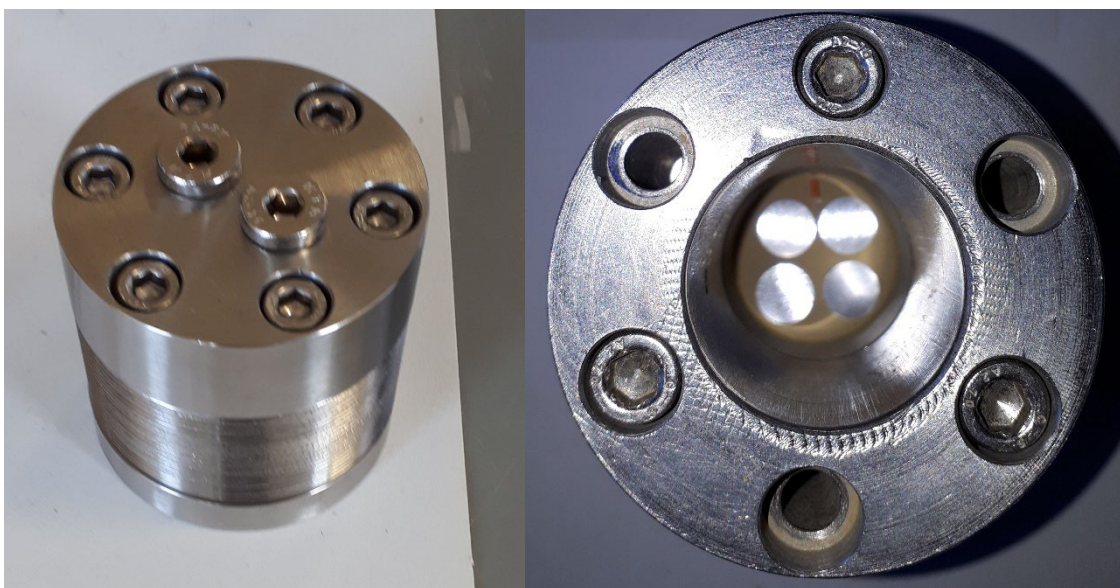
Figure 5-2. Left – corrosion cell, right – carbon steel samples inside of the corrosion cell.

The cells were connected to capillaries and saturated under the pressure of 5 MPa for the whole loading period (Figure 5-3). The saturation pressure was applied through pressure exchanger in which a piston is pressurized by Ar. All water used was de-oxygenated in the glove box (GP CONCEPT, Jacomex, France) prior to use. All experimental cells were loaded in an Ar atmosphere in the glove box or in the steel vessels filled by Ar prior to their welding. Nine cells were subjected to ^{60}Co irradiation (dose rate at samples ~ 0.4 Gy.h^{-1}, Figure 5-3). Nine cells were heated up without irradiation. The heating was adjusted to the appropriate temperatures (87 to 90 °C, 146 to 150 °C). The rest of the cells was saturated under an Ar atmosphere in the glove box (reference cells) at ambient temperature (~21 °C). The complete list of experimental cells and loading conditions are summarised in Table 5-2.

EURAD (Deliverable n° 15.7) – Elucidation of critical irradiation parameter
Dissemination level: Public
Date of issue of this report: 06/02/2024

Page 100

Figure 5-3. Steel vessels containing steel cells connected by metal capillaries with saturation medium situated in the irradiation area.

Table 5-2. A list of experimental cells and loading conditions.

Cell No.	Bentonite	w initial (%)	w final (%)	Loading period (months)	T (°C)	Radiation (Gy.h^{-1})	Dismantling date
1	BCV	15	21.14	6	150	0.4	2022-11-01
2	BCV	15	21.28	6	150	-	2022-11-01
3	BCV	15	25.06	9	150	0.4	2023-01-31
4	BCV	15	21.96	9	150	-	2023-01-31
5	BCV	15	20.54	12	150	0.4	2023-05-04
6	BCV	15	9.29	12	150	-	2023-05-04
7	BCV	15	22.61	18	150	0.4	2023-11-07
8	BCV	15	22.33	18	150	-	2023-11-07
9	MX-80	15	16.57	18	150	0.4	2023-11-07
10	MX-80	15	20.00	18	150	-	2023-11-07
11	MX-80	15	19.58	18	RT	-	2023-11-07
12	BCV	20	20.86	9	90	0.4	2023-01-31

EURAD (Deliverable n° 15.7) – Elucidation of critical irradiation parameter
Dissemination level: Public
Date of issue of this report: 06/02/2024

Page 101

Cell No.	Bentonite	w initial (%)	w final (%)	Loading period (months)	T (°C)	Radiation (Gy.h^{-1})	Dismantling date
13	BCV	20	24.55	9	90	-	2023-01-31
14	BCV	20	23.24	12	90	0.4	2023-05-04
15	BCV	20	23.93	12	90	-	2023-05-04
16	BCV	20	18.34	18	90	0.4	2023-11-07
17	BCV	20	21.78	18	90	-	2023-11-07
18	MX-80	20	20.57	18	90	0.4	2023-11-07
19	MX-80	20	20.42	18	90	-	2023-11-07
20	BCV	20	22.58	6	RT	-	2022-11-01
21	BCV	20	24.54	9	RT	-	2023-01-31
22	BCV	20	23.77	12	RT	-	2023-05-04
23	BCV	20	23.94	18	RT	-	2023-11-07

5.4 Disassembly and post-test analysis

5.4.1 Disassembly

Heating, saturation and irradiation of cells was stopped 1 day prior to disassembly. After cooling the steel vessels were opened and disassembled in the glove box under an Ar atmosphere. Three types of loaded material were obtained: steel specimens, bentonite for geochemical and mineralogical analyses, and bentonite for microbiological analyses (in the framework of ConCorD Task 4).

5.4.2 Post-test analysis of steel

5.4.2.1 Mass loss

Steel samples were subjected to descaling according to a standard procedure. A solution of hydrochloric acid inhibited by urotropine was applied. The standard prescribes gradual immersion of steel samples in the solution for 10 minutes. After each immersion, the samples were washed with demineralised water and ethanol and dried. Immersion and washing were repeated twice. Immediately after descaling the steel samples were weighed in triplicate using Presica 240A analytical balances (Precisa Gravimetrics AG, Switzerland) with the 0.1 mg resolution. The corrosion rate was calculated as a mass loss divided by exposure time and surface area of the steel samples and multiplied by the steel density (7.85 g·cm^{-1} (ČSN EN 10210-1).

5.4.2.2 Visual inspections

The surface of the steel samples was documented using an Olympus SZX10 stereomicroscope (Olympus Corporation, Japan). Images of both sides of the samples were taken.

EURAD (Deliverable n° 15.7) – Elucidation of critical irradiation parameter
Dissemination level: Public
Date of issue of this report: 06/02/2024

Page 102

5.4.2.3 Identification of corrosion products on steel surface by XRD and Raman spectroscopy

Corrosion products on metal samples were determined by X-ray diffraction analysis with the PANalytical XPertPRO MPD (PANalytical, B. V., Almelo, Netherlands, Co cathode, 40 kV, 30 mA) with the HighScorePlus software package (PANalytical, Netherlands, version 4.6.1), Diffrac-Plus software package (Bruker AXS, Germany, version 8.0) and JCPDS PDF-2 database (JCPDS 2016) and using Ramanan spectroscopy with DXR Smart Raman (Thermo Scientific, USA) with an excitation wavelength of 532 nm and a laser power of 5 mW.

Micro-Raman spectra of samples were measured by dispersive Raman spectrometer (Nicolet model DXR2-Raman microscopy) equipped with confocal microscope Olympus. As an excitation source, a laser having wavelength 532 nm and input power maximum 10mW was used. Full range grating (spectral range 3500 to 50 cm^{-1}), 25 μm confocal pinhole apertures and CCD detector (a multi-channel cooled CCD camera) were used. Samples were measured with following parameters: laser power: 0,5 mW – 2 mW, aperture 25 pinhole, objective L50x, collect exposure time: 2 s, sample exposures 200, background exposure 200. All recorded spectra were analyzed after fluorescence correction or baseline correction using OMNIC software.

5.4.2.4 SEM-EDX in cross-section

Microscopical analysis of corroded steel samples was conducted on stereomicroscope Nikon SMZ 745, light microscope Nikon Eclipse MA200 (Nikon Metrology, Ins.) and scanning electron microscope TESCAN AMBER (Tescan Group, a.s.) combined with energy dispersive spectrometer Oxford UltimMax 100 (SEM-EDS). Prior to the SEM-EDS analysis the steel surface was coated with carbon.

5.4.2.5 Profilometry

The profilometry was conducted employing 4-axes optical profilometer RedLux (RedLux Ltd., Southampton, UK). Laboratory of optical profilometry consisting of two sliding and two rotary axes. The rotary axes move with the sample and the shift axes move with the sensor. All axes use optical position sensors and linear motors. The sensor is a point confocal sensor. The principle of the analysis is based on the colour aberration of the lens (chromatic aberration) and is used to measure the distance from the measured object very accurately. According to the manufacturer's values, linear axes have a resolution of 100 nm, rotary axes 10''. The resolution of the point confocal sensor stated by the manufacturer is 20 nm. A profilometer records the position of individual points on a surface with a certain frequency. The frequency of point scanning can be set in both circumferential and longitudinal directions. The data were evaluated using the Matlab software.

5.4.3 Post-test analysis of bentonite

5.4.3.1 Chemical composition

The chemical composition of bentonite was determined by X-ray fluorescence analysis (XRF). The XRF method was chosen because of the small amount of sample needed to be analysed. The XRF analysis included the determination of the loss on ignition (LOI) at 850 °C. The total carbon content (Ctot) and the total sulphur content (Stot) were determined spectrophotometrically using the ELTRA CS 580 analyser from a naturally wet sample.

5.4.3.2 Water leachates

The determination of leachable ions was performed by a series of batch experiments in different ratios of solid and liquid phase (s:l) into MilliQ water. The phase ratio (s:l) used in the interpretation indicates the ratio of dried bentonite to water. The samples were dried at 105 °C prior to the leaching. The phase

EURAD (Deliverable n° 15.7) – Elucidation of critical irradiation parameter
Dissemination level: Public
Date of issue of this report: 06/02/2024

Page 103

interaction time (14 days) is considered long enough to achieve solid/liquid equilibrium. Subsequently, the liquid phase was separated by centrifugation, filtered through a 0.20 μm membrane filter. Concentrations of selected species were determined in the solutions by AAS (atomic absorption spectroscopy), capillary zone electrophoresis (CZE) and alkalimetric titration.

5.4.3.3 Scanning electron microscopy

The samples were examined using a JEOL SEM JSM 6510LV scanning electron microscope (JEOL, Ltd.) with an attached Oxford Instruments INCAx-actSN 55847 EDS analyzer (Oxford Instruments) operating at a resolution of 133 eV measured at 5.9 keV. The SEM microscope is equipped with a tungsten cathode, which allows work in the "low vacuum" mode. Due to the fact, that the studied materials were prepared from electrically non-conductive material and contained weakly bound water, the measurement was carried out in the "low vacuum" mode at an air pressure of 50 Pa. Under these conditions, there was neither charging of the surface of the samples by the action of the electron beam nor problems with achieving the necessary vacuum. The EDS analysis was carried out using a semi-quantitative method without standards using the company's software. Both microscopic images and EDS analyses were taken at an accelerating voltage of 25 kV.

6.   Results of tests performed by UJV

6.1 Mass loss

The corrosion rates indicated small variation of corrosion rate in the steel samples embedded in BCV (Bentonite Cerny Vrch) bentonite heated to 150 °C and irradiated for 6, 9, 12 and 18 months (10.1 ± 2.0 to 12.3 ± 2.1 μm y^{-1}) (Table 6-1). Unirradiated samples indicated the highest corrosion rate after 6 months of thermal loading (24.3 ± 2.2 μm y^{-1}) and the corrosion rate decreased with loading time (13.3 ± 1.6 to 18.0 ± 1.9 μm y^{-1}). The samples embedded at BCV bentonite heated to 90 °C (both irradiated and unirradiated) indicate the highest corrosion rates after 6 months of loading (14.9 ± 1.7 to 17.4 ± 4.1 μm y^{-1}) (Figure 6-1). The lowest corrosion rates were observed in samples stored at laboratory temperature without any irradiation (Figure 6-1).

EURAD (Deliverable n° 15.7) – Elucidation of critical irradiation parameter
Dissemination level: Public
Date of issue of this report: 06/02/2024

Page 104

Table 6-1. Corrosion rates (µm y^{-1}) of steel samples. AVG – average, ± L – confidence interval of the Student's distribution at the significance level α = 0.05.

Cell no.	Bentonite	AVG	± L	Cell no.	Bentonite	AVG	± L
1	BCV	12.0	1.5	15	BCV	13.1	2.1
3	BCV	11.1	1.9	17	BCV	12.9	2.3
5	BCV	12.3	2.1	20	BCV	6.0	0.8
7	BCV	10.1	2.0	21	BCV	4.7	0.2
2	BCV	24.3	3.2	22	BCV	3.6	0.6
4	BCV	18.0	1.9	23	BCV	2.6	0.1
6	BCV	13.3	1.6	9	MX-80	17.2	0.3
8	BCV	17.5	1.1	10	MX-80	18.9	0.3
12	BCV	14.9	1.7	11	MX-80	2.2	0.1
14	BCV	11.7	1.8	18	MX-80	4.7	0.1
16	BCV	9.3	1.4	19	MX-80	4.5	0.7
13	BCV	17.4	4.1				

Different corrosion rates were observed when steel samples were embedded in MX-80 bentonite (Figure 6-2). The highest corrosion rates were observed when steel samples were embedded in MX-80 bentonite and heated to 150 °C for 18 months (17.2 ± 0.3 µm y^{-1} and 18.9 ± 0.3 µm y^{-1} for irradiated and unirradiated samples, respectively). The steel samples embedded at MX-80 bentonite heated to 90 °C for 18 months had lower corrosion rates (4.7 ± 0.1 µm y^{-1} and 2.2 ± 0.1 µm y^{-1} for irradiated and unirradiated cells, respectively) comparable to those of thermally unloaded samples (4.5 ± 0.7 µm y^{-1}) (Figure 6-2).

EURAD (Deliverable n° 15.7) – Elucidation of critical irradiation parameter
Dissemination level: Public
Date of issue of this report: 06/02/2024

Page 105
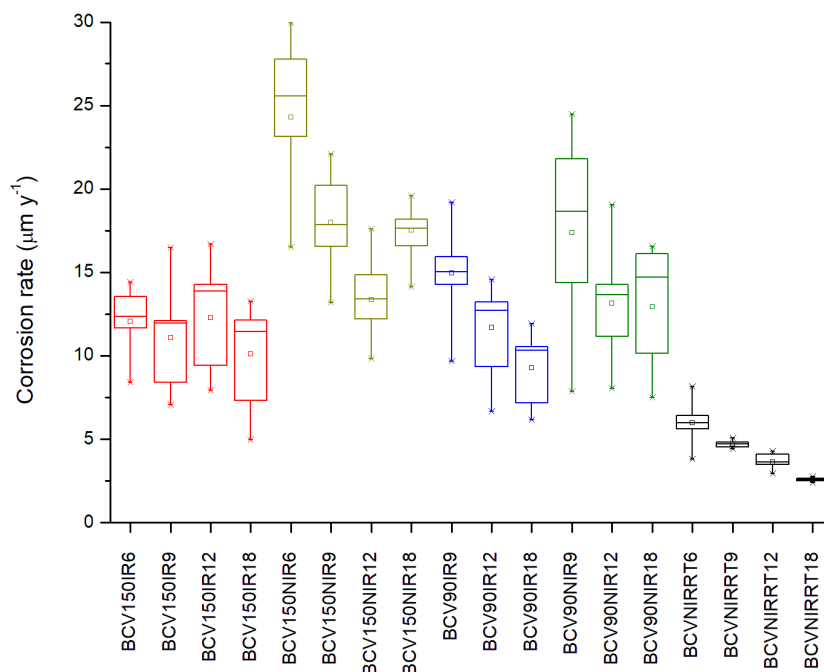
Figure 6-1. Corrosion rate of steel samples embedded in BCV bentonite at 150 °C (red – irradiated, dark yellow – unirradiated), 90 °C (blue – irradiated, green – unirradiated) and at laboratory temperature (black). The loading period is indicated by last 1-2 digits in the title of the samples (6, 9, 12 or 18).

EURAD (Deliverable n° 15.7) – Elucidation of critical irradiation parameter
Dissemination level: Public
Date of issue of this report: 06/02/2024

Page 106
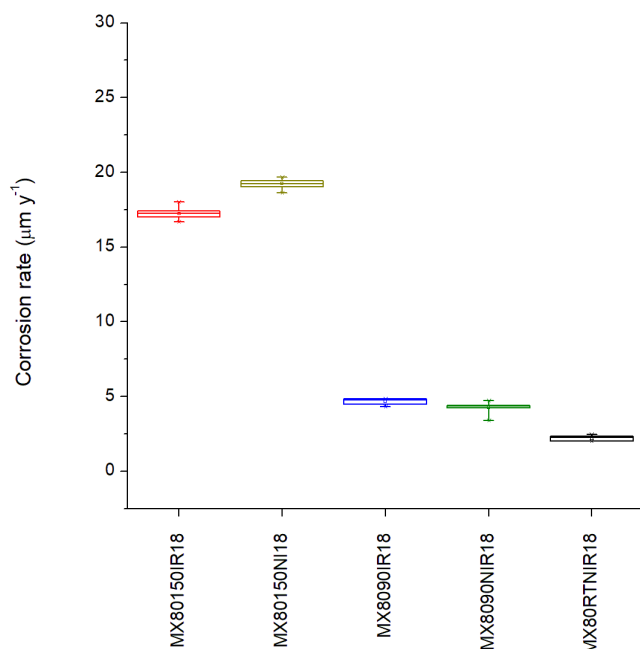
Figure 6-2. Corrosion rate of steel samples embedded in MX-80 bentonite heated to 150 °C (red – irradiated, dark yellow – unirradiated), 90 °C (blue – irradiated, green – unirradiated) and at laboratory temperature (black). The loading period was 18 months.

The steel samples were embedded in bentonite in three layers in each cell. All experiments aimed to fully homogeneous saturation of experimental cells within the experiment. Thus, corrosion rate is expected to be comparable in all steel specimens in the cell under certain conditions. Fully saturated cells exhibit very low confidence intervals (e.g., 0.1 µm y^{-1}) of corrosion rate indicating homogeneous saturation of the cell within the experiment. The cells no. 2, 3, 15, 15 and 17 indicate higher corrosion rate of the steel samples located in two layers close to the source of saturation medium. The steel samples located in the third outermost layer in the cell indicated lower corrosion rate. This heterogeneity in the individual layers is explained by inhomogeneous saturation of the cell. Lower water content decreased a corrosion rate of the steel samples. The inhomogeneity of the saturation is reflected by higher confidence intervals of corrosion rate (2.1 to 4.1 µm y^{-1}) (Table 6-1).

6.2 Visual inspections

Light optical microscopy (LOM) analysis confirmed ferritic-pearlitic microstructure of steel samples (Figure 6-3). The transition from ferritic-pearlitic microstructure to spheroidal microstructure was observed only in one steel sample in BCV bentonite in the cell no. 2 heated to 150 °C without irradiation for 6 months. Pearlite was found forming lamellae up to 30 µm thick in all steel samples. The surface roughness revealed the presence of surface depressions, which were approximately 25–30 µm deep and filled with corrosion products. These corrosion products formed a layer partially covering the steel surface for samples loaded for 6 to 9 months or completely covering it. The thickness of the corrosion layer varied, ranging from 10 to 45 µm, and was directly correlated with the duration of loading.

EURAD (Deliverable n° 15.7) – Elucidation of critical irradiation parameter
Dissemination level: Public
Date of issue of this report: 06/02/2024

Page 107

Irradiation and thermal loading at 150 °C led to the formation of thinner corrosion layers, typically ranging from 10 to 20 µm (Figure 6-4). A corrosion layer of a similar thickness (5 to 20 µm) was found in the steel samples that remained unirradiated (Figure 6-5). More extensive corrosion layers (20 to 45 µm thick) were identified in the steel samples heated to 90 °C (Figure 6-6 and Figure 6-7) showing no difference regarding to the irradiation.

Employing SEM-EDS analysis it was found different composition of corrosion products dependent on the temperature of thermal loading. Two discrete layers originated at 90 °C: a layer of Fe-oxide (Fe-oxy-hydroxide) and a layer of carbonates mixed with minerals coming from bentonite (Figure 6-6 and Figure 6-7). On the other hand, the steel samples heated to 150 °C contained: a layer composed of Fe-Si-O(OH) and a layer of carbonates mixed with minerals coming from bentonite (Figure 6-4 and Figure 6-5). The formation of Fe-Si-O(OH) layer is more obvious in samples heated at 150 °C and irradiated (Figure 6-4). These results partially correlate with the composition of corrosion products determined through XRD (X-ray diffraction) analysis. These included magnetite, Fe-rich carbonates, and a mixture of magnetite and clay minerals originating from the bentonite. The presence of Fe-Si-rich phases was not identified.
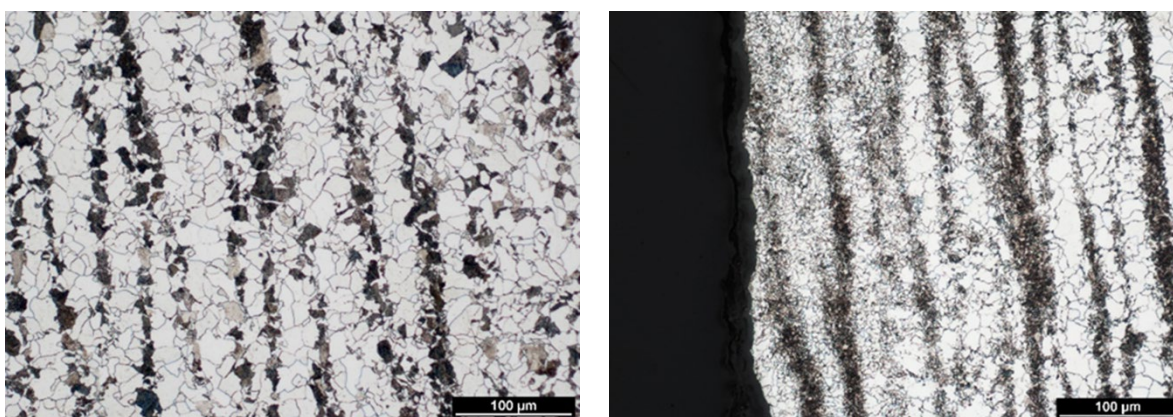
Figure 6-3. Steel microstructure ferritic-pearlitic (left) and ferritic-pearlitic with spheroidal areas (right) (cell no. 2)
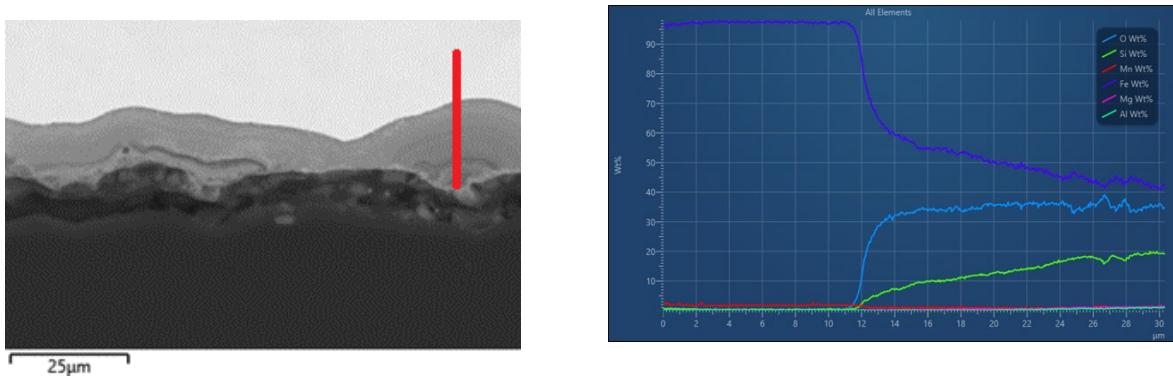
Figure 6-4. Corrosion layer on the surface of irradiated steel samples embedded in BCV bentonite heated at 150 °C (cell no. 5). SEM images including red line indicating position of the profile analysed by EDS (left) and the profile analysis.

EURAD (Deliverable n° 15.7) – Elucidation of critical irradiation parameter
Dissemination level: Public
Date of issue of this report: 06/02/2024

Page 108
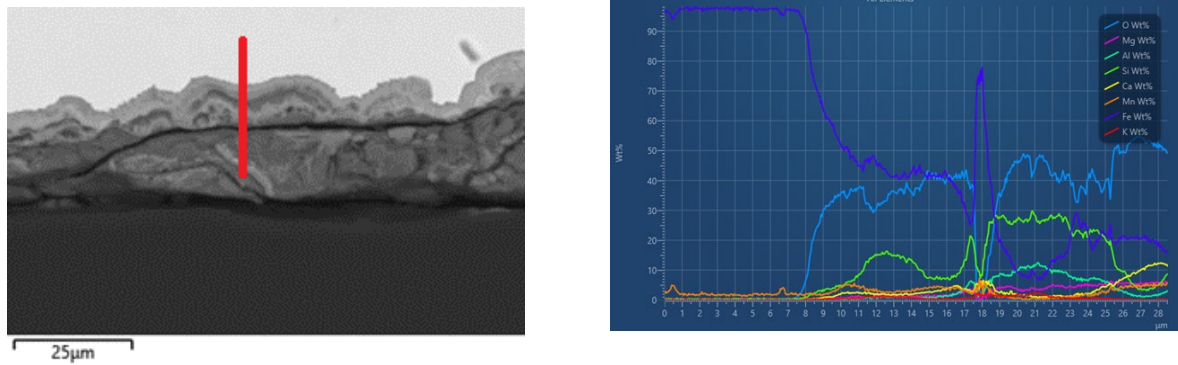
Figure 6-5. Corrosion layer on the surface of unirradiated steel samples embedded in BCV bentonite heated to 150 °C (cell no. 6). SEM images including red line indicating position of the profile analysed by EDS (left) and the profile analysis.
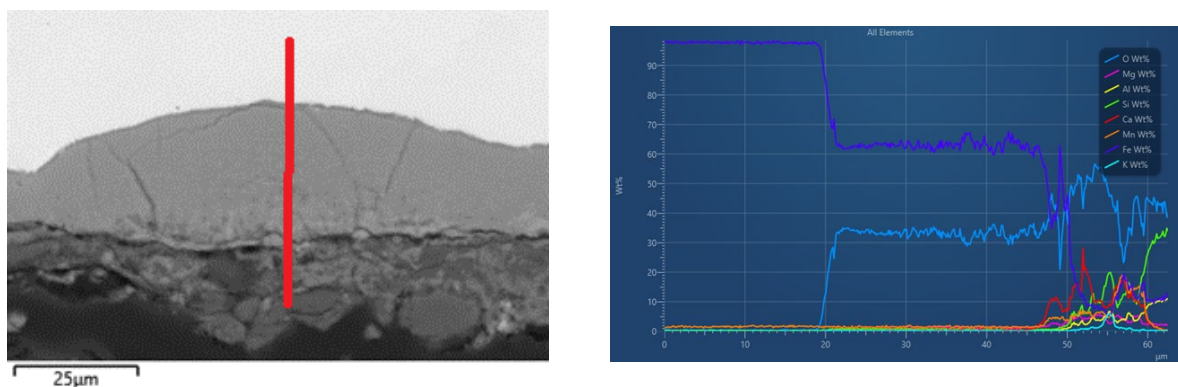
Figure 6-6. Corrosion layer on the surface of irradiated steel samples embedded in BCV bentonite heated to 90 °C and (cell no. 14). SEM images including red line indicating position of the profile analysed by EDS (left) and the profile analysis (right).
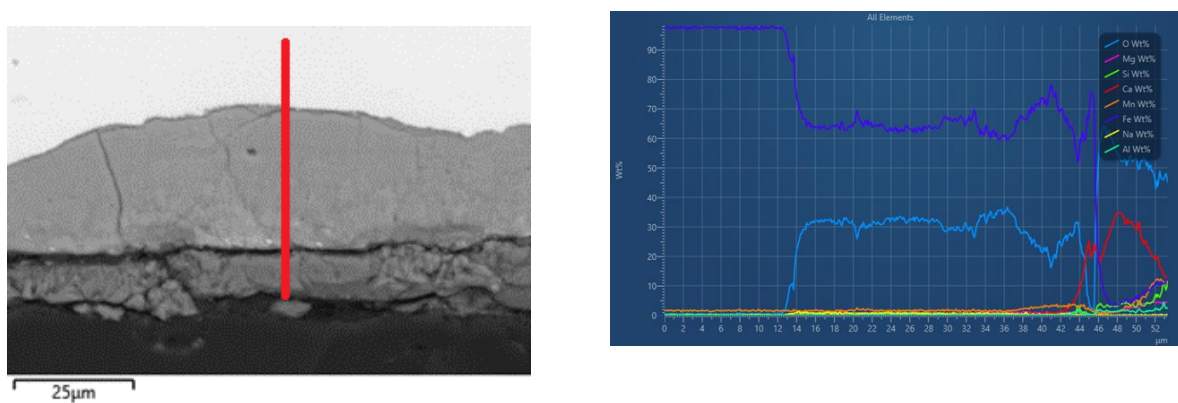
Figure 6-7. Corrosion layer on the surface of unirradiated steel samples embedded in BCV bentonite heated to 90 °C (cell no. 15). SEM images including red line indicating position of the profile analysed by EDS (left) and the profile analysis (right).

EURAD (Deliverable n° 15.7) – Elucidation of critical irradiation parameter
Dissemination level: Public
Date of issue of this report: 06/02/2024

Page 109

6.3 Profilometry

Based on the profilometry analysis it was confirmed surface corrosion of the steel samples embedded in the BCV bentonite. The degree of the corrosion was quantified based on the mean value and variation, both related to the reference plane (Table 6-2). The mean value and colour map of the BLANK sample (Figure 9-8, Table 6-2) reflects the roughness of the surface (mainly indicated as diagonal lines) related to the steel preparation and grinding prior to the experiment. Lower mean values of the selected steel samples (e.g., cells no. 1 to 5) compared to the BLANK steel sample reflect limitations with the profilometry analysis as well as surface smoothing due to corrosion (Table 6-2).

Table 6-2. Deviation from the reference Mean value and variance from reference point based on profilometry

Cell no.	Side A			Side B		
	Mean value (µm)	Standard mean deviation (µm)	Variation (µm2)	Mean value (µm)	Standard mean deviation (µm)	Variation (µm2)
1	0.00	3.35	11.24	n.a.	n.a.	n.a.
3	0.00	3.72	13.85	-0.02	4.21	17.74
5	0.16	4.95	24.46	0.18	4.54	20.61
2	0.02	3.29	10.85	n.a.	n.a.	n.a.
4	-0.03	4.43	19.59	0.08	4.21	17.71
6	0.36	4.76	22.63	0.03	5.51	30.33
12	0.28	5.54	30.66	1.15	8.64	74.65
14	-2.00	9.71	94.3	-0.64	6.73	45.25
13	-1.35	11.08	122.72	-0.46	8.13	66.07
15	-2.39	10.59	112.23	-1.11	9.31	86.67
22	0.24	4.01	16.05	0.49	3.98	15.82
BLANK	0.27	3.76	14.15	0.04	2.19	4.8

Corrosion of the steel sample embedded in BCV bentonite at laboratory temperature indicates minor corrosion propagating along the initial surface inhomogeneities (Figure 6-8). Continuous corrosion correlating with the loading period was documented in all steel samples heated to 150 °C (Figure 6-9) and 90 °C (Figure 6-10). After 12 months of loading, corrosion affected the steel surface completely. The most extensive corrosion located in the boundary parts of steel samples.

EURAD (Deliverable n° 15.7) – Elucidation of critical irradiation parameter
Dissemination level: Public
Date of issue of this report: 06/02/2024

Page 110
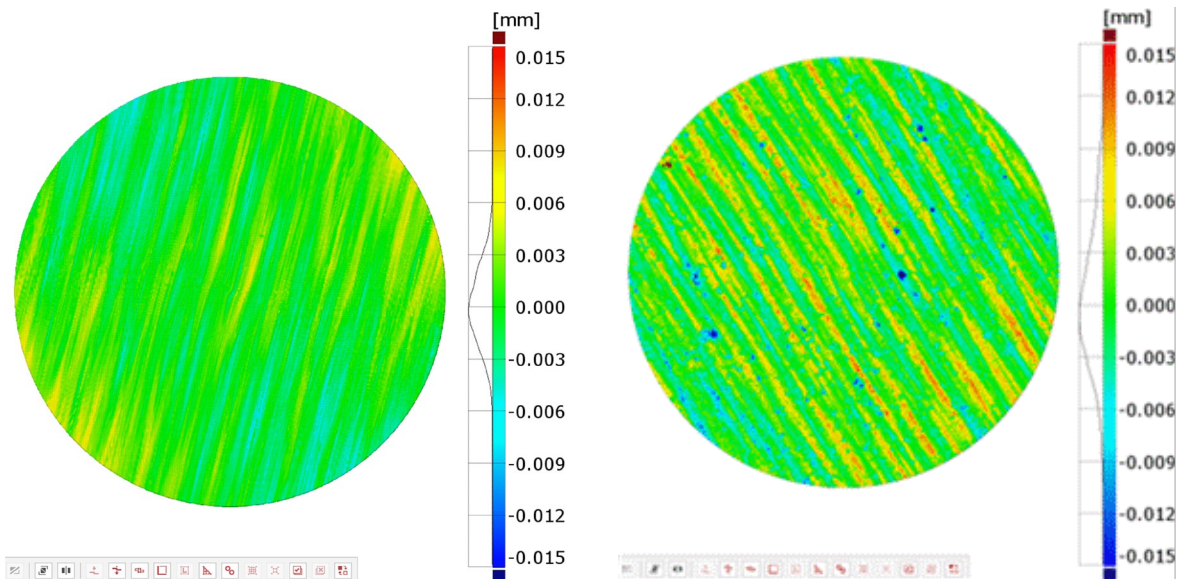
Figure 6-8. Comparison of the profilometry analysis of the BLANK steel sample (on the left) with unirradiated steel sample loaded in BCV bentonite at laboratory temperature for 12 months (on the right).

Cell no. 1   Cell no. 2

EURAD (Deliverable n° 15.7) – Elucidation of critical irradiation parameter
Dissemination level: Public
Date of issue of this report: 06/02/2024

Page 111
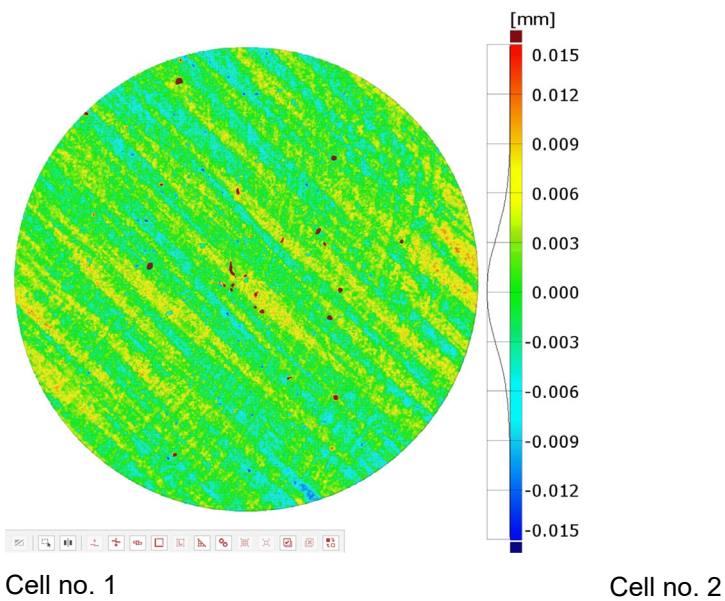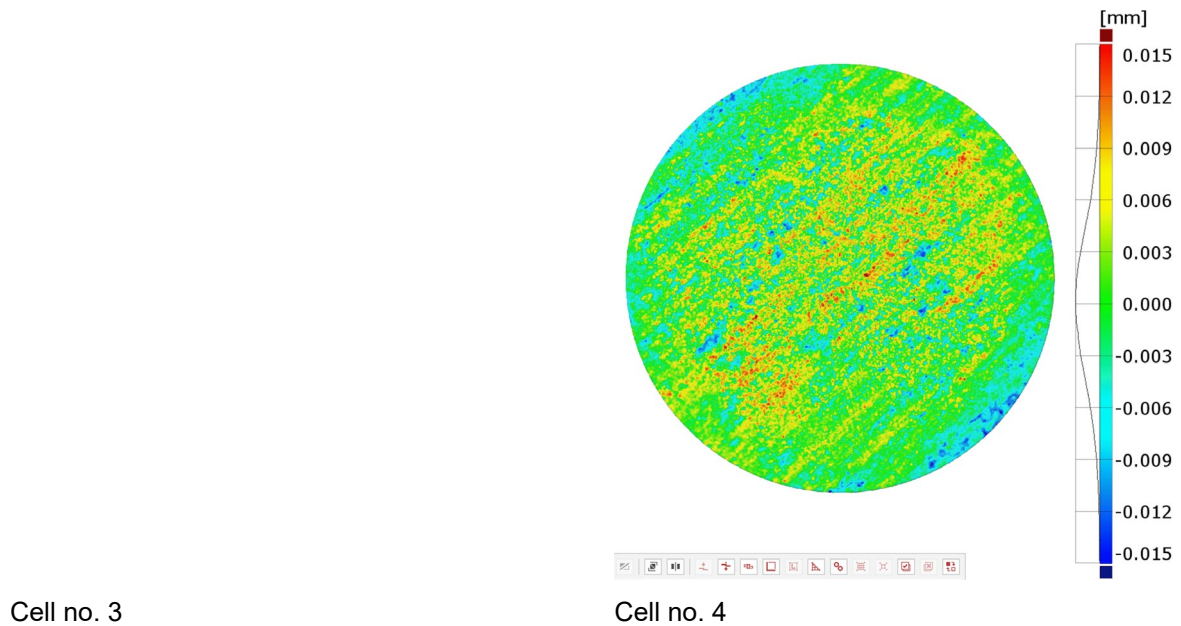
Cell no. 3   Cell no. 4

Cell no. 5   Cell no. 6

Figure 6-9. Comparison of the profilometry analysis of steel samples embedded in BCV bentonite heated to 150 °C and irradiated for 6 (cell no. 1), 9 (cell no. 3) and 12 months (cell no. 5) with the unirradiated ones (cells no. 2, 4 and 6).

EURAD (Deliverable n° 15.7) – Elucidation of critical irradiation parameter
Dissemination level: Public
Date of issue of this report: 06/02/2024

Page 112

Cell no. 12

Cell no. 13
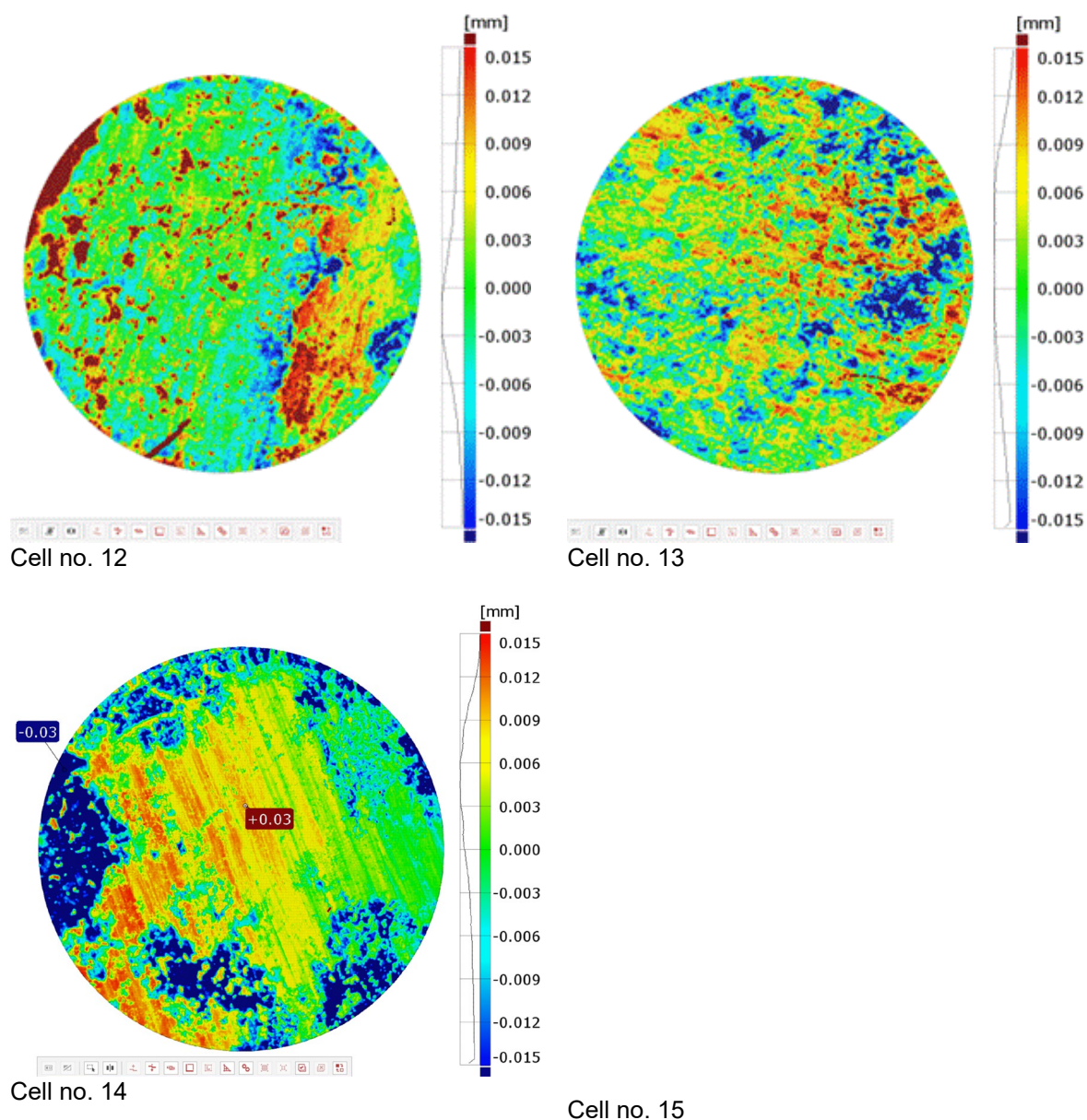
Cell no. 14

Cell no. 15

Figure 6-10. Comparison of the profilometry analysis of steel samples embedded in BCV bentonite heated to 90 °C and irradiated for 9 (cell no. 12) and 12 months (cell no. 14) with the unirradiated ones (cells no. 13 and 15).

6.4 XRD and Raman

Magnetite and Fe-rich carbonates were identified as the main corrosion products in steel samples embedded in BCV bentonite heated to 90 °C and 150 °C by XRD. Chukanovite and siderite were identified in all samples confirming anoxic conditions in the experiment. In all analyses iron and minerals coming from bentonite (montmorillonite, illite, quartz and calcite) were detected as a relic of the surrounding material.

EURAD (Deliverable n° 15.7) – Elucidation of critical irradiation parameter
Dissemination level: Public
Date of issue of this report: 06/02/2024

Page 113

6.5 Bentonite characterisation

The chemical composition of BCV bentonite (Table 6-3) indicated increased content of Fe_2O_3 in all samples (Figure 6-11a) and increased content of MnO in heated samples (Figure 6-11b, 90 °C and 150 °C). The main source of both species is regarded to be in the steel samples. Due to alteration of steel samples the corrosion products originate forming mixed structures with bentonite.

The CaO content (Figure 6-11c) decreased rapidly after 6 months in all heated samples and returned to its original values after 12 months of heating up at 150 °C. A continuous decrease of CaO content was observed in bentonite heated to 90 °C. The MgO content decreased in all heated samples for the whole loading period (Figure 6-11d). Increase in K_2O content indicated possible smectite illitization. Variable loss of ignition reflects partial drying of the samples during the bentonite pulverizing.

EURAD (Deliverable n° 15.7) – Elucidation of critical irradiation parameter
Dissemination level: Public
Date of issue of this report: 06/02/2024

Page 114

Table 6-3. Chemical composition of BCV bentonite heated to 150 °C (150), 90 °C (90) and at ambient temperature (RT), irradiated (IR) or unirradiated (NIR) (in wt%). The data were recalculated to 0.00 wt% of loss of ignition.

Bentonite no.	BCV_IN	BCV-150-IR-6	BCV-150-IR-9	BCV-150-IR-12	BCV-150-NIR-6	BCV-150-NIR-9	BCV-150-NIR-12	BCV-90-IR-9	BCV-90-IR-12	BCV-90-NIR-9	BCV-90-NIR-12	BCV-RT-NIR-6	BCV-RT-NIR-9	BCV-RT-NIR-12
Na_2O	0.35	0.42	0.40	0.35	0.42	0.39	0.42	0.33	0.33	0.35	0.33	0.32	0.31	0.28
MgO	3.34	3.24	3.27	3.02	3.32	3.20	3.13	3.27	3.22	3.29	3.23	3.30	3.28	3.25
Al_2O_3	20.31	19.47	19.00	18.80	19.05	19.08	18.73	19.10	18.92	19.18	18.93	19.31	19.38	19.01
SiO_2	54.44	55.13	54.99	54.34	54.64	54.54	54.19	54.22	54.42	54.09	54.47	54.60	54.91	54.82
P_2O_5	0.56	0.58	0.56	0.62	0.57	0.58	0.60	0.54	0.58	0.55	0.57	0.54	0.54	0.59
SO_3	0.04	0.07	0.06	0.08	0.06	0.06	0.12	0.07	0.09	0.08	0.10	0.07	0.07	0.08
K_2O	1.04	1.12	1.18	1.18	1.14	1.20	1.17	1.15	1.15	1.14	1.15	1.19	1.18	1.17
CaO	3.29	3.15	3.18	3.28	3.16	3.20	3.32	3.17	3.09	3.12	3.09	3.17	3.14	3.18
TiO_2	2.92	2.64	2.71	3.02	2.61	2.86	3.00	2.96	3.03	3.07	2.94	2.93	2.83	3.05
V_2O_5	0.05	0.04	0.00	0.00	0.03	0.00	0.00	0.00	0.00	0.00	0.00	0.00	0.00	0.00
Cr_2O_3	0.07	0.08	0.08	0.09	0.09	0.08	0.08	0.08	0.08	0.08	0.08	0.08	0.08	0.08
MnO	0.21	0.23	0.22	0.24	0.24	0.25	0.26	0.23	0.23	0.22	0.23	0.20	0.20	0.26
Fe_2O_3	13.19	13.46	13.97	14.78	14.16	14.41	14.83	14.42	14.71	14.48	14.72	14.14	13.91	14.04
Co_2O_3	0.01	0.01	0.01	0.01	0.01	0.01	0.01	0.01	0.01	0.01	0.01	0.01	0.01	0.01
NiO	0.02	0.03	0.03	0.03	0.03	0.03	0.03	0.03	0.03	0.03	0.03	0.03	0.03	0.03
BaO	0.08	0.23	0.24	0.05	0.31	0.00	0.00	0.13	0.00	0.19	0.00	0.00	0.00	0.04
Others	0.08	0.10	0.12	0.11	0.16	0.12	0.11	0.30	0.11	0.12	0.12	0.12	0.12	0.12
Total	100	100.	100	100	100	100	100	100	100	100	100	100	100	100
LOI	15.95	23.50	20.70	8.02	20.20	18.70	10.30	19.20	9.37	19.20	9.66	18.70	19.50	9.51

EURAD (Deliverable n° 15.7) – Elucidation of critical irradiation parameter
Dissemination level: Public
Date of issue of this report: 06/02/2024

Page 115
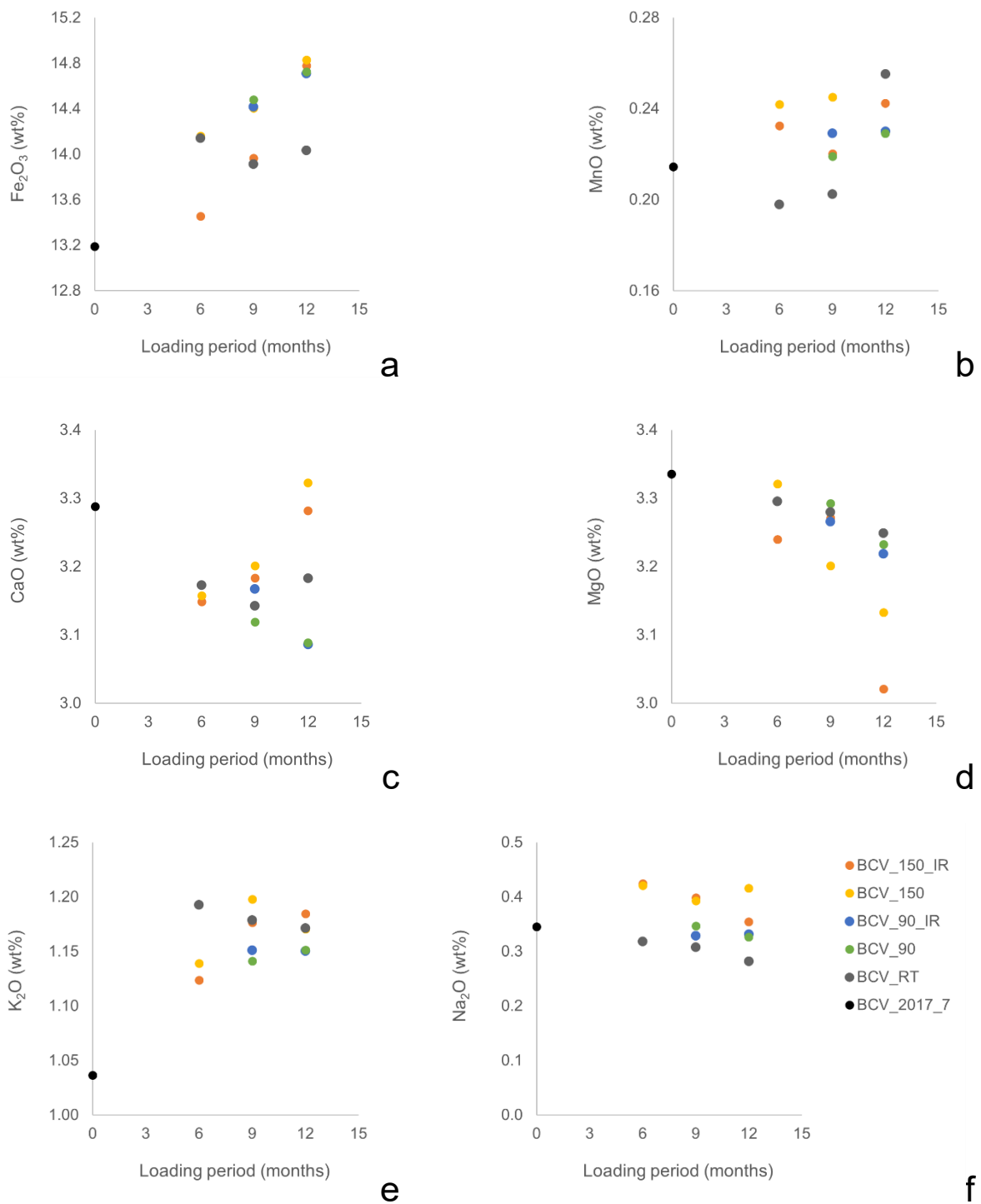
Figure 6-11. Fe_2O_3 (a), MnO (b), CaO (c), MgO (d), K_{ϵ}(e) and Na_2O (f) content in original bentonite (BCV_2017_7) and bentonite heated to 150 °C (150), 90 °C (90) and at ambient temperature (RT), irradiated (IR) or unirradiated (NIR).

EURAD (Deliverable n° 15.7) – Elucidation of critical irradiation parameter
Dissemination level: Public
Date of issue of this report: 06/02/2024

Page 116

6.6 Bentonite water leachates

The chemical composition of water leachates of BCV_input bentonite and bentonite heated to 90 °C and 150 °C indicates prevailing Na-HCO$_3$ type (Table 6-4). The concentration is dependent on the solid-to-liquid (s:l) ratio (Figure 6-12). A significant effect of both temperature and irradiation on the concentration of water leachable species was observed.

Thermal loading at 150 °C decreased the concentration of water leachable Na$^+$, K$^+$ and Mg^{2+} and slightly increased the concentration of Ca^{2+} and Cl$^-$. Only a minor effect was observed for SO$_4^{2-}$ in unirradiated BCV bentonite. Thermal loading at 90 °C decreased the concentration of water leachable Na$^+$ and Mg^{2+} and slightly increased the concentration of K$^+$, Ca^{2+}, Cl$^-$ and SO$_4^{2-}$. Only a minor effect was observed on Mg^{2+} and the concentration of HCO$_3^-$ decreased in all heated samples. Irradiation was found to decrease the concentration of water leachable Na$^+$, Ca^{2+}, Cl$^-$ and SO$_4^{2-}$. No effect of irradiation was observed on K$^+$, Mg^{2+} and HCO$_3^-$.

EURAD (Deliverable n° 15.7) – Elucidation of critical irradiation parameter
Dissemination level: Public
Date of issue of this report: 06/02/2024

Page 117

Table 6-4. Concentration (g/L) of water leachates in BCV_input and BCV heated to 150 °C (150), 90 °C (90), ambient temperature (RT), irradiated (IR) and unirradiated (NIR).

Sample no.	s:l (g/L)	Na$^+$	K$^-$	Ca^{2+}	Mg^{2+}	Fe^{x+}	Cl$^-$	SO$_4^{2-}$	NO$_3^-$	F$^-$	HCO$_3^-$
BCV_input	25.18	1.41	0.13	0.06	0.11	bdl	0.01	0.06	bdl	0.03	1.73
	114.03	3.80	0.26	0.10	0.23	bdl	0.03	0.25	bdl	0.09	4.19
	201.94	4.95	0.33	0.13	0.29	bdl	0.05	0.44	bdl	0.10	5.17
BCV150 IR6	23.82	1.51	0.12	0.04	0.03	bdl	0.04	0.09	bdl	bdl	1.54
	115.97	3.14	0.16	0.06	0.04	bdl	0.10	0.29	bdl	bdl	2.81
	209.18	4.09	0.20	0.10	0.05	bdl	0.16	0.45	bdl	bdl	3.52
BCV150 NIR6	23.55	1.56	0.12	0.05	0.02	bdl	0.04	0.11	bdl	bdl	1.57
	113.39	3.36	0.18	0.08	0.03	bdl	0.12	0.28	bdl	bdl	3.06
	203.69	4.47	0.22	0.12	0.03	bdl	0.20	0.43	bdl	bdl	3.93
BCV150 IR9	118.10	2.73	0.22	0.06	0.04	bdl	0.06	0.28	bdl	bdl	2.56
BCV150 NIR9	22.67	1.31	0.14	0.04	0.02	bdl	0.05	0.10	bdl	bdl	1.32
	113.22	2.64	0.19	0.07	0.02	bdl	0.11	0.27	bdl	bdl	2.36
	203.12	3.50	0.22	0.11	0.02	bdl	0.13	0.38	bdl	bdl	3.09
BCV150 IR12	21.82	1.17	0.15	0.07	0.03	bdl	0.01	0.08	bdl	bdl	1.36
	109.75	2.76	0.22	0.11	0.04	bdl	0.03	0.21	bdl	bdl	2.82
	196.70	3.41	0.23	0.13	0.04	bdl	0.06	0.30	bdl	bdl	3.31
BCV150 NIR12	21.93	1.50	0.14	0.07	0.02	bdl	0.08	0.11	0.04	bdl	1.48
	109.47	3.46	0.21	0.10	0.03	bdl	0.07	0.28	bdl	bdl	3.28
	196.60	4.64	0.25	0.16	0.04	bdl	0.16	0.42	bdl	bdl	4.30
BCV90I R9	117.54	3.20	0.29	0.11	0.21	bdl	0.11	0.31	bdl	bdl	3.39
BCV90N IR9	119.87	3.19	0.26	0.11	0.19	bdl	0.14	0.42	bdl	bdl	3.06
BCV90I R12	22.81	1.29	0.20	0.08	0.13	bdl	0.02	0.09	bdl	bdl	1.72
	107.29	3.16	0.25	0.11	0.19	bdl	0.13	0.29	bdl	bdl	3.29
	194.58	4.05	0.38	0.15	0.27	bdl	0.19	0.45	bdl	bdl	4.16
BCV90N IR12	22.89	1.18	0.20	0.08	0.14	bdl	0.07	0.12	bdl	bdl	1.53
	108.48	3.04	0.33	0.11	0.21	bdl	0.18	0.33	bdl	bdl	3.18
	194.33	4.30	0.40	0.17	0.29	bdl	0.30	0.52	bdl	bdl	4.27
BCVRT NIR6	116.32	2.91	0.39	0.11	0.27	bdl	0.05	0.26	bdl	bdl	3.49
BCVRT NIR9	22.77	1.19	0.25	0.10	0.22	bdl	0.04	0.11	bdl	bdl	1.83
	112.12	2.86	0.39	0.11	0.29	bdl	0.05	0.26	bdl	bdl	3.51
BCVRT NIR12	22.03	1.11	0.28	0.12	0.24	bdl	0.02	0.10	bdl	bdl	1.88
	107.87	3.03	0.49	0.16	0.37	bdl	0.01	0.19	bdl	bdl	4.18
	194.91	4.26	0.53	0.20	0.50	bdl	0.02	0.28	bdl	bdl	5.64

EURAD (Deliverable n° 15.7) – Elucidation of critical irradiation parameter
Dissemination level: Public
Date of issue of this report: 06/02/2024

Page 118
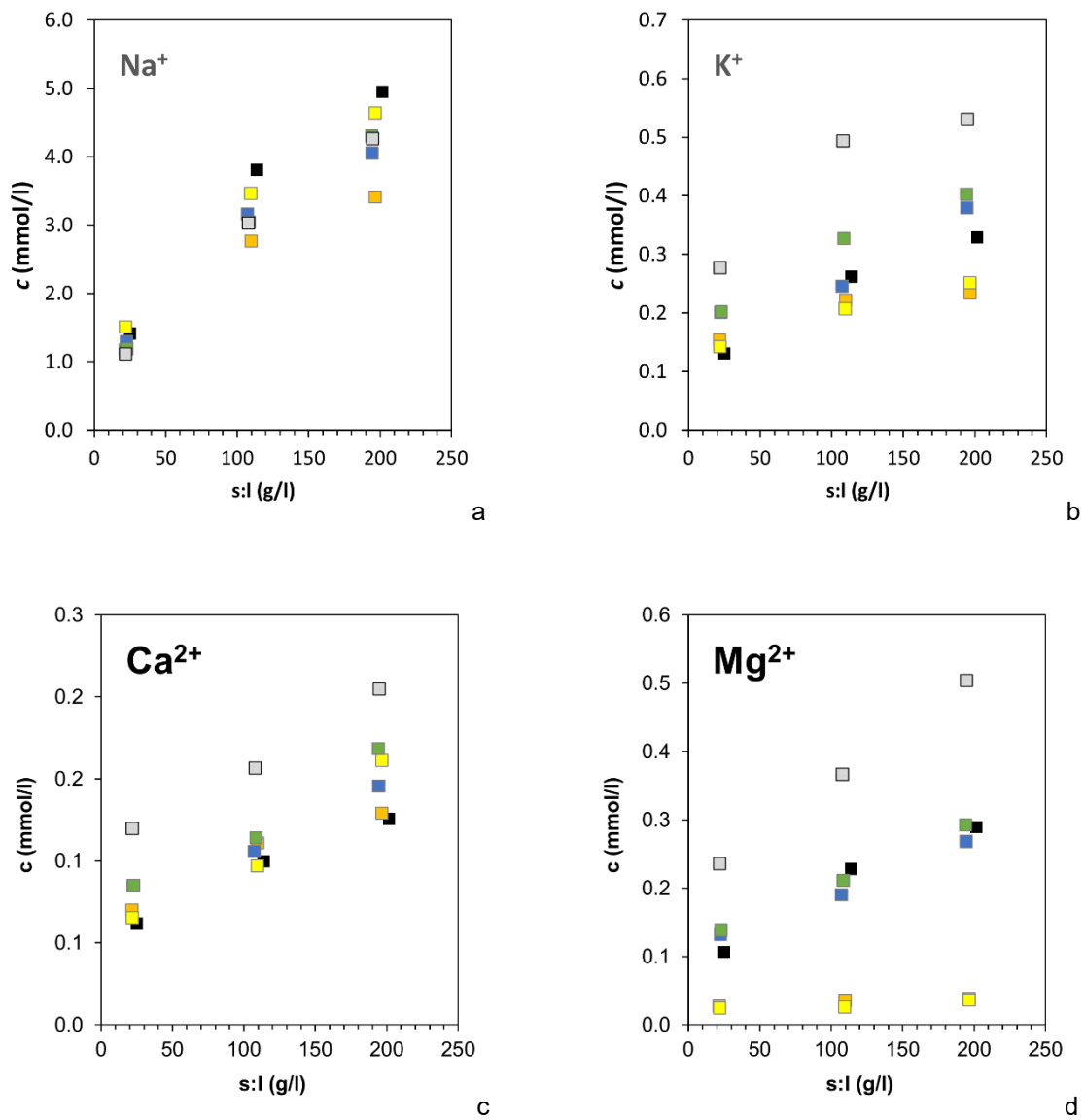
Figure caption provided on following page

EURAD (Deliverable n° 15.7) – Elucidation of critical irradiation parameter
Dissemination level: Public
Date of issue of this report: 06/02/2024

Page 119
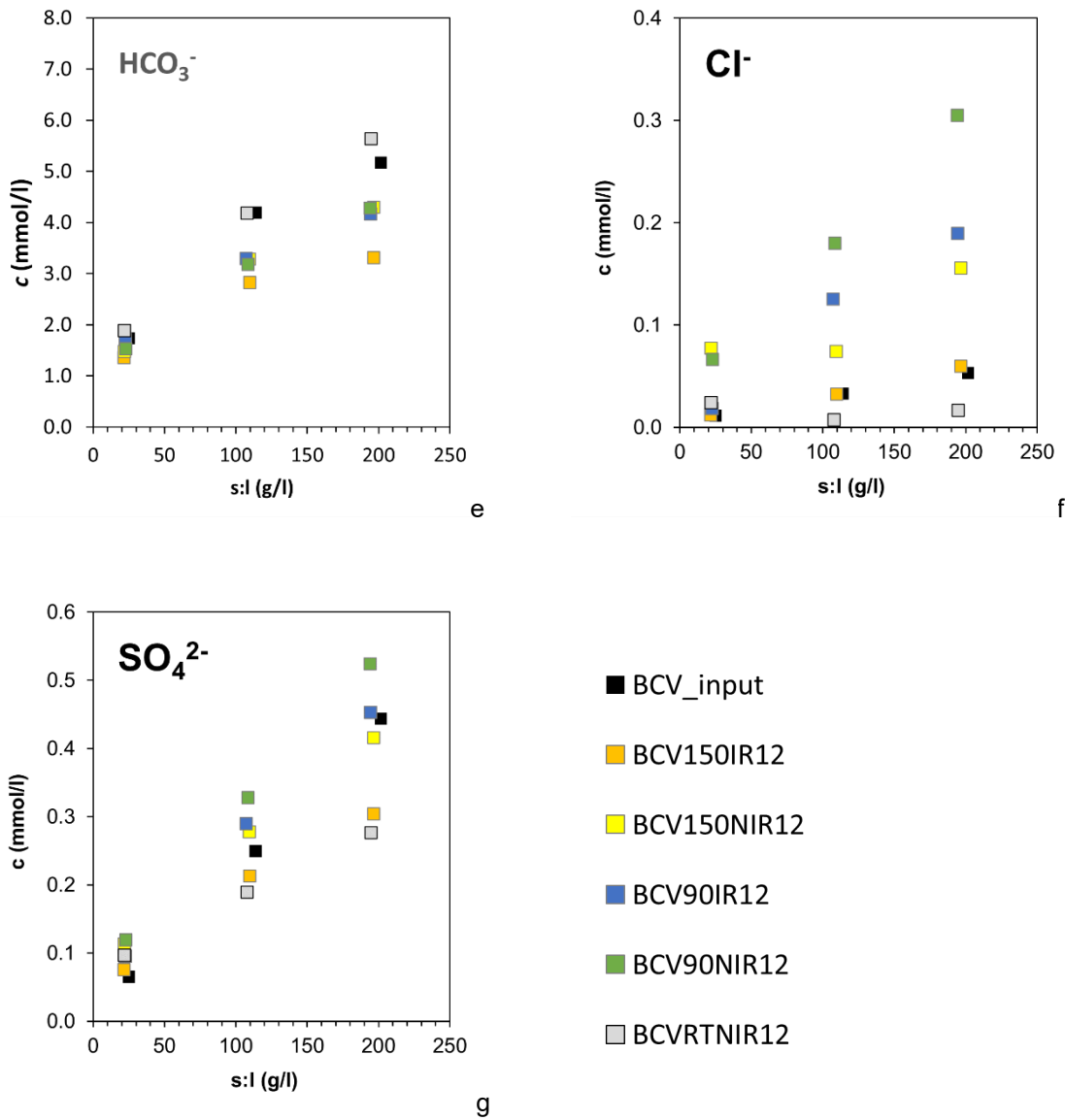
Figure 6-12. Concentration of Na^+ (a), K^+ (b), Ca^{2+} (c), Mg^{2+} (d), €₃⁻ (e), Cl^- (f) a SO_4^{2-} (g) in water leachates from BCV bentonite heated to 150 °C (150), 90 °C (90) or laboratory temperature (RT), irradiated (IR) or unirradiated (NIR), loaded for 12 months.

7. Discussion of UJV results

7.1 Impact of radiation on corrosion rate

Irradiation was found to decrease the corrosion rate of steel samples in BCV bentonite at both tested temperatures (150 and 90 °C). This trend was confirmed by corrosion rates calculated based on mass loss and by mean values and deviations calculated based on profilometry analysis. A similar trend was indicated in MX-80 bentonite heated to 150 °C. A very minor effect of irradiation on steel corrosion was observed in MX-80 bentonite heated to 90 °C.

EURAD (Deliverable n° 15.7) – Elucidation of critical irradiation parameter
Dissemination level: Public
Date of issue of this report: 06/02/2024

Page 120

7.2 Impact of radiation on corrosion product formation

Fe-oxy-hydroxide and Fe-carbonates were analysed on steel-BCV bentonite surfaces heated to 90 °C. A formation of Fe-Si-O(OH) layer was analysed in samples heated to 150 °C. Minimal difference was found in the composition of corrosion products regarding to the irradiation.

The thickness of corrosion layer well correlated with the length of loading period. More extensive and thicker layers were identified on steel samples heated to 90 °C. This feature is explained by higher saturation of bentonite and higher water content, which can facilitate formation of corrosion products. Regarding to the bentonite parameters, irradiation decreased the content of CaO and MgO in the loaded BCV bentonite. Irradiation also decreased concentration of water leachable Na^+, Ca^{2+}, Cl^- and SO_4^{2-}. No effect of irradiation was observed on water leachable K^+, Mg^{2+} and HCO_3^-.

7.3 Summary and conclusions of UJV testing

The steel samples embedded in the BCV bentonite heated to 150 °C indicate a lower corrosion rate when irradiated compared to unirradiated samples. The thickness of the surface corrosion products identified on irradiated samples heated to 150 °C indicated an almost constant corrosion rate for the whole testing period. Unirradiated samples heated up to 150 °C showed the highest corrosion rate after 6 months with decreasing tendency when the loading period was increased to 18 months. The decreasing corrosion rate was observed in both irradiated and unirradiated steel samples heated to 90 °C correlating with increasing loading period. Particularly low corrosion rates were found on steel samples embedded in water saturated BCV bentonite stored under laboratory temperature without irradiation. An inhibiting effect of irradiation on steel corrosion was observed when the steel samples were embedded in MX-80 bentonite heated to 150 °C. Almost no effect was observed when the MX-80 bentonite was heated to 90 °C.

Longer loading periods led to the formation of a higher amount of corrosion products facilitating their identification. Formation of hematite and Fe-rich carbonates (chukanovite and siderite) were identified in the corrosion layers on the steel surface. The thickness of the corrosion layer varied, ranging from 10 to 45 μm, and was directly correlated with the duration of loading. Steel samples that remained unirradiated and were heated to 90 °C exhibited corrosion layers up to 45 μm in thickness after 12 months of loading. In contrast, irradiation and thermal loading at 150 °C led to the formation of thinner corrosion layers, typically ranging from 10 to 20 μm. A corrosion layer composed of Fe-Si-O was identified on the surface of steel subjected to thermal loading of 150 °C. The layer was identified only by SEM-EDS indicating an amorphous or poorly crystalline structure. The origin of Fi-Si-rich corrosion products needs to be confirmed by future research.

8. Implications of the combined findings

8.1 Comparison of the Jacobs and UJV results

Direct comparison of the UJV and Jacobs results is difficult owing to a large number of different variables between the tests, however some inferences can be made by comparing the two data sets. The only direct comparison that can be made is between the tests operated at ambient temperature in the absence of radiation, which gives an indication of the inherent difference in corrosion rate caused by the two test configurations. From the UJV tests in BCV bentonite, the corrosion rate in ambient conditions varied from 6 μm yr^{-1} to 2.6 μm yr^{-1} after being exposed for ~4400 to ~13000 hours, respectively. In comparison, in the unirradiated Jacobs tests, the corrosion rate varied from 3.5 μm yr^{-1} to 1.5 μm yr^{-1} after being exposed for 5000 to 10000 hours. This shows that despite the very different test

EURAD (Deliverable n° 15.7) – Elucidation of critical irradiation parameter
Dissemination level: Public
Date of issue of this report: 06/02/2024

Page 121

configurations, the magnitude of the corrosion rate due to water reduction and the rate of attenuation is similar in UJV test and Jacobs tests.

UJV tests that were subjected to radiation, at 90°C and 150 °C, received total doses between 1.8 and 5.3 kGy, which were applied at a dose rate of 0.4 Gy h^{-1}. The closest conditions to these from the Jacobs testing program were tests run at dose rates of between 0.1 and 1 Gy h^{-1}, which received total doses of between 1 and 10 kGy, but were performed at ambient temperature. In the UJV tests, under all conditions tested, radiation either conferred an inhibiting effect or had no significant influence on corrosion rate. The magnitude of the inhibiting effect was greater at higher temperature, and from the tests in BCV bentonite the effect appeared to be broadly greater at shorter durations. Comparing these results with those of the Jacobs testing under the aforementioned exposure conditions shows that in Jacobs tests no inhibiting effect was observed; there was a slight increase in corrosion rate when radiation was present but at 0.1 to 1 Gy h^{-1} for total doses between 1 to 10 kGy the effect was not significant. However, when the total dose of 1 to 10 kGy was applied at higher dose rates between 10 to 1000 Gy h^{-1}, a significant increase in corrosion rate compared to unirradiated conditions was observed for several of the tests. These results invite the question as to whether the inhibiting effect that is observed in the UJV tests at high temperature would give way to a corrosion rate enhancement at dose rates higher than the 0.4 Gy h^{-1} that was tested, as observed in the Jacobs tests, or whether the inhibiting effect is solely related to the presence of bentonite and/or elevated temperature? Conversely, if the Jacobs tests were performed at higher temperature would an inhibiting effect have been observed at lower dose rates?

A key observation from the UJV tests was the substantial influence of temperature on corrosion rate, both in the presence and absence of radiation. At 150 °C, in the absence of radiation the corrosion rate in BCV bentonite varied between 24 µm yr^{-1} and 13 µm yr^{-1} with an experimental repeatability of roughly 10 to 25 µm yr^{-1} based on the ranges of corrosion rates reported. In the Jacobs tests, the increase in corrosion rate due to the presence of radiation was less than 1 µm yr^{-1} at a dose rate of 10 Gy hr^{-1} following exposure durations of between 5000 to 10000 hours. Hence, the same 1 µm yr^{-1} enhancement would probably not be detectable if the unirradiated corrosion rate was as high as was observed in the UJV tests performed at 150 °C, as it is considerably lower than the repeatability. Furthermore, where the unirradiated corrosion rate is higher (e.g., 24 µm yr^{-1}) the increase in corrosion rate associated with radiolytically generated oxidants could be offset by other effects such as a change in the chemistry of the oxide.

8.2 Comparison with other studies within ConCorD

Within ConCorD Task 3, two other studies of the effect of radiation on corrosion were performed beyond those reported here. The results of these tests will be reported in more detail within Deliverable 15.8 [27], but some are briefly compared to the results of Jacobs and UJV here. One set of tests performed by Subatech comprised exposure tests on carbon steel in either unsaturated MX-80 bentonite, or under atmospheric exposure with no bentonite. The conditions of the exposure were irradiation at 25 °C, at a dose rate of 400 Gy h^{-1} for durations of 125 to 1000 hours under argon at a controlled relative humidity (RH) of 63%, 76% and 99%, and were compared to the results of control tests that were performed in the absence of radiation. It was found that, in the absence of bentonite, the corrosion rate was much greater at 63% RH than at 76% or 99%, rising from ~ 20 µm yr^{-1} to roughly 230 µm yr^{-1}, following nearly 1000 hours of radiation exposure. In bentonite, the corrosion rates were much lower, varying between 2 to 56 µm yr^{-1} after 1000 hours of exposure, with no clear impact of relative humidity. In unirradiated conditions, at RHs of 63% and 76% there was little or no corrosion (both in clay or under atmospheric exposure) and at 99% the corrosion rate in bentonite was comparable to that observed under radiation.

EURAD (Deliverable n° 15.7) – Elucidation of critical irradiation parameter
Dissemination level: Public
Date of issue of this report: 06/02/2024

Page 122

The results of the tests performed in bentonite by Subatech [27] indicated an increase in corrosion rate due to radiation at lower RH (63% and 76%), with ranges of corrosion rates overlapping those reported by Jacobs and UJV. However, at higher levels of saturation no significant influence of radiation was observed at 25 °C, which is consistent with the results of the UJV tests performed at 90 °C in MX-80 bentonite. In the absence of clay, a similar increase in corrosion rate was observed in the presence of radiation for tests performed at 76% RH. However, for tests performed at 63% RH, the corrosion rate in the presence of radiation was extremely high even after nearly 1000 hours of testing (~230 $\mu m\ yr^{-1}$) and was greater than the corrosion rate observed in the Jacobs tests performed in porewater simulant for durations between 100 and 1000 hours at dose rates between 100 and 1000 Gy h^{-1}, which are the closest comparable irradiation conditions.

A second set of tests, performed by CIEMAT [27], comprised exposure tests on copper and carbon steel in FEBEX bentonite at either full saturation or 60% water content, or in FEBEX porewater with no bentonite present. The exposure conditions were irradiation at ambient temperature at 66 Gy h^{-1} and 697 Gy h^{-1} to give total doses of 14 and 140 kGy, respectively. Unirradiated control tests were run under comparable conditions. For carbon steel tests performed in the presence of bentonite, the average corrosion loss was greater under radiation than in unirradiated conditions, but the differences were small compared to the variations associated with repeatability. Furthermore, there was no significant difference in the measured corrosion rates between the two dose rates (and resulting total doses – same test durations were used). For tests performed in porewater in the absence of bentonite, there was an increase in average corrosion loss under radiation and the corrosion loss increased with increasing dose/dose rate. As with the tests performed in bentonite, the difference in corrosion rate under different radiation exposures (i.e., 0, 14 and 140 kGy) was smaller than the differences observed between nominally identical repeat tests. For tests performed on copper in the presence of bentonite, the corrosion rates were all below 10 $\mu m\ yr^{-1}$, but there appeared to be an inhibiting influence of radiation on corrosion with lower average corrosion rates observed at increasing dose rates. Interestingly, for the copper tests that were performed in porewater without bentonite, there was a substantial increase in corrosion rate in the presence of radiation compared to the unirradiated control tests, broadly consistent with the general observations reported in the tests performed by Jacobs. In the absence of radiation the corrosion rate was ~3 $\mu m\ yr^{-1}$, but following irradiation exposure to 14 and 140 kGy, the corrosion rates were ~49 and 25 $\mu m\ yr^{-1}$, respectively.

From the CIEMAT results, the increase in corrosion rate of steel during exposure to bentonite contrasts the results of the test performed by UJV, which were also performed in bentonite. The key differences between the two test configurations are the dose rate, temperature, and type of bentonite. Of these parameters, the higher dose rate in the CIEMAT tests would be expected to result in an increased corrosion rate, owing to the greater rate of formation of radiolytically generated oxidants. However, there may also be an impact of bentonite type and temperature given that they appeared to have an influence on the UJV results. The results for carbon steel performed in porewater without bentonite are broadly similar to the results observed in the Jacobs tests; namely, there does appear to be an enhancement of corrosion rate by radiation, however it is difficult to resolve above the noise of the measurement for short duration tests.

The results of the tests on copper in porewater are in fair agreement with the Jacobs tests, showing an increase in corrosion rate due to radiation. However, unlike in the Jacobs tests, which were performed over the dose rate range 0.1 to 10 Gy h^{-1}, the CIEMAT tests showed that the corrosion loss with radiation did not increase with increasing dose rate between 66 Gy h^{-1} and 697 Gy h^{-1}. This is an important observation as it demonstrates that, whilst there is a dose rate effect at very low dose rates, this influence cannot be accelerated linearly by increasing the dose rate up to very high dose rates (i.e, 697 Gy hr^{-1}). A further key observation was that the increase in corrosion rate due to radiation that was observed in

EURAD (Deliverable n° 15.7) – Elucidation of critical irradiation parameter
Dissemination level: Public
Date of issue of this report: 06/02/2024

Page 123

porewater did not occur in bentonite. In fact, in the latter, an inhibiting effect was possibly observed. The reason for the difference in results between porewater tests and those performed in bentonite is not yet certain, but it is anticipated that the reduced transport of oxidants in bentonite compared to porewater, the reduced water density in bentonite, and the ability of bentonite to react with radiolytically generated oxidants could all be contributing factors. These parameters may also explain the inhibiting influence of radiation on the corrosion rate of carbon steel that was observed in the UJV tests. Consequently, a key aspect for future work would be to assess the impact of bentonite on mitigating RIC under a wider range of conditions e.g., different bentonites, temperatures, and saturation levels. Additionally, it might be important to consider any effect of gamma radiation on the properties of the bentonite that may influence its ability to self-seal (e.g., a possible reduction in swelling pressure if there is a shift from monovalent to divalent cations in the smectite interlayers of the montmorillonite [58]).

EURAD (Deliverable n° 15.7) – Elucidation of critical irradiation parameter
Dissemination level: Public
Date of issue of this report: 06/02/2024

Page 124

References

1.   F King, M Behazin, *A Review of the Effect of Irradiation on the Corrosion of Copper-Coated Used Fuel Containers*. Corrosion and Materials Degradation,20212, 4,2021, pp. 678-707.

2.   C Liu, J Wang, Z Zhang, E-H Han, *Studies on corrosion behaviour of low carbon steel canister with and without γ-irradiation in China's HLW disposal repository*. Corrosion Engineering, Science and Technology,201752, sup1,2017, pp. 136-140.

3.   GS Was, Y Ashida, PL Andresen, *Irradiation-assisted stress corrosion cracking*. Corrosion Reviews,201129, 1-2,2011, pp. 7-49.

4.   P Scott, *A review of irradiation assisted stress corrosion cracking*. Journal of Nuclear Materials,1994211, 2,1994, pp. 101-122.

5.   K Daub, X Zhang, JJ Noël, J Wren, *Gamma radiation-induced carbon steel corrosion*. ECS Transactions,201133, 25,2011, pp. 15.

6.   K Daub, X Zhang, JJ Noël, JC Wren, *Gamma-radiation-induced corrosion of carbon steel in neutral and mildly basic water at 150°C*. Corrosion Science,201153, 1,2011, pp. 11-16.

7.   Å Björkbacka, S Hosseinpour, M Johnson, C Leygraf, M Jonsson, *Radiation induced corrosion of copper for spent nuclear fuel storage*. Radiation Physics and Chemistry,201392, 2013, pp. 80-86.

8.   A Björkbacka, S Hosseinpour, C Leygraf, M Jonsson, *Radiation Induced Corrosion of Copper in Anoxic Aqueous Solution*. Electrochemical and Solid-State Letters,201215, 5,2012.

9.   M Jonsson, *Exploring the impact of groundwater constituents and irradiation conditions on radiation-induced corrosion of copper*. Radiation Physics and Chemistry,2023211, 2023, pp. 111048.

10.   M Behazin, S Briggs, F King, *Radiation-induced corrosion model for copper-coated used fuel containers. Part 1. Validation of the bulk radiolysis submodel*. Materials and Corrosionn/a, n/a.

11.   DW Shoesmith, F King, *The Effects of Gamma Radiation on the Corrosion of Candidate Materials for the Fabrication of Nuclear Waste Packages,*University of Western Ontario*, AECL-11999, 1999

12.   RP Morco. *Gamma-Radiolysis Kinetics and Its Role in the Overall Dynamics of Materials Degradation*: The University of Western Ontario (Canada); 2020.

13.   I Soroka, N Chae, M Jonsson, *On the mechanism of γ-radiation-induced corrosion of copper in water*. Corrosion Science,2021182, 2021, pp. 109279.

14.   P Bouniol, W Guillot, V Dauvois, W Dridi, S Le Caër, *Original behavior of pore water radiolysis in cement-based materials containing sulfide: Coupling between experiments and simulations*. Radiation Physics and Chemistry,2018150, 2018, pp. 172-181.

15.   C Padovani, F King, C Lilja, D Féron, S Necib, D Crusset, et al., *The corrosion behaviour of candidate container materials for the disposal of high-level waste and spent fuel – a summary of the state of the art and opportunities for synergies in future R&D*. Corrosion Engineering, Science and Technology,201752, sup1,2017, pp. 227-231.

16.   AU Abdelouas A., Bernier-Latmani R., Bosch C., Cherkouk A., Dobrev D., Fernández A.M., Finck N., Gaggiano R., Havlová V., Hesketh J., Idiart A., Mijnendonckx K., Montoya V., Muñoz A.G., Padovani, C., Pont A., Rajala P., Riba O., Sarrasin L., Sayenko S., Smart N., Texier-Mandoki N., Wersin P, *Initial State-of-the-Art of WP ConCorD,Final version as of 17.08.2022 of deliverable D15.1 of the HORIZON 2020 project EURAD,* EC Grant agreement no: 847593, 2022

17.   JP Simpson, *Experiments on container materials for Swiss high-level waste disposal projects Part 2,Switzerland,* NAGRA-NTB--84-01, 1984

18.   F King, C Litke, *The Corrosion of Copper in Synthetic Groundwater at 150 C--Part I. The Results of Short-Term Electrochemical Tests*.19871987.

EURAD (Deliverable n° 15.7) – Elucidation of critical irradiation parameter
Dissemination level: Public
Date of issue of this report: 06/02/2024

Page 125

19.   K Daub, X Zhang, JJ Noël, JC Wren, *Effects of γ-radiation versus H_2O_2 on carbon steel corrosion*. Electrochimica Acta,201055, 8,2010, pp. 2767-2776.

20.   G Marsh, K Taylor, *An assessment of carbon steel containers for radioactive waste disposal*. Corrosion Science,198828, 3,1988, pp. 289-320.

21.   R Westerman, J Nelson, S Pitman, W Kuhn, S Basham, D Moak, *Evaluation of iron-base materials for waste package containers in a salt repository*. MRS Online Proceedings Library (OPL),198326, 1983.

22.   E Smailos, W Schwarzkopf, R Koester, B Fiehn, G Halm, *Corrosion testing of selected packaging materials for disposal of high-level waste glass in rock-salt formations,Commission of the European Communities (CEC),* EUR--13672, 1991

23.   RE Westerman, SG Pitman, JL Nelson, *General corrosion, irradiation-corrosion, and environmental-mechanical evaluation of nuclear-waste-package structural-barrier materials Progress report,United States,* PNL--4364, 1982

24.   S-I Giannakandropoulou, H Desjonqueres, C Wittebroodt, G Baldacchino, *"Impact of γ-radiation on carbon steel anaerobic corrosion and H2 production."*. Radiation Physics and Chemistry,20222022, pp. 110742.

25.   N Fujita, C Matsuura, K Saigo, *Radiation-induced preferential dissolution of specific planes of carbon steel in high-temperature water*. Radiation Physics and Chemistry,200160, 1,2001, pp. 53-60.

26.   NR Smart, AP Rance, LO Werme, *The effect of radiation on the anaerobic corrosion of steel*. Journal of Nuclear Materials,2008379, 1,2008, pp. 97-104.

27.   *Synthesis of irradiation results under repository conditions,*Draft Version as of 22.01.2024 of Deliverable D15.8 of the HORIZON 2020 project EURAD. EC Grant agreement no: 847593., 2024.

28.   ASTM. G1-03 Standard Practice for Preparing, Cleaning, and Evaluating Corrosion Test Specimens. 2011.

29.   *Deliverable D55, DISCO project, grant agreement 755443, Horizon 2020 Framework Programme, European Commission, Development of a reactive transport model of spent fuel dissolution under near field environmental conditions,* 2021

30.   B Pastina, JA LaVerne, *Effect of molecular hydrogen on hydrogen peroxide in water radiolysis*. The Journal of Physical Chemistry A,2001105, 40,2001, pp. 9316-9322.

31.   M Kelm, E Bohnert. *A kinetic model for the radiolysis of chloride brine, its sensitivity against model parameters and a comparison with experiments*: Forschungszentrum Karlsruhe; 2004.

32.   JK Heuer, JF Stubbins, *An XPS characterization of FeCO3 films from CO2 corrosion*. Corrosion Science,199941, 7,1999, pp. 1231-1243.

33.   MC Biesinger, BP Payne, AP Grosvenor, LWM Lau, AR Gerson, RSC Smart, *Resolving surface chemical states in XPS analysis of first row transition metals, oxides and hydroxides: Cr, Mn, Fe, Co and Ni*. Applied Surface Science,2011257, 7,2011, pp. 2717-2730.

34.   SW Goh, AN Buckley, RN Lamb, RA Rosenberg, D Moran, *The oxidation states of copper and iron in mineral sulfides, and the oxides formed on initial exposure of chalcopyrite and bornite to air*. Geochimica et Cosmochimica Acta,200670, 9,2006, pp. 2210-2228.

35.   J Hesketh, H Haynes, B Reddy, A Rance, C Bevas, C Padovani, et al., *Carbon steel corrosion in a bentonite buffer: A comparison between in situ exposure and lab based experiments*. Materials and Corrosion,20232023.

36.   N Diomedes, B Reddy, *Corrosion of Canister Materials in Anaerobic Saturated Bentonite: In Situ and Ex Situ Experiments,Wettingen, Switerland,* Nagra, NAB 20-10, 2022

37.   B Kursten, NR Smart, NA Senior, DD Macdonald, S Caes, V de Souza, et al., *Overview of anaerobic corrosion of carbon steel radioactive waste packages in alkaline media in support of the Belgian supercontainer concept*. Materials and Corrosion,202172, 1-2,2021, pp. 32-51.

EURAD (Deliverable n° 15.7) – Elucidation of critical irradiation parameter
Dissemination level: Public
Date of issue of this report: 06/02/2024

Page 126

38.   G Hultquist, P Szakalos, M Graham, AB Belonoshko, G Sproule, L Gråsjö, et al., *Water corrodes copper*. Catalysis Letters,2009132, 2009, pp. 311-316.

39.   F King, *Critical review of the literature on the corrosion of copper by water,*Swedish Nuclear Fuel and Waste Management Co., Stockholm*, SKB-TR-10-69, 2010

40.   E Toijer, M Jonsson, *H2O2 and γ-radiation induced corrosion of 304L stainless steel in aqueous systems*. Radiation Physics and Chemistry,2019159, 2019, pp. 159-165.

41.   A Barreiro Fidalgo, Y Kumagai, M Jonsson, *The role of surface-bound hydroxyl radicals in the reaction between H2O2 and UO2*. Journal of Coordination Chemistry,201871, 11-13,2018, pp. 1799-1807.

42.   JM Joseph, B Seon Choi, P Yakabuskie, J Clara Wren, *A combined experimental and model analysis on the effect of pH and O2(aq) on γ-radiolytically produced H2 and H2O2*. Radiation Physics and Chemistry,200877, 9,2008, pp. 1009-1020.

43.   M Pérez Sánchez, M Barrera, S González, RM Souto, RC Salvarezza, AJ Arvia, *Electrochemical behaviour of copper in aqueous moderate alkaline media, containing sodium carbonate and bicarbonate, and sodium perchlorate*. Electrochimica Acta,199035, 9,1990, pp. 1337-1343.

44.   M Pérez Sánchez, RM Souto, M Barrera, S González, RC Salvarezza, AJ Arvia, *A mechanistic approach to the electroformation of anodic layers on copper and their electroreduction in aqueous solutions containing NaHCO3 and Na2CO3*. Electrochimica Acta,199338, 5,1993, pp. 703-715.

45.   F King, L Ahonen, C Taxen, U Vuorinen, L Werme, *Copper corrosion under expected conditions in a deep geologic repository,*Sweden, SKB-TR--01-23, 2001

46.   AD Modestov, G-D Zhou, H-H Ge, BH Loo, *A study by voltammetry and the photocurrent response method of copper electrode behavior in acidic and alkaline solutions containing chloride ions*. Journal of Electroanalytical Chemistry,1995380, 1,1995, pp. 63-68.

47.   BR N. Diomidis, *Corrosion of canister materials in anaerobic saturated bentonite: In situ and ex situ experiments – Part 1,*Nagra working report NAB 20-10, 2022

48.   S Sim, IS Cole, YS Choi, N Birbilis, *A review of the protection strategies against internal corrosion for the safe transport of supercritical CO2 via steel pipelines for CCS purposes*. International Journal of Greenhouse Gas Control,201429, 2014, pp. 185-199.

49.   NR Smart, B Reddy, AP Rance, DJ Nixon, M Frutschi, R Bernier-Latmani, et al., *The anaerobic corrosion of carbon steel in compacted bentonite exposed to natural Opalinus Clay porewater containing native microbial populations*. Corrosion Engineering, Science and Technology,201752, sup1,2017, pp. 101-112.

50.   B Reddy, C Padovani, NR Smart, AP Rance, A Cook, A Milodowski, et al., *Further results on the in situ anaerobic corrosion of carbon steel and copper in compacted bentonite exposed to natural Opalinus Clay porewater containing native microbial populations*. Materials and Corrosion,202172, 1-2,2021, pp. 268-281.

51.   P Wersin, J Hadi, M Kiczka, A Jenni, J-M Grenèche, N Diomidis, et al., *Unravelling the corrosion processes at steel/bentonite interfaces in in situ tests*. Materials and Corrosion,202374, 11-12,2023, pp. 1716-1727.

52.   P Wersin, A Jenni, UK Mäder, *Interaction of Corroding Iron with Bentonite in the ABM1 Experiment at Äspö, Sweden: A Microscopic Approach*. Clays and Clay Minerals,201563, 1,2015, pp. 51-68.

53.   P Wersin, J Hadi, A Jenni, D Svensson, J-M Grenèche, P Sellin, et al., *Interaction of Corroding Iron with Eight Bentonites in the Alternative Buffer Materials Field Experiment (ABM2)*. Minerals,202111, 8,2021, pp. 907.

54.   S Kaufhold, R Dohrmann, N Götze, D Svensson, *Characterization of the Second Parcel of the Alternative Buffer Material (ABM) Experiment — I Mineralogical Reactions*. Clays and Clay Minerals,201765, 1,2017, pp. 27-41.

EURAD (Deliverable n° 15.7) – Elucidation of critical irradiation parameter
Dissemination level: Public
Date of issue of this report: 06/02/2024

Page 127

55.   M Behazin, S Briggs, F King, *Radiation-induced corrosion model for copper-coated used fuel containers. Part 1. Validation of the bulk radiolysis submodel*. Materials and Corrosion,202374, 11-12,2023, pp. 1834-1847.

56.   I Pospiskova, D Dobrev, M Kouril, J Stoulil, D Novikova, P Kotnour, et al., *Czech national programme and disposal canister concept*. Corrosion Engineering, Science and Technology,201752, 1_suppl,2017, pp. 6-10.

57.   R Červinka, M Klajmon, J Zeman, Z Vencelides,   *The geochemical evolution of DGR/preparation of geochemical model-geochemical calculations and reactive transport modelling,*Radioactive Waste Repository Administration*, 2018*

58.   O Karnland, S Olsson, U Nilsson, *Mineralogy and sealing properties of various bentonites and smectite-rich clay materials,*Swedish Nuclear Fuel and Waste Management Co.*, 2006*

EURAD (Deliverable n° 15.7) – Elucidation of critical irradiation parameter
Dissemination level: Public
Date of issue of this report: 06/02/2024

Page 128